4

RESULTS AND DISCUSSION

The results of the present investigation ***"Corrosion Mitigation Effect of Synthesized Water Soluble Acryl Terpolymers on Mild Steel in HCl and Preliminary Investigation as Oil Filed Inhibitor on N80 steel"*** are discussed in the light of the objectives set forth. The present study aims to synthesize water soluble acryl terpolymers and analyze their inhibitive properties on mild steel in 1M HCl medium. In order to test the effectiveness of the terpolymer inhibitors as oil field inhibitors, studies were conducted using N80 steel in selected media.

Efforts are taken to discuss the results in the following headings

- Synthesis of Water Soluble Acryl Terpolymers
- Characterization of Water Soluble Acryl Terpolymers
- Effectiveness of Water Soluble Acryl Terpolymers as corrosion inhibitors-Weight loss methods and electrochemical measurements.
- Adsorption properties of the inhibitors, Surface analysis of mild steel in the presence and absence of the inhibitors-SEM&AFM, and Mechanism of adsorption.
- Effectiveness of synthesized terpolymers as oil field inhibitors

4.1 Synthesis of Water Soluble Acryl Terpolymers

A series of five graft terpolymers was synthesized based on poly(vinyl alcohol) as given in section 2.1. The photographic images of the synthesized terpolymers are shown in Figure 7. The synthesis was carried out for five graft terpolymers with different combinations of monomers, while concentration of PVA and initiator were fixed. The synthetic details of the grafted terpolymers are given in Table 6. From the Table 6, it is clear that the reaction rate of the acrylamide terpolymers is higher than the other terpolymeric systems. This fact is also manifested in the terms of conversion percentage and grafting percentage. The terpolymers were soluble in hot water and Dimethyl sulfoxide (DMSO) and almost insoluble in the organic solvents. The terpolymers initially swell and then get gradually dispersed in the medium. The slow solubility is an indication of the high molecular weight and cross-linking nature of the polymers.

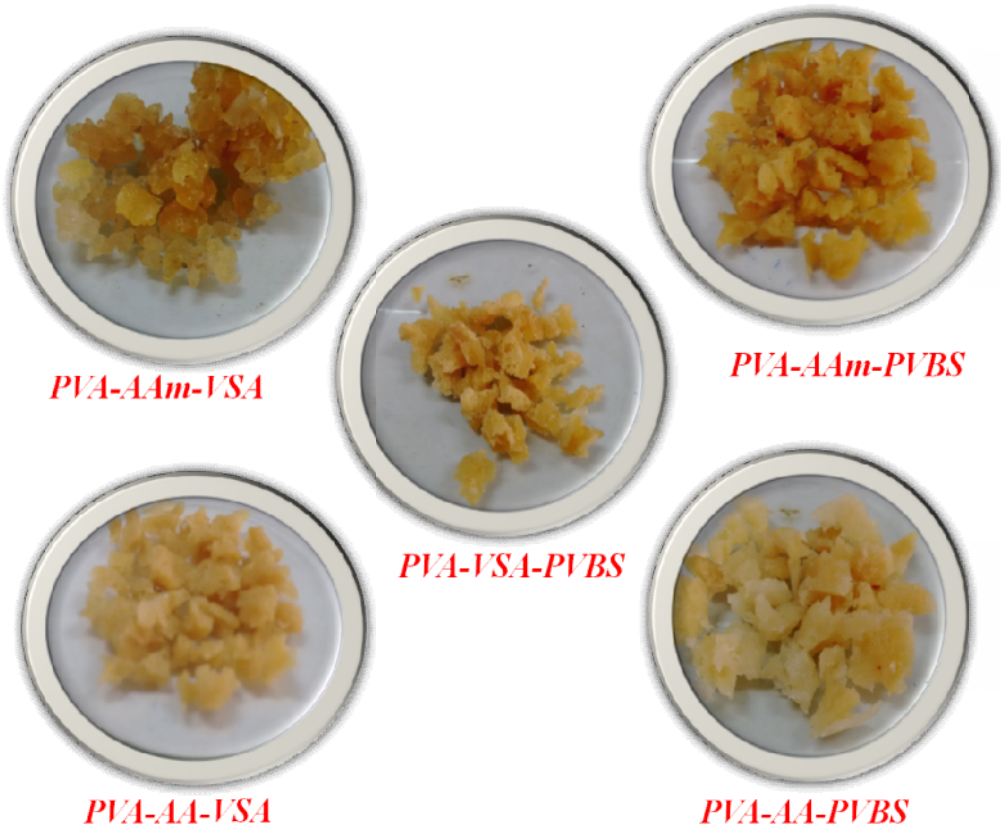

Figure - 7 Photographic images of the synthesized grafted terpolymers

Table - 6 Synthetic details of the grafted terpolymers and their solvents

S. No.	Terpolymer	Yield (%)	Conversion (%)	Grafting (%)	Soluble in	Insoluble in
1	PVA-AAm-VSA	90.4	80.8	190	Water and DMSO (heated wherever required)	NaOH, Ethanol, Toluene, Benzene $CHCl_3$, N,N-DMF, THF.
2	PVA-AAm-PVBS	94.7	85.9	180		
3	PVA-AA-VSA	85.3	70.6	160		
4	PVA-AA-PVBS	83.5	56.0	125		
5	PVA-VSA-PVBS	75.1	33.6	150		

4.1.1 Mechanism of the grafting reaction

The mechanism of grafting reaction involves the formation of free radical initiator that generate free-radical sites on the PVA backbone. These active free radical sites generated on the polymer backbone, in the presence of acrylic monomers produce graft polymers **(Krishnamoorthi and Singh, 2006; Marin *et al.*, 2014).** In the present study, free radicals are expected to get generated on the PVA backbone and on the vinyl monomers. It is expected that vinyl monomers tend to copolymerize faster, and may tend to get terminated with the radical formed in the PVA backbone. As this is not a controlled polymerization reaction, the reaction sequence cannot be confined holistically to the above hypothesis. Several reactions could have taken place in all possible ways to produce a cross-linked product. The plausible mechanism of the polymerization reaction can be given as follows:

Initiation

During the initiation reaction free radicals may be formed on the PVA and vinyl monomer unit. M1 is the acrylamide or acrylic acid or sodium salt of vinyl sulfonic acid, M2 is the sodium salt of vinyl sulfonic acid or p-vinyl benzene sulfonic acid. I is the initiator.

$$I\text{-}I \rightarrow 2I^*$$

$$PVA + I^* \rightarrow PVA^*$$

$$M1 + I^* \rightarrow M1^*$$

$$M2 + I^* \rightarrow M2^*$$

Propagation

The propagation of the reactions can proceed through the following steps.

$$PVA^* + M1 \rightarrow PVA\text{-}M1^*$$

$$PVA^* + M2 \rightarrow PVA\text{-}M2^*$$

$$M1 + M2^* \rightarrow M2\text{-}M1^*$$

$$M2 + M1^* \rightarrow M1\text{-}M2^*$$

$$PVA\text{-}M1/2^* + M1/2^* \rightarrow PVA\text{-}M1/2\text{-}M1/2^*$$

Termination

The termination reactions can occur as follows.

$$PVA\text{-}M1^* + M1^*/M2^* \rightarrow PVA\text{-}M1\text{-}M1 \text{ or } PVA\text{-}M1\text{-}M2$$

$$PVA^* + M1\text{-}M2^* \rightarrow PVA\text{-}M1\text{-}M2$$

Hence the expected structure of the grafted terpolymers can be depicted as follows:

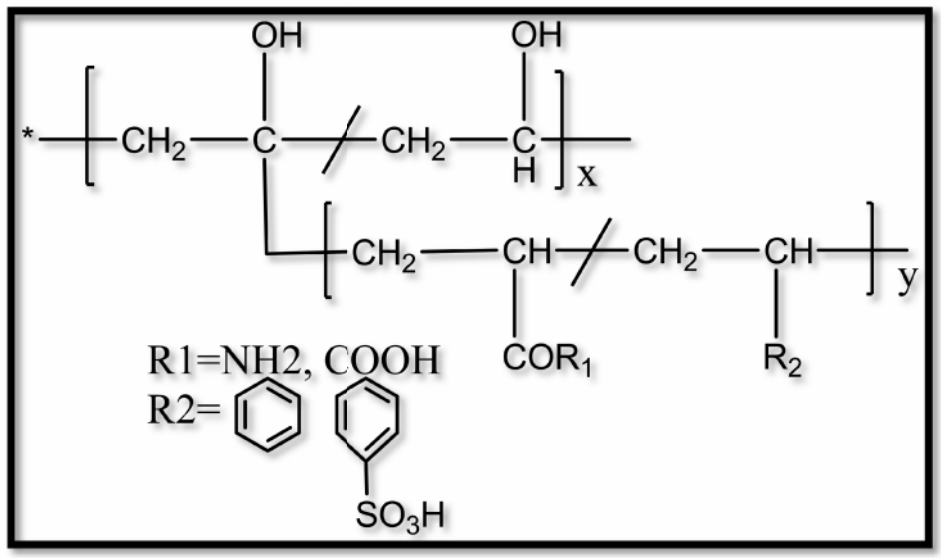

Figure - 8 Proposed structure of the grafted terpolymer

4.2 Characterization

4.2.1 Ultraviolet Visible spectroscopy

The synthesized terpolymers have some of the conventional transfers in the UV region such as n-σ^*, π -π* and n -π*. The UV Visible spectrometric scan of polyvinyl alcohol and grafted terpolymers in the wavelength region of 200-400 nm is shown in Figure 9 and the corresponding transitions are briefed in Table 7.

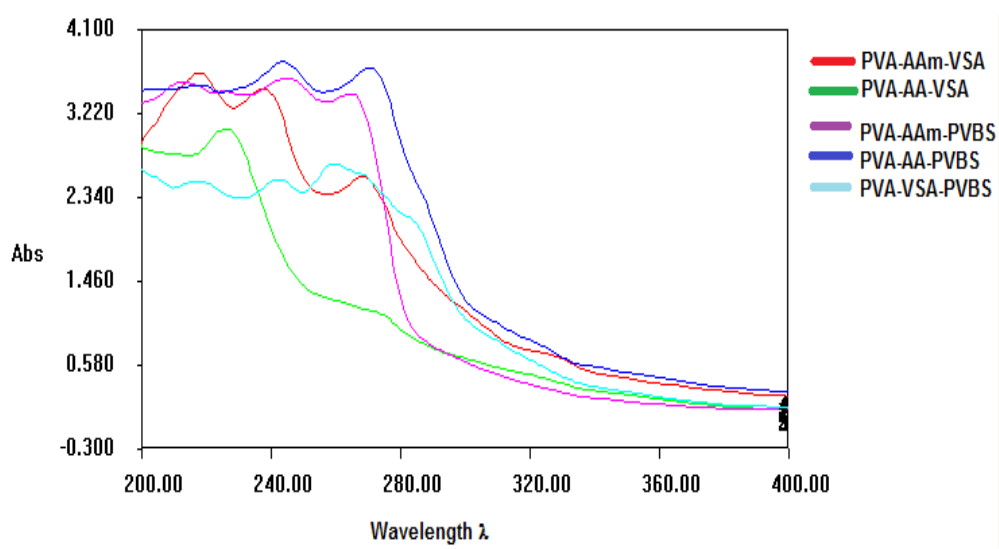

Figure – 9 UV absorption peaks of Terpolymers under investigation

Table – 7 Characteristic UV-visible transitions in the grafted terpolymers

S.No.	Polymer	Chromophores and Auxochromes	Absorbance (λ) nm		
			n-σ*	π -π*	n -π*
1	PVA	OH	204		
2	PVA-AAm-VSA	OH, CO, NH, SO	218	237	268
3	PVA-AAm-PVBS	OH, CO,NH,Ar.,SO	212	244	274
4	PVA-AA-VSA	OH,CO, SO	225		270(w)
5	PVA-AA-PVBS	OH,CO,Ar.,SO	217	243	270
6	PVA-VSA-PVBS	OH,Ar.,SO	242		260

All the transitions were found to occur in the range of 200-300 nm. Based on the auxochromes and chromophores present in the investigated polymers the transtions are classified and explained as follows:

n-σ* transition

This transition is a characteristic transition of saturated molecules that contain atoms bearing non-bonding pairs of electrons. Alcohols were found to absorb in the range of 175-200 nm. PVA reflects n-σ* transition at 204 nm which is shifted to higher wavelength in the case of all grafted terpolymers studied. This bathochromic shift is caused because of the extended chain length after polymerization.

π -π* transition

This transition occurs when the unsaturated molecules are excited under UV irradiation. π-π* is a high energy transition, but still the position is affected significantly by the presence of substituted groups. A typical carbonyl compound undergoes π -π* transition at 188 nm. The carbonyl group present in the grafted terpolymers show π -π* transition at 225-244 nm. This bathochromic shift is due to the polymerization resulting in extended chain length leading to resonance interaction and presence of other substituted groups. PVBS polymers show greater bathochromic shift than the VSA polymers, because of the presence of an extra aromatic ring system that renders extended conjugation.

n -π* transition

n-π* is generally called as forbidden transition as it requires high energy for excitation and appears as a low intensity signal. This transition is very slightly affected by substitution or conjugation. If the chain length is too long it may sometimes be buried under the more intense π -π* transition. The grafted terpolymers undergo this transition in the range of 260-274 nm which are generated by the lone pair of electrons present on O, N and S atom.

4.2.2 Fourier Transform Infrared Spectroscopy (FTIR)

The structural changes of the terpolymers were confirmed by Fourier Transform Infrared Spectroscopy (FTIR) and briefed in the following sections.

4.2.2.1 Analysis of molecular vibrations of PVA-AAm-VSA

Table 8 shows the characteristic bands of PVA, AAm, VSA and the grafted polymer PVA-AAm-VSA and their assignments to respective functional groups.

Table - 8 Characteristic FTIR vibrations of PVA-AAm-VSA

PVA (cm^{-1})	AAm (cm^{-1})	VSA (cm^{-1})	PVA-AAm-VSA (cm^{-1})	Assignment
3000-3600		2900-3700	3000-3700	OH str. Inter and intra molecular hydrogen bonding
-	3379, 3182	-	-	Symmetric and asymmetric NH str.
2923,2878	-	-	2941(w)	Alkyl –CH str.
1706	-	-	-	C=O str.
-	1680	1655(C=C)	1653	Amide I C=O
-	1600	-	-	Amide II N-H bending
1430	1421	1394	1429	C-O-H bending/C-H bending vibrations
	1358		1367	Amide III C-N
1250	1260	-	1268	C-O str.
-	-	1188, 1036	1153-1089(w) 1268	Asymmetric and symmetric S=O str.
1000-1071	1125	-	-	C-O-C str. /Additional NH bending bands
839	822	-	-	CH rocking/N-H wagging
-	956	956	-	Out-of-plane bending vibrations of vinyl unit

PVA Vs. PVA-AAm-VSA

All the major peaks related to the hydroxyl groups and acetate groups are observed in the FTIR spectrum of PVA. The large bands appearing in the region of 3000-3600 cm^{-1} are due to the stretching vibrations of -OH arising from the intermolecular and intramolecular hydrogen bonds. In the same region, a broader peak corresponding to OH group can be figured out for the grafted polymer, which may be due to the overlapping of -OH and -NH stretching vibrations of polyacrylamide. The vibrational bands observed in the region of

2923 cm^{-1} and 2878 cm^{-1} are linked to the alkyl -CH stretching vibrations of PVA, which is slightly shifted to 2941 cm^{-1} in the case of the grafted polymer.

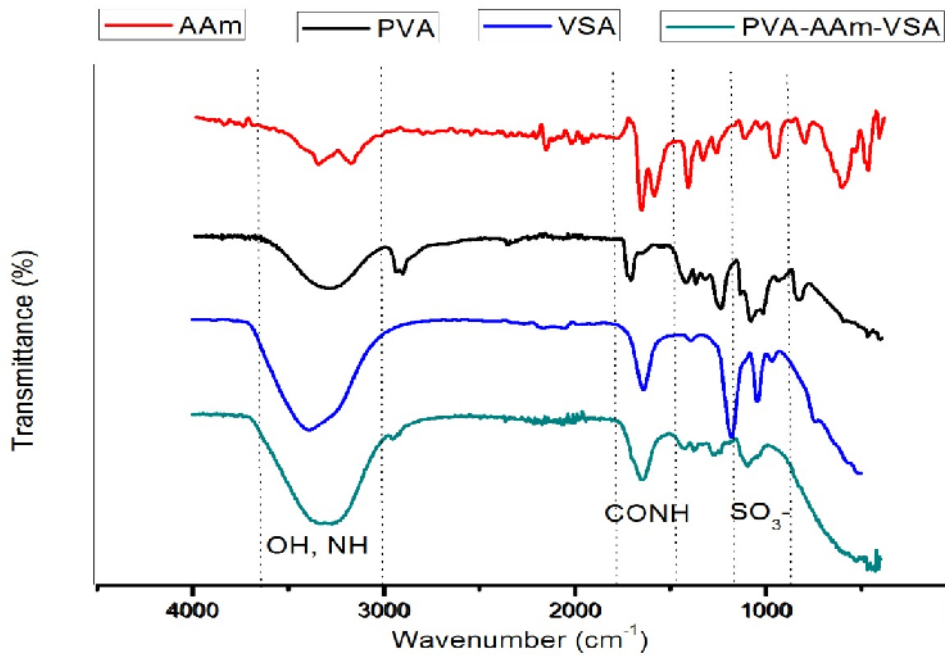

Figure - 10 Comparative FTIR spectrum of PVA-AAm-VSA with its respective monomers

The peak found at 1706 $cm^{-1}$is correlated to the C=O stretching of the unhydrolyzed acetate groups of PVA, but shifted to lower wavenumber in the grafted terpolymer. The intensity of this peak also provides information about the degree of hydrolysis of the PVA **(Mansur *et al.*, 2008).** The absorption pointed around 1430 cm^{-1} is pertained to C-O-H bending vibrations and/or C-H bending vibrations, and these absorptions remain the same for the grafted polymer. The absorptions around 1250 cm^{-1} and a broad peak positioned in the range of 1000-1071 cm^{-1} are attributable to the C-O stretching and C-O-C stretching of the acetyl groups of PVA respectively. The C-O stretching vibrations of the polymer can be pointed at 1268 cm^{-1}.The peak at 839 cm^{-1} can be assigned to -CH rocking vibrations which are distinctively absent in the PVA-AAm-VSA **(Pavia *et al.*, 2001;Silverstein *et al.*, 2005).**

AAm Vs. PVA-AAm-VSA

The absorptions at 3379 cm^{-1} and 3182 cm^{-1} belong to the symmetric and asymmetric stretching vibrations of –NH moiety of the amide. In the case of amide polymers, 3 types of amide bands viz. amide I, amide II and amide III are expected. Amide I is the C=O stretching of the amide group, amide II is the N-H bending and amide III is C-N stretching

(Cavus, 2010; Zhang and Easteal, 2007). When the absorptions of the monomer acrylamide is observed, the bands amide I, II and III appear at 1680 cm^{-1}, 1600 $cm^{-1}$and 1358 cm^{-1} respectively. But the amide I and II are shifted to a lower wave number and appears as a single broad peak at 1653 cm^{-1} in the polymer due to the lengthening of the bond after polymerization. This peak is the characteristic peak of polyacrylamide. The amide I and II band of the polymer are overlapped with those peaks corresponding to C=O stretching of PVA and amide III is shifted to 1367cm^{-1}. The CH bending vibrations of the monomer is present at 1421 cm^{-1} and has shifted to 1429 cm^{-1} after polymerization. The weaker bands observed at 1260 cm^{-1} and 1125 cm^{-1} are additional bands which can result from the interactions between N-H bending and C-N stretching of the C-N-H group of acrylamide and have shifted to 1268 cm^{-1} in the polymer. The absorption positioned around 822 $cm^{-1}$and 956 cm^{-1} can be assigned to NH wagging of the amide and out-of plane bending vibrations of the vinyl unit which are absent in the polymer.

VSA Vs. PVA-AAm-VSA

The strong peak at 2900-3700 cm^{-1} is due to the OH groups of VSA. The C=C stretching of the monomer is observed at 1655 cm^{-1} which is obviously absent in the polymer. The asymmetric and symmetric stretching modes of vibrations of $-SO_3$ group can be observed at 1188 cm^{-1} and 1036 cm^{-1} respectively **(Yadav *et al*., 2013; Roy *et al*., 2013)**. For grafted terpolymer, these stretching modes are shifted and observed in the form of a small single broadened peak in the region of 1153-1089 cm^{-1}. This shift could be because of the following reasons: Copolymerization of vinyl sulfonic acid with acrylamide, followed by grafting on the backbone of PVA matrix. This hypothesis is further supported by the **Neira-carrillo *et al*. (2011)** who has reported a peak at 1195 cm^{-1} corresponding to the S=O group of Polyvinyl sulfonate. These evidences confirmed the grafting of poly(vinyl sulfonic acid) chains on the PVA. The out-of-plane bending modes of the monomer vinyl unit of vinyl sulfonic acid positioned at 956 cm^{-1} disappear in the spectrum of the polymer **(Hobson and Feast, 1999; Gu *et al*., 2012).**

4.2.2.2 Analysis of molecular vibrations of PVA-AA-VSA

Table 9 shows the characteristic bands of PVA, AA, VSA and the grafted polymer PVA-AA-VSA with their assignments to respective functional groups.

PVA Vs. PVA-AA-VSA

The large bands appearing in the region of 3000-3600 cm^{-1} due to the stretching vibrations of -OH in PVA can be figured out for the grafted polymer in the range of 3000-3700 cm^{-1}. The alkyl -CH stretching vibrations at 2923 cm^{-1} are slightly shifted to

2941 cm^{-1} in the grafted polymer. The C=O stretching of unhydrolyzed acetate groups of PVA at 1706 cm^{-1} is shifted to 1661 cm^{-1} in the grafted terpolymer. The C-O-H bending vibrations and/or C-H bending vibrations appear at 1437 cm^{-1} in the grafted polymer. The C-O absorptions around 1250 cm^{-1} and C-O-C absorptions in the range of 1000-1071 cm^{-1} of acetyl groups of PVA can be pointed at 1260 cm^{-1} in the terpolymer.

Table - 9 Characteristic FTIR vibrations of PVA-AA-VSA

PVA (cm^{-1})	AA (cm^{-1})	VSA (cm^{-1})	PVA-AA-VSA (cm^{-1})	Assignment
3000-3600	2800-3400	2900-3700	3000-3700	OH str. Inter and intra molecular hydrogen bonding
2923,2878	-	-	2941	Alkyl –CH str.
1706	1697	-	1661	C=O str.
-	1608	1655	-	C=C str.
1430	1421	-	1437	C-O-H bending/C-H bending vibrations
1250	1286 1054	-	1260	C-O str.(COOH)
-	-	1188, 1036	1106-1044 small peak	Asymmetric and symmetric S=O str.
-	1120	-	-	Monosubstituted vinyl bond
1000-1071	-	-	-	C-O-C str.
839	804	-	-	CH rocking
-	983	956	-	Out-of-plane bending vibrations of vinyl unit

AA Vs. PVA-AA-VSA

A broad and weak peak for -OH is found in the range of 2800-3400 cm^{-1} for the acrylic acid monomer, because of the strong intramolecular hydrogen bonding the free hydroxyl stretching is less pronounced. But a broad deep peak is obtained for the grafted polymer in the range of 3000-3700 cm^{-1} as a result of polymerization and –OH groups of PVA and Vinyl sulfonic acid. A sharp peak for C=O absorption is found at 1697 cm^{-1}, which shifts to lower wave number of 1661 cm^{-1} in the polymer. The shift in the absorption of C=O to lower wave number may be because of Hydrogen bonding, Resonance stabilization and lengthening of the bond **(Silverstein *et al*., 2005)**. The absorption pointed around 1430 cm^{-1} is pertained to C-O-H bending vibrations and/or C-H bending vibrations, and these absorptions are shifted to 1437 cm^{-1} in the grafted polymer. The stretching modes of C-O are

associated with absorptions present at 1286 cm^{-1} and 1054 cm^{-1} for monomer, and 1260 cm^{-1} for the polymer. The absorption peaks at 1120 cm^{-1}, 804 cm^{-1} and 989 cm^{-1} are assigned to the mono-substituted vinyl bond, -CH rocking modes of vibrations and -CH bond of alkene respectively which are typically absent in the polymeric form **(Hobson and Feast, 1999 ; Gu *et al*. 2012).**

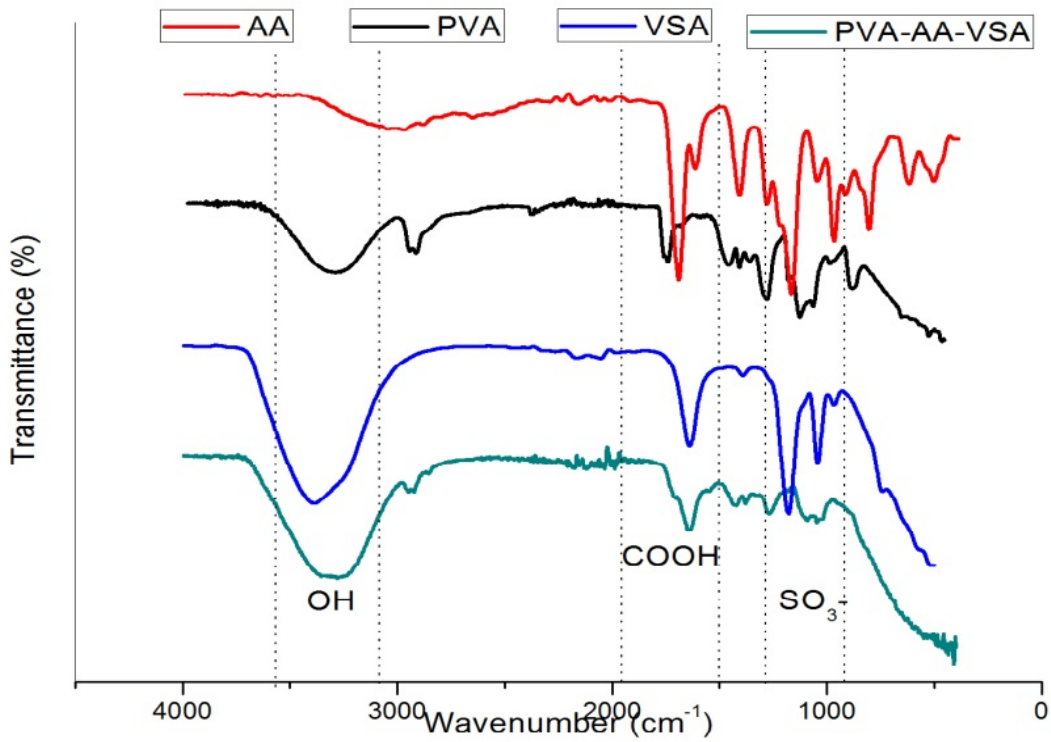

Figure - 11 Comparative FTIR spectrum of PVA-AA-VSA with its respective monomers

VSA Vs. PVA-AA-VSA

The OH stretching, C=C stretching, SO_3 group's asymmetric and symmetric stretching vibrations of the monomer VSA appeared at 2900-3700 cm^{-1}, 1655 cm^{-1}, 1188 cm^{-1} and 1036 cm^{-1} respectively. For grafted terpolymer, the SO_3 group's stretching modes are shifted and observed in the form of a small single broadened peak in the region of 1106-1044 cm^{-1}. This shift could be because of copolymerization of vinyl sulfonic acid with acrylic acid, followed by the grafting on the backbone of PVA matrix. The out-of-plane bending modes of the vinyl unit of monomers acrylamide and vinyl sulfonic acid at 956 cm^{-1} has disappeared in the spectrum of the polymer **(Hobson and Feast, 1999; Gu *et al*., 2012).**

4.2.2.3 Analysis of molecular vibrations of PVA-AAm-PVBS

Table 10 shows the characteristic bands of PVA, AAm, PVBS and the grafted polymer PVA-AAm-PVBS and their assignments to respective functional groups.

PVA Vs. PVA-AAm-PVBS

The major absorption bands of PVA are discussed in the previous sections 4.2.2.1. The broader peak of the grafted polymer appears in the range of 3000-3700 cm^{-1}, which may be due to the overlapping of -OH and -NH stretching vibrations of polyacrylamide. The peaks at 2923 cm^{-1} and 2842 cm^{-1} is due to the alkyl–CH and aromatic –CH stretching vibrations in the grafted The absorption pointed around 1430 cm^{-1} is pertained to C-O-H bending vibrations and/or C-H bending vibrations in PVA, and these absorptions can be figured at 1438 cm^{-1} for grafted polymer. The absorptions around 1250 cm^{-1} and a broad peak positioned in the range of 1000-1071cm^{-1} are attributable to the C-O stretching and C-O-C stretching of the acetyl groups of PVA respectively. The C-O stretching vibrations of the polymer can be pointed at 1259 cm^{-1}. The peak at 839 cm^{-1} can be assigned to -CH rocking vibrations and are absent in the polymer.

Table - 10 Characteristic FTIR vibrations of PVA-AAm-PVBS

PVA (cm^{-1})	AAm (cm^{-1})	PVBS (cm^{-1})	PVA-AAm-PVBS (cm^{-1})	Assignment
3000-3600	-	-	3000-3700	OH str. Inter and intra molecular hydrogen bonding
-	3379,3182	-	-	Symmetric and asymmetric NH str.
2923,2878	-	-	2923,2842	Alkyl –CH str. /alkene =CH str.
1706	-	-	-	C=O str.
-	1680	-	1644	Amide I C=O
-	1600	-	-	Amide II N-H bending
-	-	1590, 1429 1358,1322	-	Aromatic skeleton str.
1430	1421	-	1438	C-O-H bending/C-H bending vibrations
	1358	-	1376	Amide III C-N
1250	1260	-	1259	C-O str.
-	-	1197, 1116, 1045	1197-1098(w) 1009 (s)	Asymmetric and symmetric S=O str.
1000-1071	1125	-	-	C-O-C str. /Additional NH bending bands
839	822	-	-	CH rocking/N-H wagging
-	956	983, 919	-	Out-of-plane bending vibrations of vinyl unit
-	-	839,669,508	660, 446	Out-of-plane bending vibrations of para-substituted benzene unit

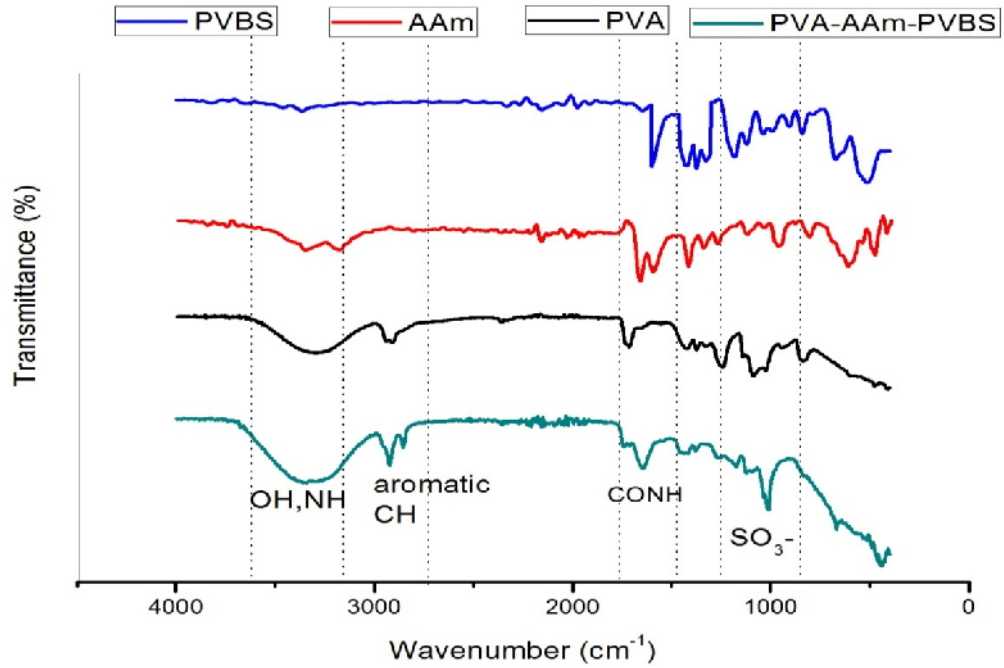

Figure - 12 Comparative FTIR spectrum of PVA-AAm-PVBS with its respective monomers

AAm Vs. PVA-AAm-PVBS

The vibrational bands of the monomer acrylamide are as discussed in the previous section 4.2.2.2. The amide I and II are shifted to a lower wave number and appear as a single broad peak at 1644 cm^{-1} in the polymer due to the lengthening of the bond after polymerization. This peak is the characteristic peak of polyacrylamide, and amide III is shifted to 1376 cm^{-1}. The amide I and II band of the polymer are overlapped with the C=O stretching of PVA. The CH bending vibrations appear at 1438 cm^{-1} in the polymerized form. The weaker bands observed at 1260 cm^{-1} and 1125 cm^{-1} are additional bands which may be due to the interactions between N-H bending and C-N stretching of the C-N-H group of acrylamide and is present as a single peak at 1259 cm^{-1} in the polymer. The NH wagging of the amide and out-of plane bending vibrations of the vinyl unit of the monomer are absent in the polymer.

PVBS Vs. PVA-AAm-PVBS

Gu *et al.* (2012) has assigned the absorption peaks at 1590, 1429, 1358 and 1322 cm^{-1} are due to the aromatic skeleton stretching vibrations of PVBS**. Orler *et al.* (1993)** observed peaks at 1128, 1175 and 1095 cm^{-1} for styrene sulfonic acid. For sodium styrene sulfonic acid, **Yang *et al.* (2002)** observed peaks at 1184 and 1042 cm^{-1} for asymmetric and symmetric SO_3^- stretching. Thus the peaks at 1197, 1116 cm^{-1} for the monomer can be attributed to the asymmetric and symmetric stretching vibration of sulfonic acid group.

The sulfonic peaks formerly described in the monomer have a slight shift with a peak in the range of 1197-1098 cm^{-1} for asymmetric SO_3^- stretching and a peak at 1009 cm^{-1} for symmetric SO_3^- stretching. The absorption peaks at 983 and 919 cm^{-1} are the out-of-plane bending vibrations of vinyl unit and the absorption peaks at 839, 669 and 508 $cm^{-1}$are the out-of-plane bending vibrations of the Ar-H bond of para-substituted benzene ring **(Gu *et al*., 2012).** The out-of-plane bending vibrations of Ar-H bond of the substituted benzene ring are manifested from the peaks at 660 and 446 cm^{-1} in the polymer.

4.2.2.4 Analysis of molecular vibrations of PVA-AA-PVBS

Table – 11 Characteristic FTIR vibrations of PVA-AA-PVBS

PVA (cm^{-1})	AA (cm^{-1})	PVBS (cm^{-1})	PVA-AA-PVBS (cm^{-1})	Assignment
3000-3600	2800-3400	-	3000-3700	OH str. Inter and intra molecular hydrogen bonding
2923, 2878	-	-	2923, 2842	Alkyl –CH str.
1706	1697	-	1644	C=O str.
-	1608	-	-	C=C str.
1430	1421	-	1456	C-O-H bending/C-H bending vibrations
		-	1376	
1250	1286 1054		1260	C-O str.(COOH)
		1590, 1429 1358,1322		Aromatic skeleton str.
-	-	1197, 1116, 1045	1179 1116 (w) 1009	Asymmetric and symmetric S=O str.
-	1120	-		Mono-substituted vinyl bond
1000-1071	-	-	-	C-O-C str.
839	804			CH rocking
-	983	983, 919	-	Out-of-plane bending vibrations of vinyl unit
		839,669, 508	678,455	Out-of-plane bending vibrations of para-substituted benzene unit

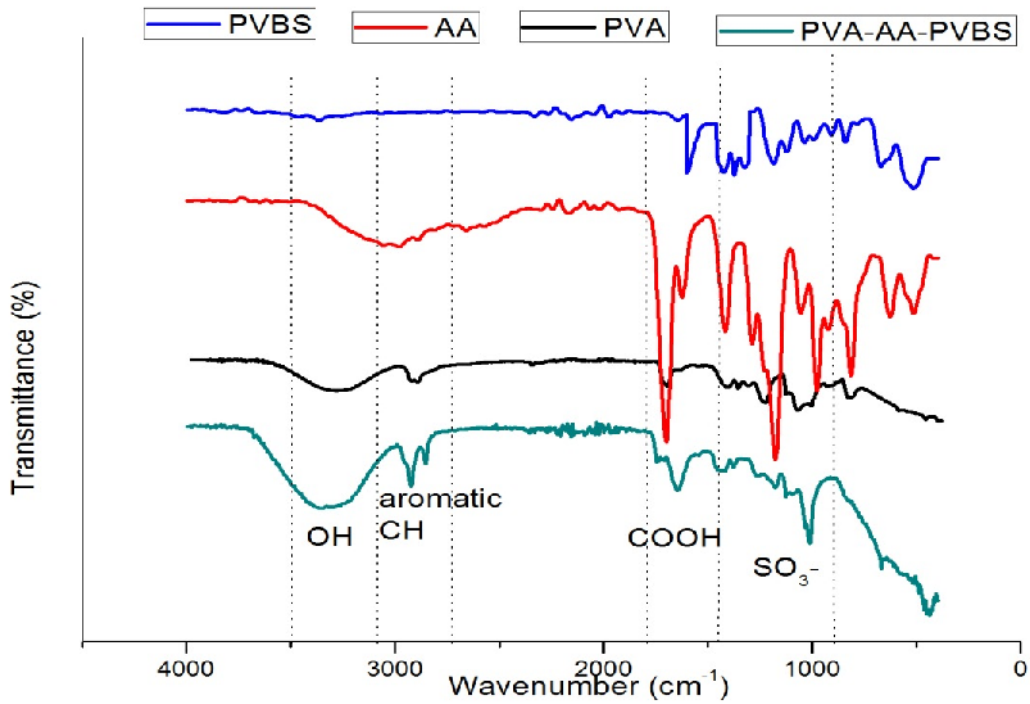

Figure – 13 Comparative FTIR spectrum of PVA-AA-PVBS with its respective monomers

Table 11 shows the characteristic bands of PVA, AA, PVBS and the grafted polymer PVA-AA-PVBS and their assignments to respective functional groups.

PVA vs PVA-AA-PVBS

A broader peak corresponding to OH group is present in the range of 3000-3700 cm^{-1} in the grafted polymer. These peaks at 2923 and 2842 cm^{-1} can be assigned to alkyl –CH and aromatic –CH stretching vibrations respectively in the grafted terpolymer. The C=O stretching (1706 cm^{-1}) of the unhydrolyzed acetate groups of PVA is shifted to 1644 cm^{-1} in the grafted terpolymer. The absorption pointed around 1430 cm^{-1} pertained to C-O-H bending vibrations and/or C-H bending vibrations in PVA, are positioned at 1456 cm^{-1} in grafted polymer. The C-O stretching vibrations of the polymer can be found at 1260 cm^{-1}. The peak at 839 cm^{-1} can be assigned to -CH rocking vibrations of PVA which is absent in the polymer.

AA vs PVA-AA-PVBS

The vibrational bands of the acrylic acid are as discussed in the previous section 4.2.2.2. A broad deep peak in the range of 3000-3700 cm^{-1} is due to the –OH groups of PVA and acrylic acid after polymerization. The C=O absorption (697 cm^{-1}) of the acrylic acid is shifted to 1644 cm^{-1} in the polymer. The absorption pointed around 1421 cm^{-1} is pertained to

C-O-H bending vibrations and/or C-H bending vibrations, and these absorptions are shifted to 1456 cm^{-1} in the grafted polymer. The C-O stretching modes associate with peaks present at 1286 cm^{-1} and 1054 cm^{-1} for monomer, appear as a single peak at 1260 cm^{-1} in the polymer.

PVBS vs PVA-AA-PVBS

The sulfonic peaks of the monomer as described in the previous sections are slightly shifted and appear as a weak peak in the range of 1179-1116 cm^{-1} which is assignable for asymmetric SO_3^- stretching, and a strong peak at 1009 cm^{-1} for symmetric SO_3^- stretching. The absorption peaks at 983 and 919 cm^{-1} are the out-of-plane bending vibrations of vinyl unit and the absorption peaks at 839, 669 and 508 cm^{-1} are the out-of-plane bending vibrations of the Ar-H bond of para-substituted benzene ring **(Gu *et al.*, 2012).** The out-of-plane bending vibrations of Ar-H bond of substituted benzene ring are manifested from the peaks at 678 and 455 cm^{-1} in the polymer.

4.2.2.5 Analysis of molecular vibrations of PVA-VSA-PVBS

Table – 12 Characteristic FTIR vibrations of PVA-VSA-PVBS

PVA (cm^{-1})	VSA (cm^{-1})	PVBS (cm^{-1})	PVA-VSA-PVBS (cm^{-1})	Assignment
3000-3600	2900-3700	-	3000-3600	OH str. Inter and intra molecular hydrogen bonding
2923, 2878	-	-	2985	Alkyl –CH str.
1706	-	-	1697	C=O str.
-	1655	-	1626	C=C str.
1430	-	-	1421	C-O-H bending/C-H bending vibrations
		-		
1250	-		1295	C-O str.
		1590, 1429 1358,1322		Aromatic skeleton str.
-	1188, 1036	1197, 1116, 1045	1170 1054	Asymmetric and symmetric S=O str.
1000-1071	-	-	-	C-O-C str.
839	-	-	-	CH rocking
-	956	983, 919	-	Out-of-plane bending vibrations of vinyl unit
-	-	839, 669508	974,804 643,481	Out-of-plane bending vibrations of para-substituted benzene unit

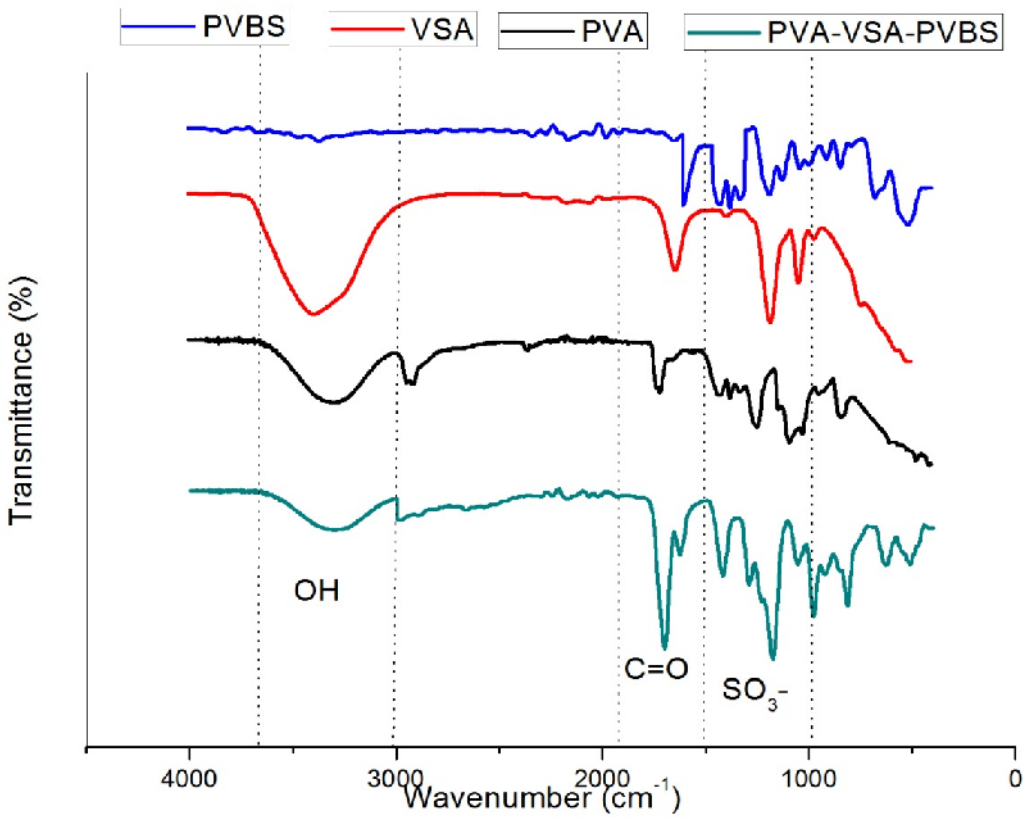

Figure - 14 Comparative FTIR spectrum of PVA-VSA-PVBS with its respective monomers

Table 12 shows the characteristic bands of PVA, VSA, PVBS and the grafted polymer PVA-VSA-PVBS and their assignments to respective functional groups.

PVA vs PVA-VSA-PVBS

All the major peaks related to the hydroxyl groups and acetate groups are discussed in the previous sections. A broader peak corresponding to OH group can be figured out for the grafted polymer in the range of 3000-3600 cm^{-1}, which is due to the -OH stretching vibrations of PVA and VSA. The vibrational bands observed at 2985 cm^{-1} may be assigned to alkyl –CH and/or aromatic –CH stretching vibrations in the grafted terpolymer. The C=O stretching of the unhydrolyzed acetate groups of PVA is present at 1697 cm^{-1} in the grafted terpolymer. The absorptions around 1250 cm^{-1} and a broad peak positioned in the range of 1000-1071 cm^{-1} are attributable to the C-O stretching and C-O-C stretching of the acetyl groups of PVA respectively. The C-O stretching vibrations of the polymer can be pointed at 1295 cm^{-1}. The -CH rocking vibrations of PVA at 839 cm^{-1}, are absent in the polymer.

VSA vs PVA-VSA-PVBS

The peak at 2900-3700 cm^{-1} arises from the OH groups of SO_3H of the monomer. The asymmetric and stretching modes of vibrations of SO_3 group can be observed at 1170 cm^{-1} and weak peak at 1054 cm^{-1}. The polymerization of the VSA monomer has been confirmed by the following peaks: This polymerized form of the monomer has been reported with a peak at 1195 cm^{-1} corresponding to the S=O group. The peak corresponding to the C=C str. in the monomer is absent in the polymer. The out-of-plane bending modes of the monomer vinyl unit of acrylamide and vinyl sulfonic acid positioned at 956 cm^{-1} disappear in the spectrum of the polymer.

PVBS vs PVA-VSA-PVBS

The absorption peaks at 1197, 1116 and 1046 cm^{-1} can be attributed to the asymmetric and symmetric stretching vibration of sulfonic acid group of the monomer. These peaks are slightly shifted and appear as a strong peak at 1170 $cm^{-1}$and weak peak at 1054 cm^{-1} in the grafted terpolymer. The out-of-plane bending vibrations of vinyl unit are observed at 983 and 919 cm^{-1} and the out-of-plane bending vibrations of the Ar-H bond of para-substituted benzene ring are observed at 839, 669 and 508 cm^{-1}. The grafted polymer has out-of-plane bending vibrations corresponding to Ar-H bond of substituted benzene ring at 974, 804, 643 and 481 cm^{-1} in the polymer.

4.2.3 NMR Spectroscopy

The grafted terpolymers were characterised by proton nuclear magnetic resonance (^{1}H NMR) spectrum with a NMR instrument DMX-500 (Bruker, Germany) and the solvents were D_2O/ DMSO-D6. The spectral data corresponding to protons of the terpolymers under investigation are discussed in the following sections.

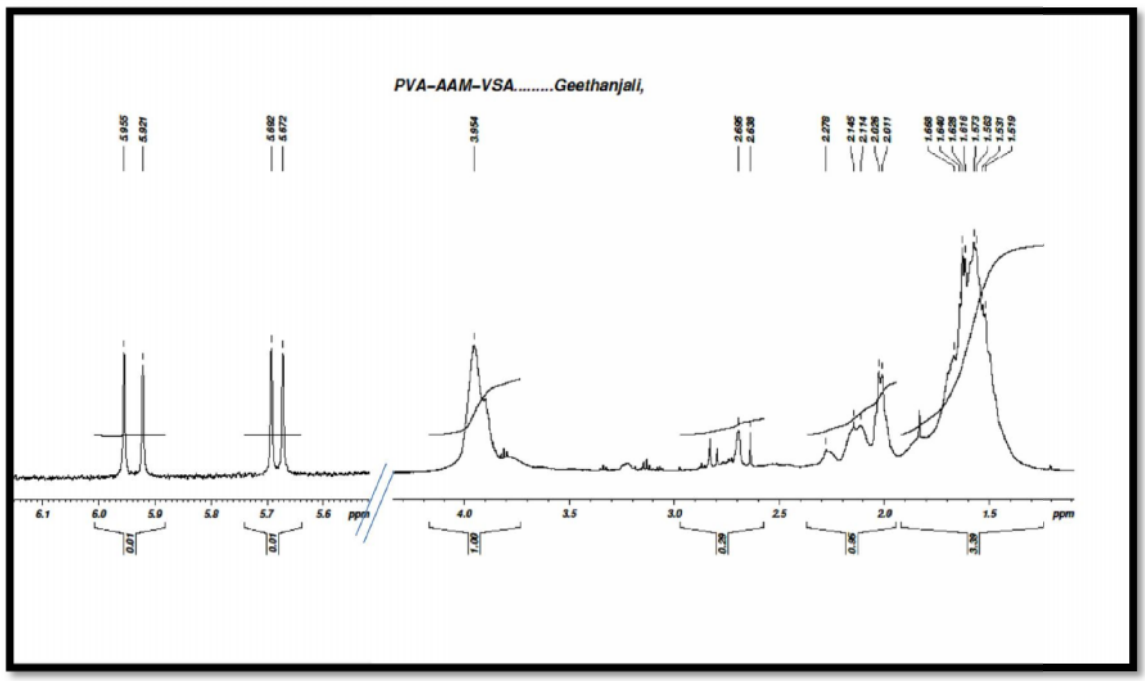

Figure - 15 Proton NMR spectrum of sample PVA-AAm-VSA in D_2O-d6

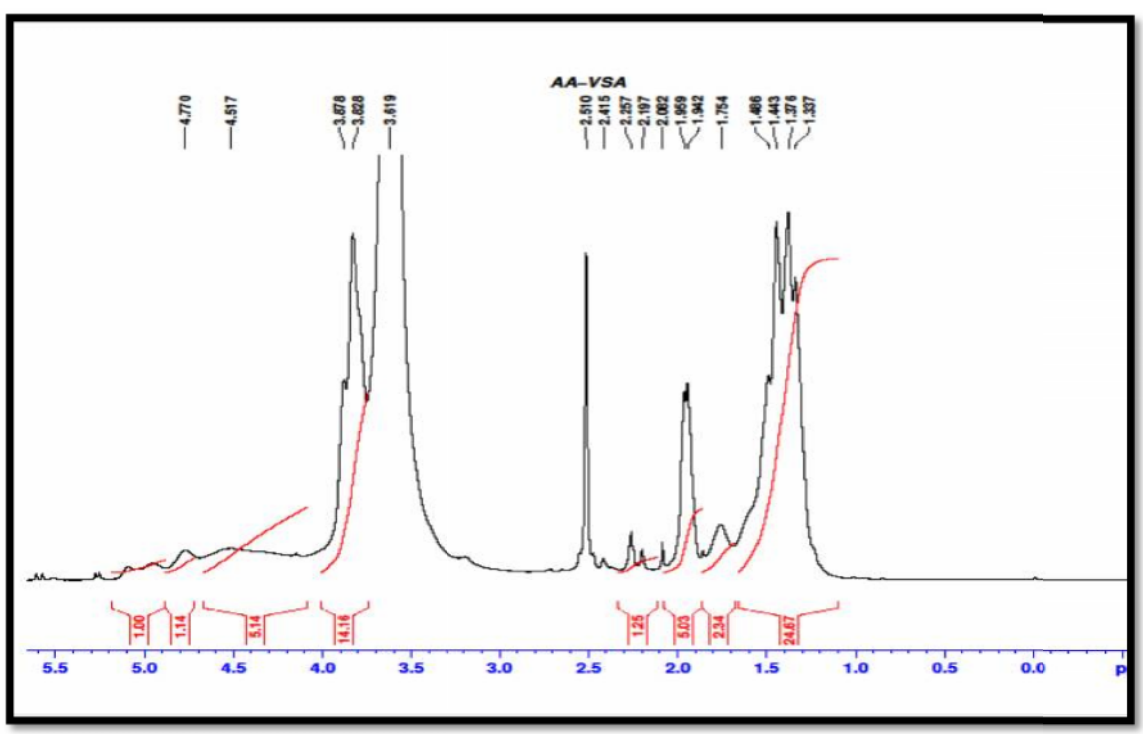

Figure - 16 Proton NMR spectrum of sample PVA-AA-VSA in DMSO-d_6

4.2.3.1 Analysis of ^{1}H NMR spectra of PVA-AAm-VSA and PVA-AA-VSA

PVA-AAm-VSA: *^{1}H NMR (500 MHz, D_2O-d6, δ ppm): 1.51-1.66 (CH_2), 2-27 (CH), 3.9 (CH-OH), 5.5 & 5.9 (d, NH_2).*

PVA-AA-VSA*: ^{1}H NMR (500 MHz, DMSO-d6, δ ppm): 1.33-1.75 (CH_2), 1.94-1.95(CH), 3.6-3.8 (CH-OH).*

Chemical shifts in the range of 1.66-1.51 ppm can be assigned to the methylene -CH_2- protons in the polymer chain. For PVA-AA-VSA the methylene –CH_2- protons appears at 1.75-1.33 ppm. The broad methylene peak bears three maxima owing to difference in the chemical environment. In PVA-AAm-VSA, chemical shifts in the range of 2.3-2.01 ppm are assigned to methine protons of PVA, PAAm and PVSA present in the polymer chain. In PVA-AA-VSA the chemical shifts of methine protons can be figured at 1.95-1.94 ppm **(Grassl *et al*., 2008; Gui *et al*., 2009)** of the grafted terpolymer. The O**H** and C**H**-OH protons are shifted and appear as broad peak at 3.9 ppm, and 3.8-3.6 ppm **(Fernández *et al*., 2008)** for PVA-AAm-VSA and PVA-AA-VSA respectively. In PVA-AA-VSA the OH of PVA and COOH of acrylic acid could have formed intermolecular hydrogen bonding and hence have shifted to upfield region **(Rivas and Nicolas, 2003).** The peak at 4.7 ppm is due to the solvent proton of D_2O and 2.5 ppm is due to solvent proton of deuterated DMSO. The less intense signals observed at 5.5 ppm and 5.9 ppm can be attributed to the NH_2 protons of polyacrylamide **(Calandrelli *et al*., 2001)** which is obviously absent in the case of PVA-AA-VSA.

4.2.3.2 Analysis of ^{1}H NMR spectra of PVA-AAm-PVBS and PVA-AA-PVBS

PVA-AAm-PVBS*: ^{1}H NMR (500 MHz, DMSO-d6, δ ppm): 1.33-1.5(CH_2), 1.94 (CH), 3.83 -3.89(CH-OH), 4.67,4.47,4.23 (t,Ar-H), 5-5.1(CONH),7.5 (H_a Ar-CH), 6.83 (H_b Ar-CH).*

PVA-AA-PVBS: *^{1}H NMR (500 MHz, DMSO-d6, δ ppm): 1.33-1.5(CH_2), 1.95 (CH), 3.7-3.8(CH-OH), 7.4 and 6.7 (Ar-CH).*

The weak multiple signal owing to the unsaturated pattern in the region of 7.5 ppm and 6.83 in PVA-AAm-PVBS, and 7.4 ppm and 6.7 ppm in PVA-AA-PVBS are due to aromatic protons **(Yang *et al*., 2002)** of p-vinyl benzene sulfonic acid sodium salt. The amide proton signal in shifted to the upfield region to 5.1-5 ppm which may be due to hydrogen bonding **(Batista *et al.,* 2006).** A triplet signal appeared in the region of 4.67 ppm, 4.47 ppm and 4.23 ppm corresponds to the benzyl proton of PVBS **(Hiran and Paliwal, 2008).** The benzyl protons are not distinctively shown in the PVA-AA-PVBS because of the extensive overlapping of OH of PVA and COOH of acrylic acid in the specified region. The solvent peak of DMSO-D_6 appears at 2.5 ppm, 3.4 ppm and 2.3 ppm. .

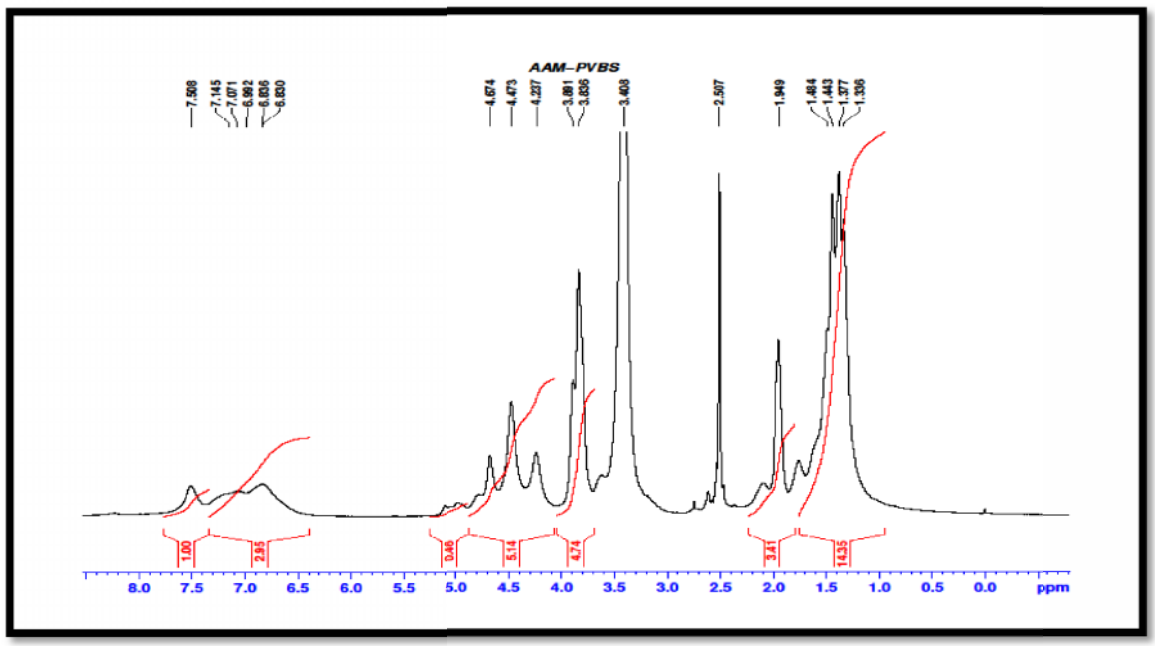

Figure - 17 Proton NMR spectrum of sample PVA-AAm-PVBS in DMSO-d6

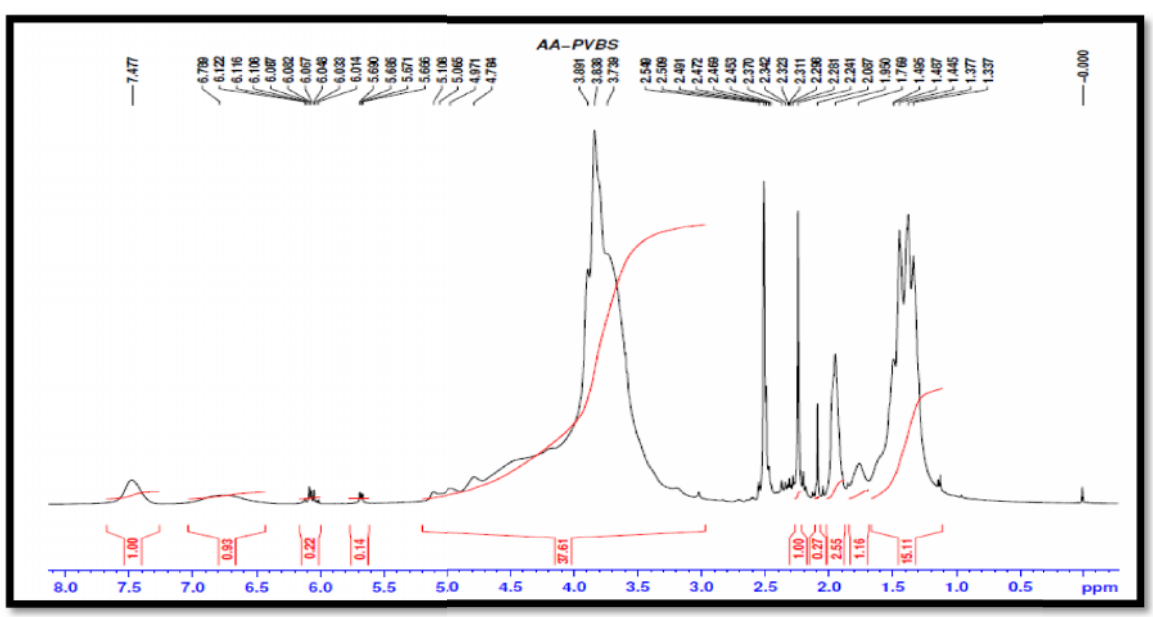

Figure – 18 Proton NMR spectrum of sample PVA-AA-PVBS in DMSO-d6

The O**H** and C**H**-OH protons are shifted and appear as broad peak at 3.83-3.89 ppm, and 3.7-3.8 ppm **(Fernández *et al*., 2008) f**or PVA-AAm-PVBS and PVA-AA-PVBS respectively. Intense signals appeared in the region of 1.94/1.95 and signals at 1.55-1.33 ppm are due to methine protons and the methylenic bridges(-CH_2) of polymer chain **(Mansri *et al*., 2013)**.

4.2.3.3 Analysis of ^{1}H NMR spectrum of PVA-VSA-PVBS

PVA-VSA-PVBS: *^{1}H NMR (500 MHz, DMSO-d6, δ ppm): 1.33-1.52(CH_2), 1.76, 1.91-1.97 (CH), 3.83-3.89(CH-OH), 4.67,4.47,4.23 (t,Ar-H), 7.49 and 6.35-6.57 (Ar-CH).*

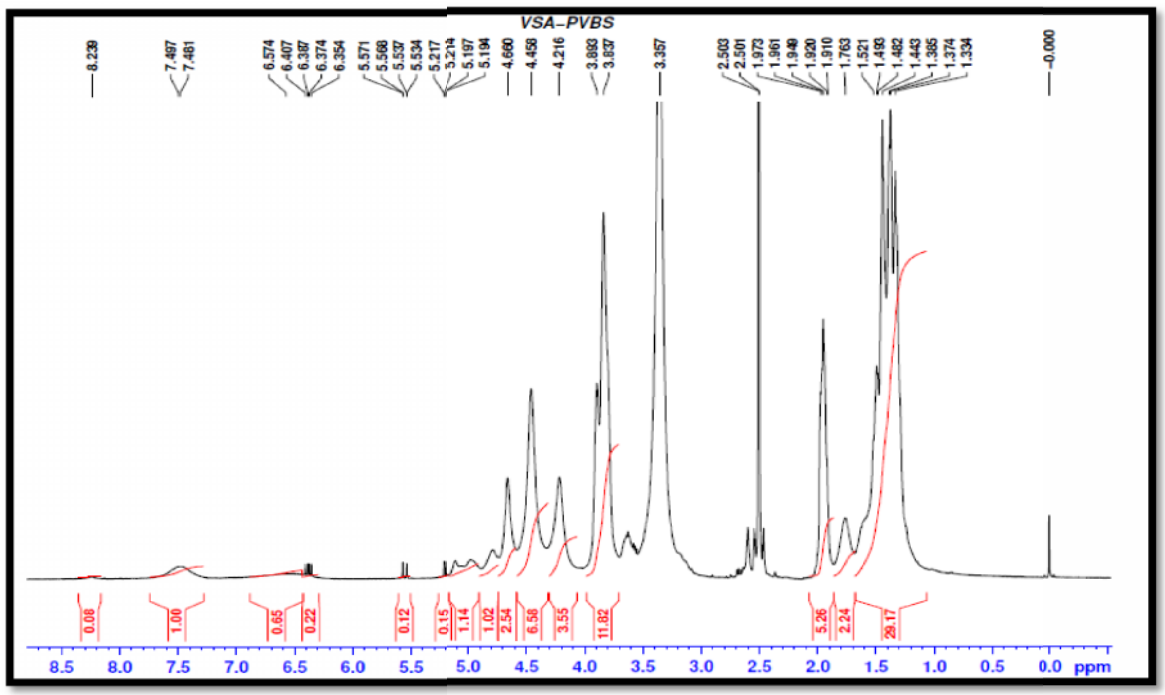

Figure – 19 Proton NMR spectrum of sample PVA-VSA-PVBS in DMSO-d6

The ^{1}H- NMR spectrum of the PVA-VSA-PVBS exhibit the strongest peaks respectively at, 1.49 (CH_2-PVBS) ,1.44 (CH_2- PVSA), 1.37 (CH_2-PVA) due to the three different methylene bridges in the terpolymer **(Mansri *et al*., 2013)**. The second-strongest peaks respectively at 1.97-1.91 ppm and 1.76 ppm could be because of the methine groups. The solvent peaks are manifested as sharp strong peaks at 2.5 ppm and 3.35 ppm. The broad peak centered at 3.89-3.83 ppm arises due to the –CH-OH of PVA **(Fernández *et al*., 2008)**. The triplet positioned at 4.67, 4.47, 4.23 ppm is a manifestation of benzyl unit **(Hiran and Paliwal, 2008)** of p-styrene sulfonic acid. The chemical shifts at 7.49 ppm (H_a) and 6.57-6.35 (q)(H_b) **(Yang *et al*., 2002)** are due to 2 different benzene protons. H_b protons are split into a quartet initially by H_a proton followed by long range coupling with benzyl -CH_2 moiety of the polymer chain.

4.2.4 Thermogravimetric analysis

The thermogravimetric analysis (TGA) and differential thermogravimetry (DTG) shows the onset of thermal degradation and several degradation steps of small moieties, branches

and interlinks from the polymer matrix. The degradation is initiated by the heat and progressed with molecular chain scission by breaking down the matrix structure.

4.2.4.1 Interpretation of TGA curves of PVA, PVA-AAm-VSA, PVA-AA-VSA

It is observed that the thermal degradation of PVA has taken place within the programmed temperature range of 350 to 480 ^{o}C. Decomposition of PVA proceeds in three stages. The first weight loss of 8 wt.% at 103 ^{o}C is due to the moisture vaporization. The second stage, occurs in the range of 328 ^{o}C corresponding to a weight loss of 5 % mainly involves dehydration and degradation of some volatile products. The third stage (431 ^{o}C) with a maximum weight loss of 84 % is correlated to the polyene residues which degrades on further heating to yield carbon and hydrocarbons **(Lewandowska, 2009).** The DTG curves of PVA shows 3 humps with maxima at 328 ^{o}C which is in well agreement with the three stages of degradation. The initial decomposition temperature of PVA was 328 ^{o}C and gets completely decomposed after 470 ^{o}C.

The TGA and DTG curves of PVA-AAm-VSA (Figure 20) shows 10 % weight loss around 160 ^{o}C due to the evaporation of the absorbed moisture. Further, the degradations are exhibited as two step degradation processes with two maxima at 337 and 440 ^{o}C in the DTG curve. These degradation steps can be possibly related to the imine reaction of amide group and desulfonation followed by thermal decomposition of polyacrylamide chain **(Zhong *et al*., 2010; Lee *et al*., 2011)**. The % wt. loss observed at these temperatures corresponds to 40 % and 90 %. The complete degradation was found to occur from 470 ^{o}C.

The DTG curve of PVA-AA-VSA (Figure 20) shows two small humps around 100 ^{o}C and 200 ^{o}C which can be attributed to the loss of water molecules and volatile groups. 50 % decomposition of PVA-AA-VSA started at a temperature of 340 ^{o}C exhibiting maxima in the DTG curve. At this stage decarboxylation and degradation of organosulfonic acid linkages could have taken place **(Devrim *et al*., 2007)**. Nearly 95% decomposition started at 450 ^{o}C after which a very less quantity of polymeric residue was left due to the thermal degradation of polymers into gaseous products at higher temperature.

When compared to that of PVA, all the degradations are slightly shifted indicating the change in thermal stability of the grafted polymer. When compared with PVA, the thermal stability of PVA-AA-VSA is lower due to its hygroscopic nature and flexible chain linkages. Polyacrylic acid has a large number of strong hydrophilic groups that could impart the hygroscopic nature of the polymer. But PVA-AAm-VSA has a slightly improved thermal stability due to the strong intermolecular linkages resulting from increased hydrogen bonding formation and improved compact/stiff nature of the polymer **(Cavus, 2010).**

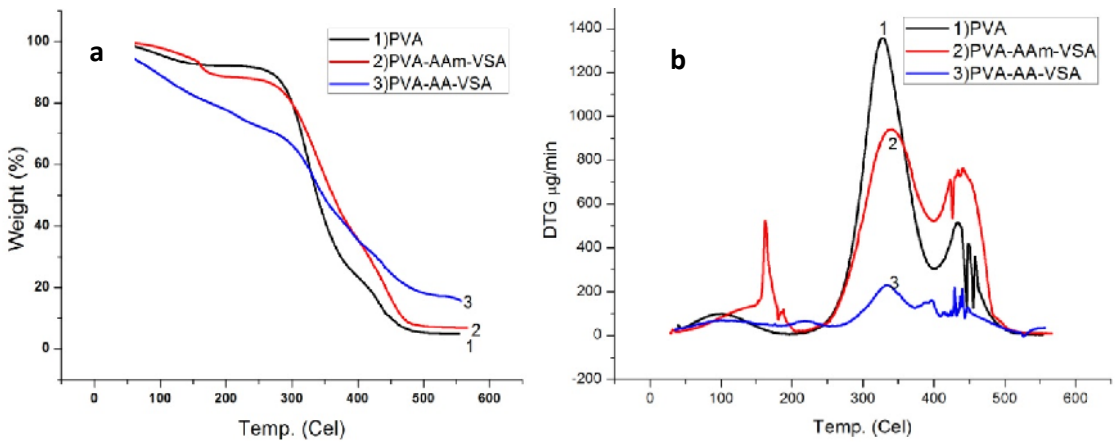

Figure - 20 TGA(a) and DTG(b) curves of 1) PVA; 2) PVA-AAm-VSA; 3) PVA-AA-VSA

4.2.4.2 Interpretation of TGA curves of PVA-AAm-PVBS, PVA-AA-PVBS and PVA-VSA-PVBS

The thermogram of PVA-AAm-PVBS (Figure 21) exhibits a multiple-stage thermal decomposition. The first stage involves dehydration with 10 % loss in weight at 158 °C. The initial decomposition (Ti) starts at 314 °C which can be assigned to the decomposition of the amide groups through imine reaction. This peak appears as maxima in DTG plot and corresponds to a weight loss of 30 %. The literature reports reveal that desulfonation and imidation reaction occurs at a temperature range of 250-350 ^{o}C. **(Hazer *et al*., 2007; Zhang and Easteal, 2007).** The final decomposition occurs at 431 ^{o}C resulting in 60 % wt.loss from the initial mass. This step is accounted for the decomposition of entire matrix that involves breakdown of C-H bonds, decompositions of any intermediate macromolecular product, and degradation of aromatic fragments of styrene units **(Kavlak *et al*., 2012)**. As can be seen in Figure 21, when the temperature reaches 480 °C the weight of the sample was constant and the residue was 25 %.

PVA-AA-PVBS undergoes a three step degradation process and is exhibited in the form of three peaks in the DTG curve (Figure 21). According to DTG curves, the first step is small and the main degradations occur in the second and third steps. The first step with a weight loss of 7 % can be ascribed to the water loss. The second degradation step reflects a large peak with two peak maxima at 317 and 362 ^{o}C. At this stage 50 % of the degradation has taken place corresponding to decarboxylation and desulfonation from the terpolymer. Similar to PVA-AAm-PVBS, the final decomposition at 416 ^{o}C resulting in 74 % wt.loss from the initial mass can be ascribed to the breakdown of C-H bonds, decompositions of any

intermediate macromolecular product, and degradation of aromatic fragments of styrene units. The complete degradation of the terpolymer starts at 450 ^{o}C.

Analysis of the TGA and DTG thermograms of PVA-VSA-PVBS (Figure 21), degradations are found to occur in three stages. The first step with a weight loss of 8 % can be due the loss of water molecules. The second degradation step is a peak at 263 ^{o}C with a small hump at 325 ^{o}C. In this range 50 % of the degradation has taken place that can be attributed to the desulfonation of the terpolymer. The final decomposition was found to occur at at 422 ^{o}C resulting in 74 % weight loss from the initial mass can be due to the breakdown of C-H bonds, decompositions of any intermediate macromolecular product, and degradation of aromatic fragments of styrene units.

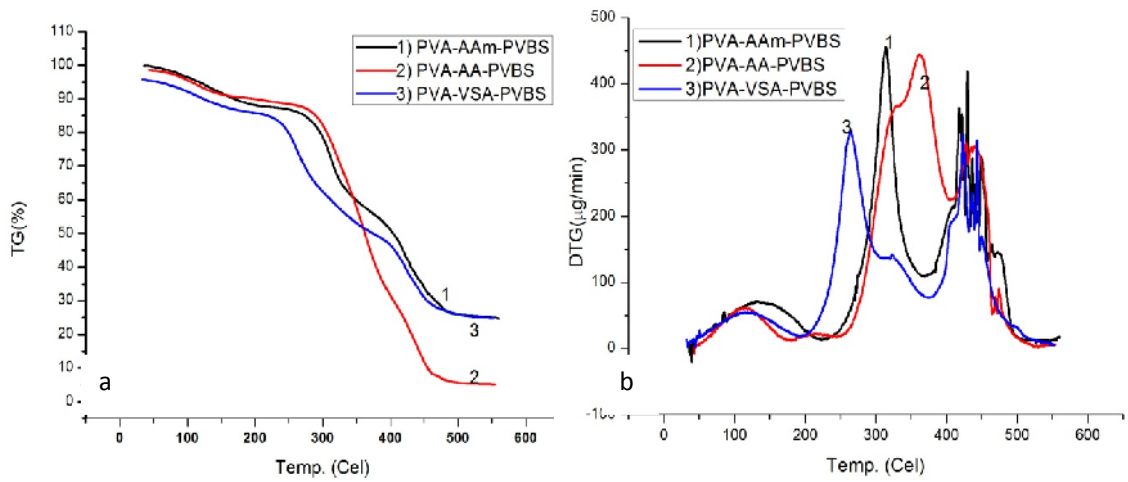

Figure – 21 TGA(a) and DTG(b) curves of 1) PVA-AAm-PVBS; 2) PVA-AA-PVBS; 3) PVA-VSA-PVBS

The initial and final degradation temperatures are similar to that of PVA, except for PVA-AA-VSA having reduced thermal stability. Usually incorporation of sulfonic acid groups result in reduced thermal stability. But due to the high reactivity of acrylamide polymers, they form rigid structure with several cross linking units. As a result their thermal degradation properties are at par with PVA. But acrylic acid polymers have reduced thermal stability due to their hygroscopic nature and flexible chain links.

Table - 13 Stepwise thermal degradation with corresponding weight loss % from TGA and DTG

S.No.	Name of the polymer	TG Wt. Loss in %			DTG (^oC)	
		100-200 ^oC	200-350 ^oC	350-450 ^oC	Td_i ^oC	Td_f ^oC
1	PVA	8	5	84	328	431
2	PVA-AAm-VSA	10	40	90	337	440
3	PVA-AA-VSA	27	54	80	340	-
4	PVA-AAm-PVBS	10	30	60	314	431
5	PVA-AA-PVBS	8	50	83	317	416
6	PVA-VSA-PVBS	5	55	84	282	422

4.2.4.3 Comparison of thermal stabilities of all the investigated terpolymers

All the investigated terpolymers are completely stable till 100 ^oC which indicates that the polymers can be used for high temperature applications. Most of the loss around 100 ^oC occurred at initial stage can be ascribed to the water loss. The TGA and DTG curves of all the terpolymers are different from PVA confirming the difference in their molecular structure due to the grafting reaction. However all the polymers undergo a major degradation in the range of 300-400 ^oC which is obviously seen in the DTG figures. At this temperature range an intermolecular chain breakage and partial scission of the molecular structure could have taken place. The other degradation steps can be due to decomposition of amide group, sulfonic acid groups, acrylic acid group and backbone decompositions.

4.2.5 Differential Scanning Calorimetry

Differential Scanning Calorimetry (DSC) is a thermal analysis tool which tracks the heat capacity changes in terms of heat flow when a material is heated. Interpretation of the DSC curves generates useful information regarding amorphous, crystalline and semi-crystalline behaviour, eutectic transitions, curing and polymorphism. The different types of transitions a polymer exhibits are glass transition, melting, crystallization and decomposition **(http://faculty.olin.edu/~jstolk/matsci/Operating%20Instructions/DSC%20Operating%20Instructions.pdf)**.

The glass transition temperature (Tg) is an important property to be analysed in the case of polymers. The Tg is an important characteristic of noncrystalline and semicrystalline polymers. Tg is a temperature below which the polymer is hard and brittle in nature because the polymer chains are locked in tangled and coiled position. Above the Tg, the polymer

becomes rubbery because the chains gain degree of freedom to move in any direction and slip past each other. In this phase the polymer is more soft and ductile in nature. Glass transition is an endothermic process as it requires energy to break the bonds. The Tg values was estimated as the temperature corresponding to the intercept of the tangent drawn to the baseline of the DSC thermogram. The endothermic baseline shift is as shown in the following DSC traces.

Melting of polymers occurs when the heating slowly loosens and breaks the bond and changes the material to liquid phase. Melting is an endothermic process with a temporary loss in heat flow. The melting endotherms are differentiated from other endotherms as the heat flow regains its original base line after the melting process.

Crystallization is an exothermic event where solid amorphous structure (cold crystallization on heating) or liquid amorphous structure (cooling) is converted to a more organized solid crystalline structure. This is depicted as a peak. The extrapolated onset is the nucleation temperature and peak maximum is the crystallization temperature.

The decomposition of the polymers is an exothermic process that usually occurs after complete melting of the polymer.

DSC and TGA curves can be used to figure out thermal profile during heat treatment. TGA basically senses the change in weight of the substance while DSC is a calorific phenomenon which occurs with less/no detectable weight change. Differential scanning calorimetry analysis was carried out using SDTQ 600 V8.0 Build 95 Instrument. The DSC thermograms were obtained at a heating rate of 10 ^{o}C per minute in the temperature range of 30-500 ^{o}C.

4.2.5.1 DSC analysis of Polyvinyl alcohol

Osiris *et al*. (2012) have reported a DSC curve of PVA containing two endothermic peaks and explain the nature of the peaks as follows. The peak appearing at 88.1°C is assigned for the moisture evaporation from the sample and also for the glass transition with an enthalpy 130.9 J/g. The second sharp endothermic melting transition was figured out at 209.6°C with an enthalpy 67.4 J/g. But the heat required for melting of 100% crystalline PVA, was reported as 138.60 J/g. **Thakur *et al*. (2011)** reported the Tg of polyacrylamide and polyacrylic acid as 190.45 ^{o}C and 105 ^{o}C.

Table - 14 Characteristic transitions of terpolymers under investigation and its respective monomers during DSC anlaysis

Material	T_G (°C)	T_m (°C)				T_d (°C)		
		Onset	I	II	III	I	II	III
PVA	88.1	-	209.6	-	-	-	-	-
PAAm	190.45							
PAA	105							
PVA-AAm-VSA	101(enthalpy relaxation 185)	239	291	385	-	-	-	-
PVA-AAm-PVBS	100(enthalpy relaxation=185)	205	311	418	477	-	-	-
PVA-AA-VSA	87	-	180	222	-	263	369	419
PVA-AA-PVBS	80	223	189	259	-	358	-	-
PVA-VSA-PVBS	45	237	332	-	-	-	-	-

4.2.5.2 Comparison of Melting Behaviours of PVA-AAm-VSA and PVA-AAm-PVBS by DSC

The DSC profile of the PVA-AAm-VSA (Figure 22a) shows three subsequent endothermic effects at 100, 291 and 385 °C which allows us to postulate stepwise transitions as follows. Tg is observed as a step down transition in the range of 40-162 °C with a midpoint around 101 °C. The Tg transition is accompanied by a sharp transition at 185 °C which could be accounted for glass transition with enthalpy relaxation of 48.1 mJ/mg **(http://us.mt.com/us/en/home/supportive_content/usercom/TA_UserCom11.html).**

The DSC profile of the PVA-AAm-PVBS (Figure 22b) exhibits three different melting endotherms positioned at 311, 418 and 477 °C. The glass transition remains the same as in the case of PVA-AAm-VSA around 100 °C with an enthalpy relaxation of 185 °C .

When the Tg values of the above discussed polymers are compared to that of pure PVA, it is shifted slightly to higher values as a result of crosslinking with other monomer reactants.The increase in the Tg value is due to the dispersion of the polyacrylamide and/or p-vinylbenzene sulfonic acid/vinyl sulfonic acid segments in the PVA matrix which basically hinders the motion of chains of the polymer **(Gao *et al*. 2010).**

PVA-AAm-VSA and PVA-AAm-PVBS show 2 and 3 melting points respectively. For PVA-AAm-VSA, an endothermic peak in the temperature range of 239-345 ^{o}C, has been observed which is attributed to be due to the melting of the polymer (Tm=291 ^{o}C, ΔH=378 mJ/mg). The second melting point is recorded at the peak position of 385 ^{o}C (ΔH=63.9 mJ/mg).

For PVA-AAm-PVBS, the melting onset is observed at 205 ^{o}C, with first melting peak positioned at 311 ^{o}C with an enthalpy of 173 mJ/mg and the second metling peak positioned at 418 ^{o}C with an enthalpy of 46.2 mJ/mg. The third melting peak is recorded at 477 ^{o}C, whereas the shape of the curve indicates the melting accompanied with decomposition. When compared to the pure PVA, the melting point is shifted well to a higher temperature indicating the extensiveness of cross-linking of the polymeric chain which makes them harder to melt.

The occurrence of multiple melting endotherms could be due to the following reasons: (1) melting-recrystallization-remelting cycle, (2) polymorphism (3) variation in morphology of the polymer inherited in the form of lamellar thickness, perfection, stability or distribution (4) physical aging or/and relaxation of the rigid amorphous fraction, (5) wide range of molecular weight distribution etc.

For the terpolymers under investigation, the complex melting behaviour exhibiting multiple endotherms is due to the domains with variable branching content **(Groeninckx *et al*., 2003)** Hence in the above discussed polymers, the presence of two different melting peaks could be due to two different polymeric segments. The first melting point can be accounted for melting of the main polymeric chain and second melting point for broken polymeric chains that has actually segmented from the main polymer. Moreover, the melting isotherms are broadened, possibly due to the amorphous nature of the polymer **(Parveen *et al*., 2009 [a];Parveen *et al*., 2009 [b]; Gandhi *et al*., 2011).** Random incorporation of the polyacrylamide and polyvinyl sulfonic acid chain in the polyvinyl alcohol main chain serves to further disrupt the crystalline regions of the polymer.

4.2.5.3 Comparison of Melting Behaviours of PVA-AA-VSA and PVA-AA-PVBS by DSC

In Figures 22 c & 22 d DSC traces are shown for the PVA-AA-VSA and PVA-AA-PVBS. The DSC thermogram of PVA-AA-VSA reflected Tg in the temperature range of 35-141 ^{o}C with the midpoint of 87. The peak at 154 ^{o}C associated with Tg range is attributed to the enthalpy relaxation (ΔH=134 mJ/mg). The glass transition of PVA-AA-PVBS is observed with decrease in heat capacity in the temperature range of 35-119 ^{o}C with midpoint

of 80 °C. Tg is highly dependant on polymer chain branching. Linear polymer chains possess smaller free volume than their branched counterparts and reflect higher Tg values. But in the branched polymers, if the branches contain bulkier group they impose hindrance or restriction to segmental motion, for which higher Tg values are expected. Nevertheless, crosslinked polymers also reflect higher Tg due to their restricted segmental motion, and sometimes the cross-linking is very high such that the polymer undergoes decomposition before starting the segmental motion (**Sinko and Yashveer, 2011).**

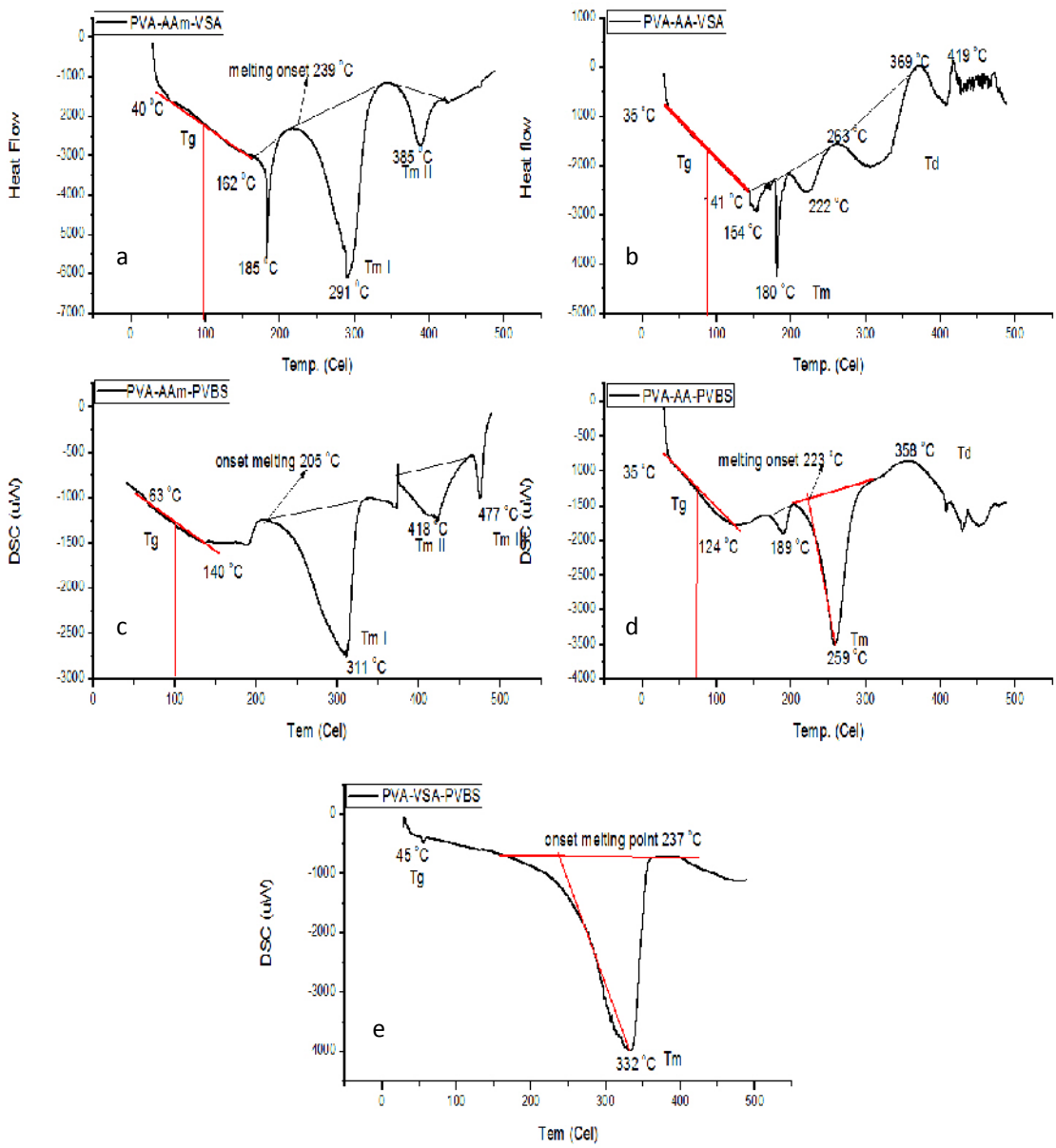

Figure - 22 DSC traces of a) PVA-AAm-VSA; b) PVA-AA-VSA; c) PVA-AAm-PVBS; d)PVA-AA-PVBS and e)PVA-VSA-PVBS

The Tg values obtained for the both the terpolymers are consistent with the values obtained for pure PVA. Grafting of PVA with acrylic acid and vinyl sulfonate/p-vinyl benzene sulfonate did not alter the Tg of pure PVA, because the polymerizaion neither imparted additional mobility or hindered mobility of the segments of PVA.

The melting of the PVA-AA-VSA is observed as a sharp endothermic transition peak at 180 ^{o}C associated with an enthalpy of 194 mJ/mg. The second melting point at 222 ^{o}C is associated with first step of polymer degradation at 263 ^{o}C (ΔH=34 mJ/mg). Further polymer degradations are reflected in the form of strong exotherms at 369 and 419 ^{o}C, having an enthalpy of 153 mJ/mg.

The DSC trace of PVA-AA-PVBS displays two endothermic peaks. The first peak at 189 °C is assigned as a thermal effect due to melting of some segments of PVA. A sharp endothermic melting transition at 259 ^{o}C (ΔH=11.2 mJ/mg) with a melting onset of 223 ^{o}C (ΔH=46.2 mJ/mg) is assignable to the melting of the complete polymer. The melting is followed by decomposition of the polymer at 358 ^{o}C.

4.2.5.4 DSC analysis of PVA-VSA-PVBS

Figure 22e shows the calorimetric curve for the terpolymer PVA-VSA-PVBS with one braod peak. Glass transition is recorded as a very small step transition in the temperature range of 36-57 ^{o}C. The small Tg values associated with the polymer can be attributed to the high mobility of the polymeric segments in the domain (**Baradie and Shoichet, 2005).**

The mobility of the polymeric segments are facilitated by the anionic repulsions that exist among the SO_3^- groups. However the melting endotherm is present as a broad peak. This widening of the transition when compared with the other polymers discussed above can be rationalized by the following arguments. The electrical charges associated with the anionic sulfonic acid groups of polyvinyl sulfonate and polyvinyl benzene sulfonic acid units are statistically distributed in the PVA domain thereby widening its chemical diversity and consequently the range of temperature leading to a broader peak. The onset melting point is recorded at 237 ^{o}C and the actual melting point is positioned at 332 ^{o}C. The enthalpy value recorded for the wide area is 491 mJ/mg.

The small difference in the Tg values can be partly attibuted to the small difference in molecular weight and polydispersities of the compared polymers. The polymer-polymer interactions produce an amorphous phase that can induce a chage in the crystalline structure of the polymer. Hence the decrease in heat of fusion or increase in melting point represents the reduced perfection/crystallinity with increase in degree of cross-linking (**Osiris *et al*., 2012).**

4.3 Corrosion studies by Weight loss technique

Weight loss is a conventional but a most reliable technique for measurement of corrosion rate and evaluation of corrosion inhibition performance of an inhibitor. Weight loss tests were conducted on the basis of three different perspectives; effect of concentration, time and temperature. The method is carried out for desired time and temperature depending upon the type of application. Hence, this method helps us to find out the most influencing factors viz. concentration of the inhibitor, effect of exposure time and effect of temperature, on corrosion inhibition. The candid inhibition efficiency (IE) results thus obtained can be employed for determination of several supporting parameters including adsorption type, mechanism and kinetics of corrosion inhibition. In order to obtain a better window for adsorption isotherms, the concentration of inhibitor is gradually increased from very low to maximum level and the increase in IE is monitored.

Though monitoring of IE with respect to concentration gives a clear picture about the optimum concentration and surface coverage, the same procedure was carried out for various time intervals. Because monitoring the IE with respect to time would provide us with conclusions about stability of the inhibitor film. The stability of the inhibitor film is an important issue to ponder as it improvise the inhibition efficiency till specific period and then may deprive the inhibition efficiency due to several reasons. Thus the ability of the inhibitor to form multilayer or monolayer is proved.

Temperature is another factor of interest for almost all corrosion inhibition applications are carried out at certain temperature. Temperature may either speed up the adsorption of inhibitor on metal surface or aids the effective rust removal of strongly adhered corrosion products during acid pickling process.

4.3.1 Weight loss results of the investigated polymeric systems as a function of concentration, time and temperature

The weight loss of mild steel strips in 100 mL of 1M HCl solution at 30 ^{o}C without and with various concentrations (0.03–0.45 wt.%) of inhibitors were determined for various immersion periods (1-12 h). The inhibition efficiency IE (%) determined from the corrosion rate is discussed in the following sections.

To investigate the mechanism of inhibition and to calculate the activation energies of the corrosion process, gravimetric measurements were taken at various temperatures (303–343 K) in the absence and presence of 0.03-0.45 wt.% of the inhibitors for ½ h of immersion.

i) PVA-AAm-VSA

Table 15 shows the calculated values of corrosion rate and IE obtained for various concentrations (0.03-0.45 wt.%) of the PVA-AAm-VSA grafted terpolymer at different time intervals (1-12 h) in 1 M HCl at 303 K. It follows from the data of Table 15 that the weight loss and corrosion rate of mild steel decreased with increasing inhibitor concentration and therefore, the IE % of the PVA-AAm-VSA is increased. It is evident that all the studied concentrations of the PVA-AAm-VSA were highly surface active, and a maximum IE (93.4 %) was achieved for 0.45 wt.% concentration of the inhibitor.

Table - 15 Corrosion rates and IE obtained for various concentrations of PVA-AAm-VSA at various time intervals

Conc. Wt.%	1 hour		3 hours		6 hours		9 hours		12 hours	
	CR (mpy)	IE (%)	CR (mpy)	IE (%)	CR (mpy)	IE (%)	CR (mpy)	IE (%)	CR (mpy)	IE (%)
Blank	2157.9		2386.9		1885.3		1971.4		1776.3	
0.03	533.1	75.3	763.2	68.0	433.2	77.0	427.3	78.3	440.7	75.2
0.09	528.8	75.5	565.5	76.3	393.9	79.1	251.0	87.3	261.2	85.3
0.18	456.3	78.9	402.7	83.1	286.4	84.8	236.4	88.0	185.9	89.5
0.27	439.3	79.6	289.3	87.9	210.8	88.8	216.6	89.0	165.6	90.7
0.36	426.5	80.2	248.6	89.6	210.1	88.9	169.6	91.4	152.5	91.4
0.45	400.9	81.4	199.2	91.7	141.0	92.5	158.9	91.9	117.6	93.4

Table - 16 Corrosion rates and IE obtained for various concentrations of PVA-AAm-VSA at 303 K-343 K

Conc. Wt.%	303 K		313 K		323 K		333 K		343 K	
	CR (mpy)	IE (%)	CR (mpy)	IE (%)	CR (mpy)	IE (%)	CR (mpy)	IE (%)	CR (mpy)	IE (%)
Blank	870.0		1825.3		5680.6		10713.1		18449.3	
0.03	416.6	52.1	790.0	56.7	1932.6	66.0	3480.0	67.5	5806.0	68.5
0.09	349.8	59.8	742.6	59.3	1443.1	74.6	2473.6	76.9	4277.2	76.8
0.18	329.2	62.2	644.0	64.7	1264.6	77.7	2379.7	77.8	4156.1	77.5
0.27	303.5	65.1	596.6	67.3	1076.0	81.1	2030.0	81.1	4039.1	78.1
0.36	293.2	66.3	523.5	71.3	1076.0	81.1	1936.2	81.9	3596.4	80.5
0.45	288.0	66.9	530.8	70.9	1019.9	82.0	1688.8	84.2	3408.4	81.5

The influence of inhibitor concentration on inhibition efficiency in the temperature range of 303-343 K is shown in Table 16. IE increased with increasing temperature in presence of optimum dose of PVA-AAm-VSA (0.45 wt.%). The efficiency at 303 K was calculated as 66.9 % which shoots up to 84.2 % at 333 K, then at 343 K, the IE decrease to 81.5 %.

ii) PVA-AA-VSA

The calculated corrosion rates and deduced IE in the presence of PVA-AA-VSA at the specified conditions are given in Table 17. The IE values increase with increase in concentration. The IE pertaining to 0.45 wt.% concentration of inhibitor gradually increases till 6 hours of immersion (89.7 %), slightly decreases at 9th hour (88.5 %) and then increases in 12th hour (90.7 %). A maximum efficiency of 90.7 % is obtained for 0.45 wt.% of inhibitor at 12 hours of immersion.

Table - 17 Corrosion rates and IE obtained for various concentrations of PVA-AA-VSA at various time intervals

Conc. Wt.%	1 hour		3 hours		6 hours		9 hours		12 hours	
	CR (mpy)	IE (%)	CR (mpy)	IE (%)	CR (mpy)	IE (%)	CR (mpy)	IE (%)	CR (mpy)	IE (%)
Blank	2157.9		2386.9		1885.3		1971.4		1776.3	
0.03	784.7	63.6	667.2	72.0	558.8	70.4	586.2	70.3	340.9	80.6
0.09	503.2	76.7	543.7	77.5	400.6	78.8	525.7	73.3	271.7	84.5
0.18	550.1	74.5	334.3	86.0	332.0	82.4	406.0	79.4	244.7	86.0
0.27	439.3	79.6	308.2	87.1	255.8	86.4	374.5	81.0	235.1	86.6
0.36	405.1	81.2	242.8	89.8	221.2	88.3	236.9	88.0	165.0	90.6
0.45	336.9	84.4	238.4	90.0	193.3	89.7	225.8	88.5	163.8	90.7

Table - 18 Corrosion rates and IE obtained for various concentrations of PVA-AA-VSA at 303 K-343 K

Conc. Wt.%	303 K		313 K		323 K		333 K		343 K	
	CR (mpy)	IE (%)	CR (mpy)	IE (%)	CR (mpy)	IE (%)	CR (mpy)	IE (%)	CR (mpy)	IE (%)
Blank	870.0		1825.3		5680.6		10713.1		18449.3	
0.03	435.0	50.0	912.7	50.0	1946.2	65.7	3512.0	67.2	5806.0	68.5
0.09	409.4	52.9	817.3	55.2	1478.9	74.0	3162.3	70.5	4277.2	76.8
0.18	366.8	57.8	653.8	64.2	1299.2	77.1	2463.0	77.0	4156.1	77.5
0.27	366.8	57.8	619.8	66.0	1083.5	80.9	2200.8	79.5	4039.1	78.1
0.36	307.1	64.7	578.9	68.3	1027.0	81.9	2030.0	81.1	3596.4	80.5
0.45	290.0	66.7	524.4	71.3	1006.5	82.3	1893.5	82.3	3408.4	81.5

The effect of acid temperature in the range of 303–343 ^{o}C on the efficiency of the PVA-AA-VSA in 1M HCl and the results obtained are tabulated in Table 18. The IE obtained for the 0.45 wt.% inhibitor concentration at temperature ranging from 303 K to 343 K in 10 K increments are listed as 66.7, 71.3, 82.3, 82.3, and 81.5 % respectively.

iii) PVA-AAm-PVBS

The effect of changing immersion time (1-12 h) and concentrations (0.03 to 0.45 wt.%) at 30 ^{o}C on the inhibition efficiency of PVA-AAm-PVBS and the respective results are shown in the Table 19. The results show that the inhibitor acts effectively in controlling the corrosion MS for all immersion times at all concentrations. At 0.45 wt.%, increasing immersion time resulted in increased IE till 6 hours (94.1 %), slight decrease at 9th hour (93.2 %) and reaches a maximum IE of 96.3 % at 12 h.

Table - 19 Corrosion rates and IE obtained for various concentrations of PVA-AAm-PVBS at various time intervals

Conc. Wt.%	1 hour		3 hours		6 hours		9 hours		12 hours	
	CR (mpy)	IE (%)	CR (mpy)	IE (%)	CR (mpy)	IE (%)	CR (mpy)	IE (%)	CR (mpy)	IE (%)
Blank	2157.9		2386.9		1885.3		1971.4		1776.3	
0.03	814.6	62.3	811.1	66.0	398.3	78.9	568.6	71.2	266.6	85.0
0.09	597.1	72.3	543.7	77.2	276.9	85.3	367.7	81.3	210.0	88.2
0.18	601.3	72.1	362.0	84.8	208.6	88.9	276.2	86.0	134.7	92.4
0.27	413.7	80.8	308.2	87.1	204.2	89.2	263.7	86.6	188.4	89.4
0.36	413.7	80.8	260.2	89.1	186.1	90.1	222.4	88.7	104.5	94.1
0.45	400.9	81.4	226.8	90.5	111.9	94.1	133.7	93.2	65.0	96.3

The values of inhibition efficiency obtained from the weight loss at various temperatures are provided in the Table 20. The data reveal that the inhibition efficiency increases with increasing temperature till 333 K (68.6 %:303 K to 84.9 %: 333 K) indicating that higher temperature favours the adsorption of inhibitor at the surface. At 343 K the IE decreased to 82.2 %. It follows from the data that corrosion process and protectiveness of an inhibitor are significantly dependent on the temperature.

Table - 20 Corrosion rates and IE obtained for various concentrations of PVA-AAm-PVBS at 303 K-343 K

Conc. Wt.%	303 K		313 K		323 K		333 K		343 K	
	CR (mpy)	IE (%)	CR (mpy)	IE (%)	CR (mpy)	IE (%)	CR (mpy)	IE (%)	CR (mpy)	IE (%)
Blank	870.0		1825.3		5680.6		10713.1		18449.3	
0.03	366.8	57.8	776.2	57.5	1876.5	67.0	2755.0	74.3	5134.8	72.7
0.09	315.6	63.7	699.4	61.7	1398.8	75.4	2268.8	78.8	4025.9	78.6
0.18	298.5	65.7	614.1	66.4	1160.0	79.6	2013.0	81.2	3829.7	79.7
0.27	290.0	66.7	520.3	71.5	1194.1	79.0	1944.7	81.8	3616.5	80.8
0.36	290.0	66.7	511.8	72.0	1177.1	79.3	1868.0	82.6	3565.3	81.1
0.45	272.9	68.6	469.1	74.3	1125.9	80.2	1620.6	84.9	3352.1	82.2

iv) PVA-AA-PVBS

The values of corrosion rate and respective IE for mild steel dissolution in 1 M HCl with and without different concentrations of PVA-AA-PVBS are depicted in Table 21. The values show that corrosion rate decreased gradually in the inhibited solution with increase in inhibitor concentration, as well as with prolonged immersion time. Inhibition efficiency can be seen to increase with increasing concentration of PVA-AA-PVBS, with maximum efficiency observed to be 94.06 % at 0.45 wt.% for 6 hour immersion. Then the IE can be seen to decrease but maintain almost steady values (91.30 %: 9 h and 91.90 %: 12 h) at 9-12 h, suggesting the stability of the inhibitor action.

Table – 21 Corrosion rates and IE obtained for various concentrations of PVA-AA-PVBS at various time intervals

Conc. Wt.%	1 hour		3 hours		6 hours		9 hours		12 hours	
	CR (mpy)	IE (%)	CR (mpy)	IE (%)	CR (mpy)	IE (%)	CR (mpy)	IE (%)	CR (mpy)	IE (%)
Blank	2157.9		2386.9		1885.3		1971.4		1776.3	
0.03	827.4	61.7	902.7	62.2	471.0	75.0	506.6	74.3	431.1	75.7
0.09	644.0	70.2	683.2	75.0	433.2	77.0	454.2	77.0	320.2	82.0
0.18	435.0	79.8	532.0	77.7	387.4	79.5	371.8	81.1	278.3	84.3
0.27	345.4	84.0	415.8	82.6	218.1	88.4	324.6	83.5	224.6	87.4
0.36	354.0	83.6	314.0	86.9	217.3	88.5	274.9	86.1	210.0	88.2
0.45	358.2	83.4	340.2	85.8	111.9	94.1	171.5	91.3	143.9	91.9

Table – 22 Corrosion rates and IE obtained for various concentrations of PVA-AA-PVBS at 303 K-343 K

Conc. Wt.%	303 K		313 K		323 K		333 K		343 K	
	CR (mpy)	IE (%)	CR (mpy)	IE (%)	CR (mpy)	IE (%)	CR (mpy)	IE (%)	CR (mpy)	IE (%)
Blank	870.0		1825.3		5680.6		10713.1		18449.3	
0.03	452.1	48.0	861.5	52.8	1808.3	68.2	3198.6	70.1	6567.7	65.1
0.09	366.8	57.8	733.5	59.8	1731.5	69.5	2959.7	72.4	6397.1	66.0
0.18	349.7	59.8	716.5	60.8	1791.2	68.5	2362.7	77.9	5271.2	72.0
0.27	307.1	64.7	622.7	65.9	1501.2	73.6	2268.8	78.8	4333.0	77.0
0.36	307.1	64.7	588.5	67.8	1330.6	76.6	2149.4	79.9	3966.2	78.9
0.45	264.4	69.6	520.3	71.5	1245.3	78.1	1748.5	83.7	3923.6	79.2

Similarly the effect of various temperature (303 K– 343 K) in the absence and presence of PVA-AA-PVBS is presented in Table 22. The data reveals the fact that the temperature till 333 K exhibits a positive effect on IE for almost all the concentrations studied. For the optimum concentration of 0.45 wt.%, a highest efficiency of 83.7 % is obtained that falls to 79.2 % with 10 K increment in temperature.

v) PVA-VSA-PVBS

The values of the efficiency obtained from the weight loss measurements for different concentrations of PVA-VSA-PVBS in 1 M HCl at 30 ^{o}C after 12 h of immersion is furnished in the Table 23. The results showed that inhibition efficiency increased as the concentration of inhibitor increased, and 0.45 wt.% was found to be the optimum concentration for the inhibitor. When the IE values obtained as a function of time is analysed, It is evident that inhibitor efficiency increases with increasing immersion time (80.6 %; 1h, 90.1 %: 6 h). Then the IE was found to drop to 86.9 % and get stabilised at the value of 91.6 % at 12 h.

Table – 23 Corrosion rates and IE obtained for various concentrations of PVA-VSA-PVBS at various time intervals

Conc. Wt.%	1 hour		3 hours		6 hours		9 hours		12 hours	
	CR (mpy)	IE (%)	CR (mpy)	IE (%)	CR (mpy)	IE (%)	CR (mpy)	IE (%)	CR (mpy)	IE (%)
Blank	2157.9		2386.9		1885.3		1971.3		1776.3	
0.03	827.4	61.7	952.1	60.1	553.8	70.6	870.5	55.8	624.1	64.9
0.09	678.1	68.6	735.5	69.2	500.3	73.5	751.4	61.9	294.3	83.4
0.18	524.6	75.7	607.6	74.5	463.0	75.4	545.9	72.3	250.2	85.9
0.27	426.5	80.2	440.5	81.5	363.7	80.7	487.0	75.3	197.2	88.9
0.36	417.9	80.6	421.6	82.3	348.9	81.5	350.8	82.2	221.8	87.5
0.45	417.9	80.6	340.2	85.7	187.1	90.1	259.2	86.9	149.3	91.6

Table - 24 Corrosion rates and IE obtained for various concentrations of PVA-VSA-PVBS at 303 K-343 K

Conc. Wt.%	303 K		313 K		323 K		333 K		343 K	
	CR (mpy)	IE (%)	CR (mpy)	IE (%)	CR (mpy)	IE (%)	CR (mpy)	IE (%)	CR (mpy)	IE (%)
Blank	870.0		1825.3		5680.6		10713.1		18449.3	
0.03	366.8	57.8	742.1	59.3	2200.6	61.3	4597.4	57.1	6235.1	66.9
0.09	349.7	59.8	742.1	59.3	2055.6	63.8	3249.7	69.7	5356.5	71.6
0.18	332.7	61.8	690.9	62.1	1535.3	73.0	2499.1	76.7	5220.1	72.3
0.27	324.1	62.7	571.5	68.7	1228.2	78.4	2396.8	77.6	4529.2	76.0
0.36	315.6	63.7	571.5	68.7	1083.2	80.9	2004.4	81.3	4213.6	77.6
0.45	290.0	66.7	503.2	72.4	887.1	84.4	1987.4	81.4	4051.5	78.5

The data collected from the experiments that were conducted to analyse the temperature effect on IE is listed in the Table 24. As discussed in the other polymeric systems under investigation, PVA-VSA-PVBS follows the same trend in extending IE. A maximum IE of 81.4 % is achieved with optimum inhibitor concentration at 333 K. This is followed by a decrease in IE to 78.5 % at 343 K.

4.3.2 Scrutiny of IE results obtained by weight loss technique

The results of weight loss measurements for mild steel dissolution in the absence and presence of different concentrations of all the inhibitors under investigation were found to follow the same trend. Figure 23 shows the variation of weight loss and corrosion rate for the highest inhibitor concentration of all grafted terpolymers at 12 hours.

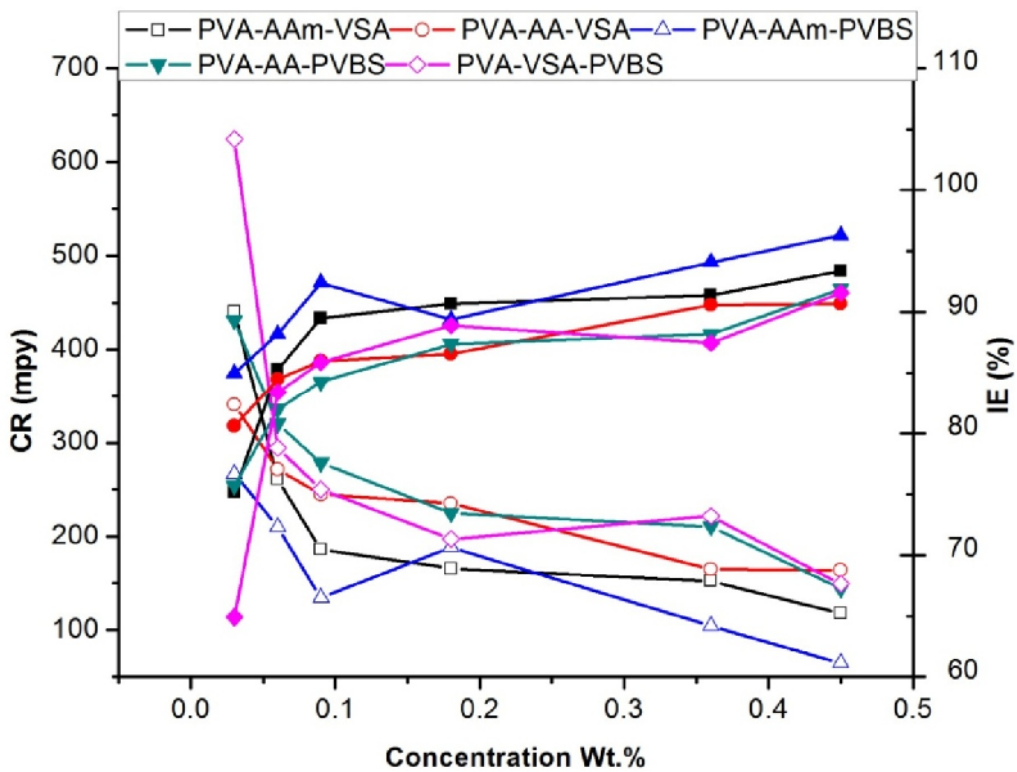

Figure-23 Variation of CR and IE with 0.45 wt.% of various terpolymers at 12 hours (○ CR and ● IE)

4.3.2.1 Effect of concentration

The IE values of the terpolymers presented in tables show a positive effect with respect to concentration. The terpolymers show an IE in the range of 65-80 % even for the low concentration, which increases to a maximum value around 90 % for the highest concentration. This is an evidence for strong adsorption of the polymers on the metal surface owing to multiple adsorption centres which makes the adsorption process favourable

(Ali *et al.*, 2012). **Amin *et al.* (2009)** explained this trend as increasing the inhibitor concentration may lead to the formation of multilayers that could furnish a maximum IE beyond which what could be achieved by monolayers at low concentration. In other words, increase in concentration increases the adsorption and surface coverage of the inhibitor molecules; thus the surface is efficiently separated from the medium. When the results of the present work is observed, increasing concentration from 0.09-0.45 wt.% lead to increase in IE with low slope values showing that increase in concentration furnished only an additional surface coverage more than what a monolayer could afford.

Generally, adsorption of the inhibitors was found to occur by the exchange of water molecules adsorbed on the metal surface with inhibitor molecules. A detailed mechanism involving two adsorbed intermediate species in relation to the retardation of anodic dissolution of iron in the presence of inhibitor as proposed by **Ashassi-Sorkhabi and Nabavi-Amri, (2000)**

$$Fe + H_2O \rightarrow Fe.H_2O_{ads}$$
$$Fe.H_2O_{ads} + Y \leftrightarrow FeOH_{ads}^- + H^+ + Y$$
$$Fe.H_2O_{ads} + Y \leftrightarrow FeY_{ads} + H_2O$$
$$FeOH_{ads}^- \text{ (rate determining step)} \rightarrow FeOH_{ads} + e^-$$
$$FeY_{ads} \rightarrow FeY^+ + e^-$$
$$FeOH_{ads} + FeY^+_{ads} \leftrightarrow FeY_{ads} + FeOH^+$$
$$FeOH^+ + H^+ \leftrightarrow Fe^{2+} + H_2O$$

Y=inhibitor system

Arukalam *et al*. (2014a) explained the above mechanism as follows: A corroding metal surface is non-homogenous due to the existence of lattice defects and dislocations, and are generally characterized by multiple adsorption centres. Inhibitor molecules having suitable adsorption enthalpies may thus be adsorbed more readily at the surface active sites, i.e. when the formation of FeY_{ads} becomes energetically more favourable, the amount of $FeOH_{ads}^-$ responsible for the rate determining step is lowered thus suppressing the anodic dissolution of iron. The inhibition efficiency discussed so far is achieved by blocking cathodic or anodic reaction through adsorption, but **Amin *et al.* (2009)** explains that it can also be achieved by simply preventing the supply of oxidant or transport of reaction products. The later occurs when the surface of the metal is saturated with monomolecular layers of the inhibitor, formation of multilayer layer occurs in which the inhibitor molecules are not in direct contact with the reactive sites of metal but offering additional resistance to transport of necessary elements for corrosion reaction. Hence, the increase in inhibition efficiency with concentration is related to adsorption and formation of a barrier film on the electrode surface.

The formation of such a barrier film is confirmed by EDX and SEM examinations of the electrode surface (ref. Section 4.5.4).

4.3.2.2 Effect of immersion Time

The weight loss of the metal coupons was monitored for a period of 12 hours at regular intervals of 3 hours to analyse the stability of the inhibitor film. The IE is directly to proportional to the inhibitor concentration and time. The high inhibition efficiency with longer immersion time is an indication of the formation of a time-dependant protective film on the MS surface **(Mu and Li, 2005)**. It has also been suggested that two-dimensional layers of inhibitor molecules were formed on metal surfaces after longer immersion times **(Oguzie *et al*. 2004; Mu and Li, 2005).**

The action of the inhibitor distinctively increased till 6 hours of immersion time and slightly decreases at 9 hours and then increases after 12 hours of immersion. **Atta *et al*. (2008)** explained that the fact of IE increasing with time is due to initial electrostatic interaction by charged groups, and as the time proceeds formation of multiple layers and/or complex formation with Fe orbital can occur. In other words, the adsorption of the inhibitor molecules on the metal surface initially takes place at some sites, and later as the time proceeds the inhibitor form monomolecular layers by forming complex with iron. Further the presence of electron donating groups $(-CH2-CH2-)_n$ enhances the electron density of the hetero atoms resulting in better efficiency. Also the solvation of the polymer is achieved gradually with time. As a consequence, the dispersion and effective adsorption of the polymer takes some time **(Arukalam *et al*., 2014a)**. There is a slight decrease in IE at 9 hours which means that the inhibitor film is not desorbed fully, and is attempting to get stabilized at this stage of time followed by formation of a stable barrier film. This slight decrease in IE after 9 hours is an indication of effort taken by the inhibitor to form a stable film. i.e. there is a competition between inhibitor molecules and chloride ions to get adsorbed on the metal surface. However, in the due course of immersion the inhibitor forms a highly adherent stable film furnishing a high IE. In some cases, when the active areas for adsorption of inhibitor molecules attain a saturated level, the development of barrier layer slows down resulting in decrease in IE.

4.3.2.3 Effect of immersion temperature

The effect of temperature on the inhibited acid-metal reaction is very complex because of certain changes that occur: Rapid etching, Desorption of the inhibitor film and decomposition of inhibitor at higher temperature **(Belkaid *et al*., 2012)**. The influence of temperature followed same trend in all inhibitor systems studied. Figure 24 explains the variation of CR and IE with 0.45 wt.% of various terpolymers at 333 K.

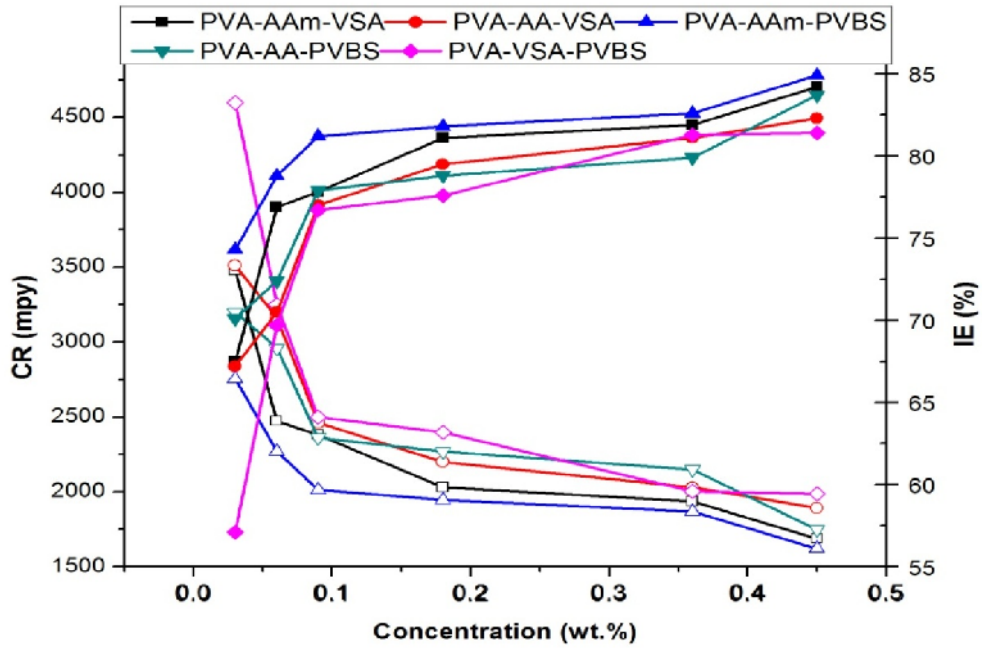

Figure - 24 Variation of CR and IE with 0.45 wt.% of various terpolymers at 333 K (○ CR and ● IE)

Observation of Tables 15-24 shows that the corrosion rate was found to increase in the presence and absence of the inhibitor. The increase in corrosion rate was found to be more pronounced with increase in temperature for blank HCl solution. However, after the addition of inhibitors the increase in corrosion rate with rise in temperature was less pronounced. This ensures the protective ability of the polymer. In the present systems studied, the IE gradually increased in the temperature domain range of 303-333 K (68.6 % to 84.9 % for 0.45 wt.% of inhibitor) and then decreased to 82.2 % at 343 K. i.e. the protective nature of the film is interfered at 343 K rendering a less protective film which in turn allows the corrodant species to diffuse into the active sites initiating the corrosion **(Arukalam *et al*., 2014a).**

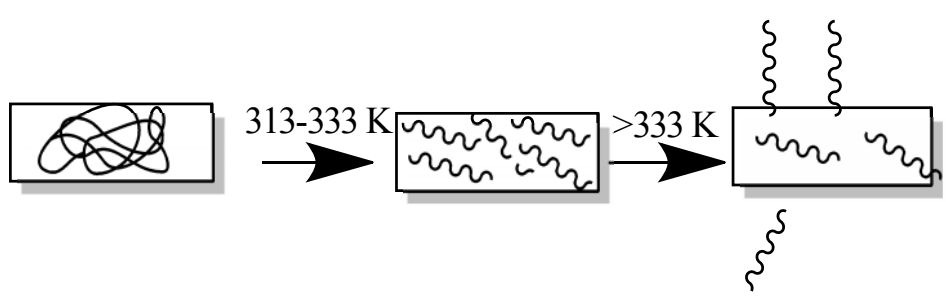

Figure - 25 Plausible transformations of the terpolymer at various temperatures on mild steel surface at various temperatures

Because increase in temperature stimulates kinetic energy of the metal surface which adversely affects the adsorption process. Hence the adsorption-desorption equilibrium is shifted more towards the desorption process **(Fares *et al*., 2012a)** and the electrode surface is more roughened owing to the enhanced corrosion. This fact can be explained on the basis of structural orientation according to **Fares *et al*. (2012a)** and **Chamovska *et al*. (2007)** as follows: At lower temperatures coiled structure of the polymer chains covers the surface and prevents the metal dissolution. But at temperatures from 313-333 K, the long chains of the coiled structure could have broken into small segments but still providing the better efficiency. At temperatures greater than 333 K, the short chains could have started desorbing from the metal surface and consequently IE starts decreasing.

4.3.2.4 Effect of terpolymer composition on IE

Inhibition efficiency is primarily due to the adsorption of inhibitor molecules. Adsorption can occur through electrostatic interaction on metal surface, electron donating hetero atoms and π electron interaction with the metal surface. The variation in corrosion inhibition performance among the terpolymers under investigation can be explained on the basis of composition of the terpolymers. Based on the composition they can be classified as VSA polymers (PVA-AAm-VSA and PVA-AA-VSA), PVBS polymers (PVA-AAm-PVBS and PVA-AA-PVBS) and sulphur polymers (PVA-VSA-PVBS). PVBS polymers have shown best performance among the other two groups. VSA polymers performed better than the sulphur polymers.

The terpolymers under investigation contain amide, acid, alcohol, sulfonic acid and benzene groups. In acid solution, the amide moiety remain protonated to form polycations of polymeric material **(Umoren and Ebenso, 2008)**, thereby promoting electrostatic interactions. Further, the chains probably remain in the unfolded form due to the presence of COOH group hindrance along with the pi electron conjugation. The lone pair of electrons of nitrogen, oxygen and sulphur present in the polymeric matrix can extend linkages with the empty d-orbitals of the iron surface thereby enabling the adsorption **(Mansri *et al*., 2013)**. The delocalised pi electrons of the aromatic ring of PVBS can also form a co-ordination type of bond by interacting with empty orbital of the metal.

From the above statements, it is clear that the reduction in anodic dissolution is highly achieved in the presence of both conjugated aromatic ring and lone pair of electrons of nitrogen atoms. This is the reason for PVBS polymers ranking first in controlling the corrosion than the VSA polymers. In the sulphur polymers, the inhibitory action is a result of interaction of electroactive sulphur with the surface of the metal **(Khaled and Al-Qahtani, 2009).**

Here the interaction of the lone pair of electrons is restricted to occur only through sulphur atom. The pi electrons of the p-vinyl benzene sulfonate also aid in the adsorption of the inhibitor molecules on metal surface. Generally the sulphur compounds are found to be less effective in HCl solutions, but they are frequently used in H_2SO_4 **(Abd-El Rehim *et al*., 2001)**. As a rule of thumb it can be stated that S-containing inhibitors are primarily useful in H_2SO_4, whilst N-containing inhibitors exert their best efficiencies in HCl. However, the sulphur compound is selected as a monomer for grafting because it is capable of exerting flexibility to the polymer matrix.

4.3.2.5 Comparison of optimum results of the grafted terpolymers with the respective monomers

Based on the distribution percentage of each monomer present in the optimum concentration (0.45 wt.%) of the terpolymer inhibitor, the monomer ratios were fixed and subjected to corrosion inhibition evaluation. The distributed ratios of monomers in the terpolymer were tested individually for its corrosion inhibition efficiency in 1 M HCl for an immersion period of 6 hours and the results are tabulated in Table 25.

Table – 25 Corrosion rates and IE obtained for individual monomers before polymerization at 303 K

Monomer ratio	Corrosion rate (mpy)	IE (%)
Blank HCl	1885.31	
PVA (50 %)	591.63	68.61
AAm (20%)	818.40	56.59
AA (20 %)	915.07	51.46
VSA (30 %)	768.98	59.21
PVBS (12.5 %)	600.35	68.15
Commercial terpolymer Inhibitor (10 mL)	208.59	88.93

It is well established that the corrosion inhibition percentage of the PVA, acrylamide, acrylic acid, vinyl sulfonic acid sodium salt, p-vinyl benzene sulfonic acid sodium salt is less than 70 %. A commercially available terpolymer inhibitor was also tested for its corrosion mitigation effect and IE of 88.9 % was obtained. The results prove that the terpolymers of the present study are a better inhibitor than their monomeric form, because of the combined effect of O, N and S hetero atoms. Moreover, the larger polymer molecule can provide an effective surface coverage area.

4.3.3 Kinetic Considerations

The effect of temperature on the MS corrosion is a complex process. Temperature can have a positive effect or negative effect on the inhibition efficiency of the corrosion process. The decrease in inhibition efficiency with rise in temperature is attributed to the shifting of the adsorption-desorption equilibrium to desorption process and vice versa. This leads to lower inhibition efficiency at higher temperatures **(Chaudhary *et al.*, 2007; Sanyal *et al.*, 2010; Jamal Abdul Nasser and Anwar Sathiq, 2012)**. The temperature dependency of the corrosion reaction can be evaluated through the activation parameters (E_a, ΔH_o, and ΔS_o) using Arrhenius equation and Transition state equation 4 and 5.

$$\log(CR) = \frac{-Ea}{2.303RT} + \log\lambda \tag{4}$$

$$CR = \frac{RT}{Nh} exp\left(\frac{\Delta So}{R}\right) exp\left(-\frac{\Delta Ho}{RT}\right) \tag{5}$$

Where E_a is the apparent activation energy, λ is the Arrhenius pre-exponential factor, CR is the corrosion rate, ΔH_o the enthalpy of activation, ΔS_o the entropy of activation, N the Avogadro's number, R the universal gas constant and T the absolute temperature.

A plot of log CR vs. 1/T is the Arrhenius plot. The activation energy E_a is calculated from the slope ($-E_a/R$) of the straight lines and the plot of log CR/T vs. 1/T is the Transition state plot. The transition state plot is also a set of straight lines with the slope value of $-\Delta H_o/R$ and intercept of (log (R/Nh)+ $\Delta S_o/R$) from which the values of ΔH_o and ΔS_o are calculated. Based on the temperature effect, the relation between IE and E_a can be classified into three types as follows: **(Radovicci, 1965**)

- When IE decreases with increase in temperature, the value of apparent activation energy for inhibitor added solution is more than the uninhibited solution
- When IE does not change with respect to temperature, then apparent activation energy does not show a significant change
- When IE increases with increase in temperature, the apparent activation energy for the corrosion process is smaller than that obtained for uninhibited solution. This is likely an indication of specific type of interaction of inhibitors with metal surface **(Jamal Abdul Nasser and Anwar Sathiq, 2012; Radovici, 1965). Al-Sabagh *et al.* (2011)** explains the higher E_a values for inhibited solutions as follows: The corrosion of steel tends to precede at uncovered surface portion or high energy sites of the steel. When the inhibitor functions by blocking high energy active sites, the E_a values

do increase significantly. **Machu (1971**) reports that the E_a values are smaller for powerful inhibitors than that obtained for blank HCl solution. This is an evidence for chemisorption nature of the inhibitor while the increased E_a values with respect to the inhibited solution is an indication of physical nature of adsorption of the inhibitor.

4.3.3.1 Thermodynamic activation parameters obtained for the grafted terpolymers by gravimetric method

Arrhenius plot is constructed by plotting logarithm of corrosion rate vs. inverse of temperature. Figures 26a and 27a shows the linear regression between log (CR) and 1/T for PVA-AA-VSA and optimum concentrations of all the other investigated terpolymers respectively. Transition state plot is constructed by plotting logarithm of corrosion rate/temperature vs. inverse of temperature. Figures 26b and 27b shows the linear regression between log (CR/T) and 1/T for PVA-AA-VSA and optimum concentrations of all the other investigated terpolymers respectively. The kinetic parameters such as Ea, ΔH_o and ΔS_o were calculated and are summarised in the Table 26.

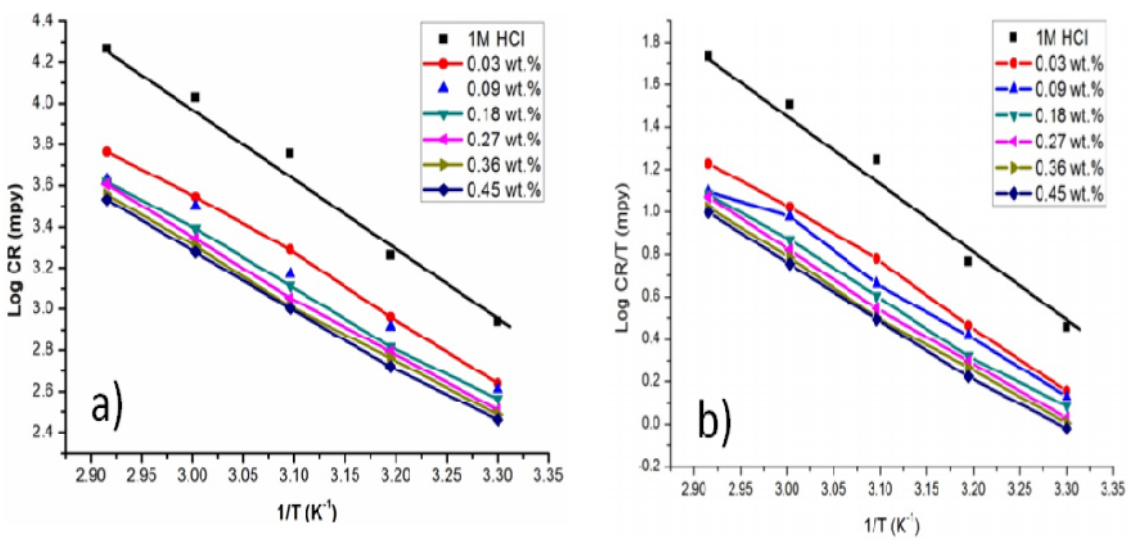

Figure – 26 a)Arrhenius Plot and b)Transition state plot of PVA-AA-VSA

The R^2 values obtained for both the plots are close to unity indicating the applicability of kinetic model for the corrosion process. Inspection of the E_a values reveal that the values obtained for blank HCl is 68 kJ mol^{-1} which is in agreement with the literature data for iron dissolution in HCl in the range of 58-100 kJ mol^{-1} **(Perboni and Rocchini, 1988; Riggs *et al,.* 1967; Larabi *et al,* 2004).** The E_a values obtained for inhibited solution is lesser than those obtained for blank HCl and lies in the range of 57-64 kJ mol^{-1}. The activation energy is lesser than the uninhibited solution, and IE increases with increase in temperature till 343 K and then decreases. The aforementioned facts are tenable to the chemisorption mode of

adsorption. The decreased E_a is explained by various authors in different perspectives as follows: **Riggs et al. (1967)** report that this decrease in the activation energy of corrosion at maximum inhibited level is a result of shift of the net corrosion reaction from that on the uncovered portion to covered portion of the metal surface. In other words, when the surface coverage is maximum, diffusion through the inhibitor layer or corrosion products will become the rate-determining step of the metal dissolution process **(Putilova *et al*., 1960)**.

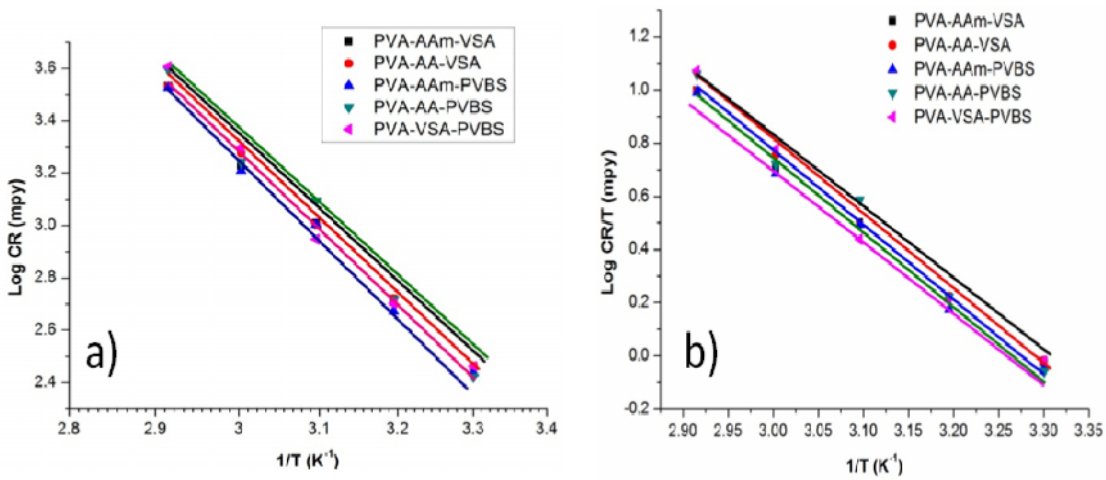

Figure – 27 a)Arrhenius Plot and b)Transition state plot of the investigated terpolymers at optimum concentration

According to **Noor and Al-Moubaraki (2008a)**, with increase in temperature, due to some chemical changes that occur in the inhibitor molecules, electron density increases at the adsorption centres of the molecule which in turn furnishes improved inhibition efficiency. In other words the decrease in apparent activation energy is a result of shift of the net corrosion reaction from uncovered surface to adsorbed sites directly. The tendency of variation of Arrhenius frequency factor λ is similar to that in apparent activation energy for most of the corrosion reactions. According to **Hoar and Holliday (1953)**, this can be pertained to the slow rate of inhibitor adsorption with a resultant closer approach to equilibrium during the experiments at higher temperature. **Schmid and Huang (1980) & Hegazy and Zaky (2010)** explain the same phenomenon as follows: When the inhibitor molecules is capable of inhibiting both anodic and cathodic partial reactions on the electrode surface while a parallel reaction takes place on the inhibitor covered surface, the reaction rate of the covered surface is considerably less than that on the uncovered surface area.

The positive values of ΔH_o reflect the endothermic metal dissolution process suggesting the slow process of metal dissolution in the presence of inhibitors. All the Ea values are larger than the analogous ΔH_o values showing that the corrosion process basically

involved a gaseous reaction i.e. hydrogen evolution reaction associated with decrease in total reaction volume **(Laidler, 1963).** Hence the corrosion process can be considered as a unimolecular reaction which obeys the relation $Ea-\Delta H_o=RT$. The results permit to verify the relation between Ea and ΔH_o: $Ea-\Delta H_o=RT$, i.e. the calculated values of RT are very close to the theoretical value 2.68 kJ/mol **(Soltani *et al*., 2012).**

Table - 26 Thermodynamic activation functions in the absence and presence of different concentrations of investigated terpolymers from Arrhenius and Transition state plots. Ea- ΔH_o = 2.68 kJ mol^{-1}

Inhibitor	Conc. (wt.%)	E_a kJ mol^{-1}	ΔH_o kJ mol^{-1}	ΔS_o J mol^{-1} K^{-1}	$\lambda^* 10^{14}$
	1M HCl	68.27	65.59	27.74	5.130
PVA-AAm-VSA	0.03	58.45	55.77	-10.92	0.049
	0.09	53.78	51.10	-27.37	0.007
	0.18	55.15	52.47	-23.77	0.011
	0.27	55.27	52.59	-24.27	0.010
	0.36	54.39	51.71	-27.50	0.007
	0.45	52.78	50.10	-32.96	0.003
PVA-AAm-PVBS	0.03	56.72	54.04	-17.17	5.130
	0.09	54.36	51.68	-25.99	0.023
	0.18	54.48	51.80	-26.36	0.008
	0.27	55.03	52.35	-25.40	0.008
	0.36	54.55	51.87	-27.09	0.009
	0.45	54.00	51.32	-29.56	0.007
PVA-AA-VSA	0.03	56.56	53.88	-16.44	0.025
	0.09	52.37	49.69	-30.87	0.004
	0.18	53.42	50.74	-28.84	0.006
	0.27	54.52	51.84	-26.19	0.008
	0.36	53.34	50.66	-30.55	0.005
	0.45	53.65	50.97	-30.07	0.005
PVA-AA-PVBS	0.03	61.32	58.64	-2.03	0.143
	0.09	62.34	59.66	0.51	0.194
	0.18	59.07	56.39	-10.71	0.050
	0.27	57.04	54.36	-17.82	0.021
	0.36	57.03	54.36	-18.51	0.020
	0.45	57.13	54.45	-19.00	0.019
PVA-VSA-PVBS	0.03	61.32	58.64	-2.03	0.143
	0.09	62.34	59.33	-0.56	0.194
	0.18	59.07	56.39	-10.71	0.050
	0.27	57.04	54.36	-17.82	0.021
	0.36	57.03	54.36	-18.51	0.020
	0.45	57.13	54.45	-19.00	0.019

The positive values of ΔS_o resulted from the blank HCl shows an increase in disorderliness that takes place during a rigorous metal dissolution. At the same time the negative values of ΔS_o obtained after the addition of inhibitor indicate that the rate determining step is association rather than the dissociation. This means that a decrease in disordering takes place on going from reactants to the activated complex **(Noor and Al-Moubaraki, 2008a; Bouklah *et al.*, 2006; El-Sherbini, 1999).**

The average value of apparent activation energies for PVA-AAm-VSA, PVA-AAm-PVBS, PVA-AA-VSA, PVA-AA-PVBS and PVA-VSA-PVBS are: 54.96, 52.10, 53.97, 58.98 and 59.44 kJ mol^{-1}, respectively. According to these values the inhibitors protection efficiency can be arranged as follows: PVA-AAm-PVBS> PVA-AA-VSA > PVA-AAm-VSA > PVA-AA-PVBS > PVA-VSA-PVBS. Activation energy, enthalpy and entropy thus obtained for the inhibition process for all the inhibitors reveals their protection efficiency.

4.4 Corrosion studies by Electrochemical technique

Corrosion is an electrochemical process and hence electrochemical techniques are used in myriad number of ways to assess the effectiveness of corrosion inhibitors and coatings for metals and alloys. Electrochemical techniques that employ direct current (DC) over a specified potential range are linear polarization/potentiodynamic polarization, and alternating current (AC) for analysis of metal/solution interface is electrochemical impedance spectroscopy (EIS).

Polarization is a technique in which the potential of the electrode is made to shift in any particular direction from its open circuit potential by applying a DC voltage. As a result current flows through the electrodes by electrochemical reaction, that takes place at the surface of the electrode. During the electrochemical reaction, the open circuit potential is controlled by two different types of reactions. The reaction that generates the cathodic current (i_c) is the cathodic reaction and the reaction that generates anodic current (i_a) is the anodic reaction. The total amount of the reaction is controlled by the kinetics of the reactions (k_{corr}) and the diffusion of reactants both towards and away from the electrode. The current thus generated by the reaction is called corrosion current which can be determined from the intersection point by the extrapolation of anodic and cathodic region.

When a metal is subjected to polarization the following reaction takes place.

$$M \underset{i_c}{\overset{i_a}{\rightleftharpoons}} M^{2+} + 2e^- \qquad (6)$$

At equilibrium conditions $i_a = i_c$, then $i_{meas} = i_a - i_c \rightarrow 0$, no net current flow. The corrosion rate for the above reaction can be written as

$$r = k_{corr}\,[reactants] \tag{7}$$

The thermodynamic relation between ΔG and equilibrium constant is given as

$$-\Delta G = RT \ln k \tag{8}$$

When ln k in the general thermodynamic equation is replaced by the k_{corr},

$$\text{Then, } k_{corr} = Ae^{\frac{-\Delta G}{RT}} \tag{9}$$

$$\text{Hence, } r = Ae^{\frac{-\Delta G}{RT}}\,[reactants] \tag{10}$$

Where A is a constant. At equilibrium conditions,

$$i_a = i_o = i_o e^{\frac{-\Delta G}{RT}}\,[reactants] \tag{11}$$

Anodic polarization can be noted as αzf and cathodic polarization can be noted as (1-αzf), the above equation 11 can be written as

$$i_a = i_o e^{\frac{\alpha \eta ZF}{RT}}] \tag{12}$$

Where R is universal gas constant, T is the temperature, Z is the number of electrons involved in the reaction and F is the Faraday.

$$i_c = i_o e^{(\frac{1-\alpha)\eta ZF}{RT}} \tag{13}$$

$$i_{meas} = i_o(i_o e^{\frac{\alpha \eta ZF}{RT}} - i_o e^{(\frac{1-\alpha)\eta ZF}{RT}}) \tag{14}$$

By substituting αZF/RT as A' and taking log

$$\ln i_a = \ln i_o + A'\eta \tag{15}$$

$$\ln \frac{i_a}{i_o} = A'\eta; \quad \eta = \frac{2.303}{A'} log \frac{i_a}{i_o} \tag{16}$$

If we replace 2.303/A' as βa, then

$$\eta a = \beta a \log i_a - \beta a \log i_o; \eta c = \beta c \log i_c - \beta a \log i_o \tag{17}$$

The above equation is called as Tafel equations for anodic and cathodic reactions respectively. From these equations, Tafel constants can be determined. Corrosion current I_{corr} is obtained by extrapolation of the linear portions of the anodic and the cathodic branches of the curve (E Vs. log I) to the corrosion potential, E_{corr}. The corrosion current is related with the slope of the line as

$$\frac{\Delta E}{\Delta i} = \frac{b_a b_c}{2.303 I_{corr}(b_a + b_c)} \quad (18)$$

The measured corrosion current density is converted into corrosion rate via Faraday's law and empirically determined Tafel slopes and other factors in the equation.

The relation between the I_{corr}, R_p, b_a and b_c is explained using the following equation.

$$\frac{\Delta i}{\Delta E} = I_{corr};\ I_{corr} = \frac{b_a b_c}{2.303(b_a + b_c)} \frac{1}{R_p} \quad (19)$$

Corrosion rate is then calculated from the Icorr using the following equation.

$$Corrosion\ rate = \frac{0.13 I_{corr}(Eq.wt.)}{d} \quad (20)$$

Where, I_{corr} is the corrosion current density (in A/cm^2), d the density of the corroding metal sample (in g/cm^3), and Eq.wt. is the equivalent weight (mass) of the corroding metal (in g).

Since corrosion is basically an electrochemical process, the determination of electrochemical properties at the metal–solution interface like corrosion potential and corrosion current density play a vital role in monitoring the corrosion reaction. From the above derivation, it is clear that the electrochemical data such as I_{corr} can be converted into corrosion rate using equations and the inhibition efficiency of an inhibitor under investigation can be determined.

4.4.1 Potentiodynamic polarization measurements

The effectiveness of the various concentrations of the inhibitor PVA-AAm-PVBS at 303 K on polarization behaviour of MS in HCl has been studied. Polarization curves for MS in HCl in the presence of various concentrations of PVA-AAm-PVBS are shown in Figure 28. The choice of the concentration is related to the efficiency of PVA-AAm-PVBS. Table 27 represents the list of polarization parameters: corrosion potential (E_{corr}), corrosion current density (I_{corr}), Tafel slopes (b_a and b_c) and inhibition efficiency (IE %) for corrosion of MS in 1 M HCl.

Table - 27 Polarization parameters of the MS in 1 M HCl containing various concentrations of PVA-AAm-PVBS at 303 to 343 K calculated from extrapolation of the Tafel lines

Temp (K)	Conc. (wt.%)	303 K		313 K		323 K		333 K		343K	
E_o (V)	Blank	-0.4842		-0.4805		-0.4671		-0.4840		-0.4853	
	0.03	-0.4796		-0.4732		-0.4651		-0.4685		-0.4408	
	0.09	-0.4822		-0.4757		-0.4715		-0.4679		-0.4407	
	0.18	-0.4803		-0.4780		-0.4748		-0.4639		-0.4383	
	0.27	-0.4774		-0.4776		-0.4778		-0.4619		-0.4378	
	0.36	-0.4775		-0.4771		-0.4832		-0.4733		-0.4392	
	0.45	-0.4708		-0.4784		-0.4737		-0.4754		-0.4384	
b_a and b_c (mV)		b_a					b_c				
	Blank	220	298	327	373	423	269	316	355	421	579
	0.03	137	184	185	267	375	150	198	209	326	471
	0.09	148	170	181	291	343	152	181	196	341	467
	0.18	152	161	181	252	360	187	172	196	300	445
	0.27	184	157	179	245	337	171	166	213	299	431
	0.36	132	155	190	260	357	147	166	219	348	468
	0.45	124	157	199	233	334	148	180	241	308	422
I_o (mA/cm^2) IE $_{Io}$		I_{corr}					% IE $_{Icorr}$				
	Blank	15.3	37.2	65.9	120.4	231.7	-	-	-	-	-
	0.03	1.5	6.4	7.4	31.0	61.5	89.96	82.80	88.74	74.28	73.46
	0.09	1.5	4.5	7.4	27.1	59.0	90.02	87.97	88.73	77.49	74.53
	0.18	1.3	3.5	6.7	25.6	55.4	91.46	90.64	89.76	78.77	76.10
	0.27	1.4	3	6.7	24.9	50.6	91.01	92.06	89.83	79.30	78.15
	0.36	1.2	2.8	6.9	22.5	49.8	92.42	92.50	89.55	81.30	78.50
	0.45	0.8	2.6	5.2	20.4	44.4	94.96	92.97	91.3	83.03	80.84
R_p Ωcm^2 IE R_p		R_p					% IE $_{Rp}$				
	Blank	16.4	7.8	3.3	2.6	1.4	-	-	-	-	-
	0.03	42.8	19.6	16.7	9.1	3.3	61.70	60.30	80.00	70.90	58.50
	0.09	82.8	31.3	18.6	9.8	4.2	80.20	75.10	82.00	73.00	67.40
	0.18	100.9	53.5	44.9	10.2	5.2	83.70	85.40	92.60	74.10	73.50
	0.27	145.4	79.3	46.1	11.1	5.2	88.70	90.20	92.80	76.20	73.60
	0.36	150.8	94.8	55.7	16.1	5.6	89.10	91.80	94.00	83.60	75.50
	0.45	190.6	91.4	56.1	19.3	5.6	91.40	91.47	94.05	86.36	75.58

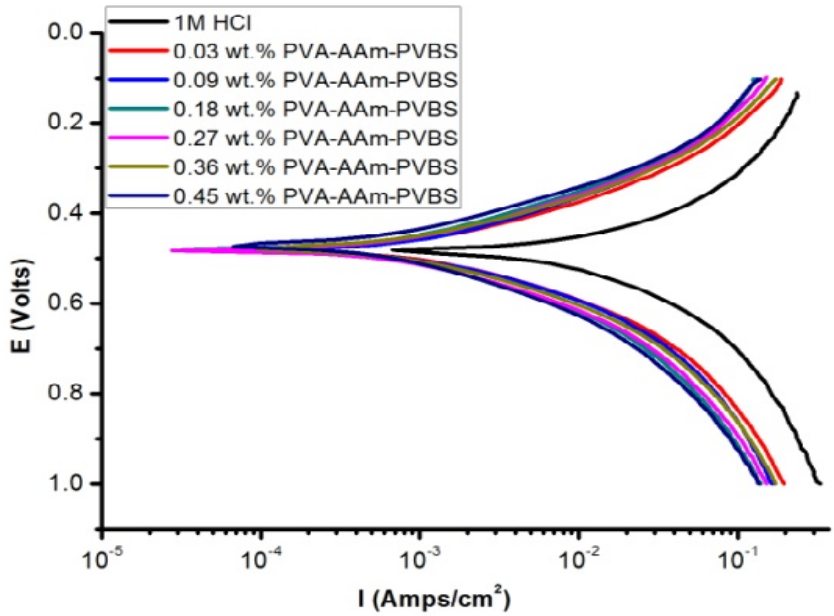

Figure - 28 Potentiodynamic polarization curves of MS in 1 M HCl in the absence and in the presence of PVA-AAm-PVBS at various concentrations

4.4.1.1 Effect of concentration on polarization behaviour of PVA-AAm-PVBS

When both the cathodic and anodic regions of the Tafel curves are observed, the current density decreases with the addition of inhibitor. Observation of the Figure 28 reveals that with progressive addition of the inhibitor (0.03-0.45 wt.%), the Tafel curves are shifted gradually to lower current densities. This shows that the inhibitor gets adsorbed on the metal surface thereby preventing the acid attack on the metal. The parallel nature of the current-potential curves, indicates that hydrogen evolution reaction is activation controlled **(Tebbji *et al*., 2007; Atta *et al*., 2008)**. The activation controlled reaction can be explained as follows: An electrochemical reaction may consist of several steps but the slowest step determines the rate of the reaction. The rate determining step in these types of reactions is the cathodic hydrogen evolution and it requires activation energy to proceed. When the current flows through the anode and the cathode electrodes, and if electrochemically active species is plenty near the electrode surface, then the reaction rate is determined by the electrode potential. Subsequent shift in potential or polarization is termed as activation polarization or activation controlled reaction. There is no notable shift in corrosion current till 323 K but at higher temperatures the Tafel lines are shifted to the anodic region indicating increased corrosion process.

The linearity of the Tafel lines is maintained with different slope values at all concentrations studied. This indicates that the adsorption of the inhibitors in the electrical double layer does not affect the mechanism of the process. When the anodic region is

observed, there is no evidence for any passive film formation either in presence or absence of the inhibitors.

b_a and b_c

The Tafel slopes b_a and b_c are described as follows:

$$b_c = -2.303 + \frac{RT}{(1-\alpha)nZF} \quad (21)$$

$$b_a = -2.303 + \frac{RT}{\alpha nZF} \quad (22)$$

Where R is universal gas constant, T is the temperature, Z is the number of electrons involved in the reaction, α is the symmetry factor and n is the number of electrons involved in the rate determining step. A typical rate determining step involving 1 electron and a symmetry factor of 0.5, results in a Tafel slope b_c of 120 mV per decade and b_a of 60 mV per decade. The present data (Table 27) obtained in the 1 M HCl solution show deviations from the expected Tafel behaviour in the cathodic and anodic region at all the concentrations studied. The deviation of b_a and b_c from the mentioned values shows that the number of the electrons involved in the reaction is increased due to complexity of the corrosion process which is reflected as higher values of b_a and b_c. The deviations in the Tafel behaviour may also be due to changes that occur in anodic kinetics caused by the presence of chloride ions **(Zecevic *et al.*, 1989; Glass and Chadwick, 1994)** explain the reasons for these deviations as follows: (a) High temperatures enhancing the rate and complexity of the reaction (b) Active cathodic and anodic areas dependancy on current and/or potential, pH and environment (c) interference from the anodic reaction kinetics. In other words, significant changes that occur in anode-cathode distributions due to an increased corrosion rate would be considered as an important factor for generating larger than expected values of slopes.

b_a and b_c values are affected by concentration of the inhibitors **(Popova *et al.*, 2007).** Both the b_a and b_c values are decreased significantly in the presence of inhibitors when compared with that of blank **(Elayyachi *et al.*, 2005).** This behaviour suggests that inhibitor under investigation have inhibition effect on both cathodic and anodic reactions of the corrosion process and can be categorised as mixed type inhibitor. The shift in the cathodic Tafel slope is an indication of the influencing nature of the inhibitor on kinetics of hydrogen evolution reaction. i.e. the inhibition takes place by simple blocking of electrode surface area thus decreasing the surface area available for hydrogen evolution reaction without affecting the reaction mechanism **(Tong *et al.*, 1983)**. Similarly, the anodic Tafel slopes also vary signifying the adsorption of chloride ions and/or inhibitor molecules onto the steel surface **(McCafferty and Hackerman, 1972; Mistry and Jauhari, 2014).**

E_{corr} values

The average value of E_{corr} observed was -0.48 V to -0.47 V for the studied concentration range, which is in agreement with corrosion potential observed by other authors **(Ashassi-Sorkhabi and Seifzadeh, 2006; Noor and Al-moubaraki, 2008a)** for mild steel corrosion in HCl. The linear relation between the corrosion potential and acid concentration is given as:

$$E_{corr} = E^{o}_{\text{corr}} + \frac{\ln RT}{ZF} \log C\,HCl \tag{23}$$

Where E^{o}_{corr} is the corrosion potential when acid concentration equals unity, R is universal gas constant, T is the temperature, Z is the number of electrons involved in the reaction. The net charge transferred during the electrode reaction is considered as Z, but when there is a deviation from equilibrium (Z=2) the Z value is modified as Z/v, where v is the number of times the elementary action has occurred for the formation of end product, which determines the rate of overall electrode reaction.

When the shift in the E_{corr} potential is >85mV with respect to E_{corr} in uninhibited solution, the inhibitor can be differentiated as cathodic or anodic type **(Mistry and Jauhari, 2014; Li *et al*., 2008a; Li *et al*., 2009).**

In the present study, the corrosion potential values remain almost same or undergo a slight shift among the various concentrations of the inhibitor. The displacement in the E_{corr} values is less than 85 mV at 303 K which is an indication of mixed type inhibitory action of the inhibitors.

I_{corr} values

For all the inhibitor concentrations studied the I_{corr} values significantly decrease corresponding to the blank HCl. The corrosion current density observed for blank HCl is 15 mA/cm^2 which is reduced to 0.7 mA/cm^2 for 0.45 wt.% concentration of PVA-AAm-PVBS. The decrease in the current densities for oxygen and hydrogen evolution is displayed by the shift of the reduction potential to more negative values. All the above results discussed indicates that the addition of inhibitor reduces the corrosion current values by adsorption on both the cathodic and anodic active sites without modifying the mechanism of corrosion reaction, or in other words inhibitor blocks the active sites and decreases the effective surface area responsible for dissolution and hydrogen evolution reaction **(Atta *et al*., 2008).**

Rp values

The current-potential plots recorded at the vicinity of the corrosion potential to determine the polarization resistance. The polarization resistance (R_p) (Table 27) was calculated using the Stern-Geary equation **(Stern and Geary, 1957).**

$$R_p = \frac{b_a b_c}{2.303 icorr(b_a + b_c)} \quad (24)$$

Where, b_a and b_c are the slopes of the anodic and the cathodic Tafel lines, respectively.

This equation clearly indicates that R_p values are inversely proportional to the I_{corr} values. When the polarization resistance values are observed from Table 27, it increases with increasing the inhibitor concentration which leads to a decrease of I_{corr} values. Increase in R_p imparts higher protection of the interface against reactions associated with metal dissolution.

Effect of concentration on IE derived from I_{corr} and R_p of PVA-AAm-PVBS

In all cases, the IE depends primarily on the concentration and molecular structure of the inhibitors considered. As discussed earlier, both anodic and cathodic reactions of mild steel corrosion were inhibited by increasing the concentration of the polymeric inhibitors. This indicates that the inhibiting effect of the studied polymers on the mild steel corrosion can be related to its adsorption on the steel surface which is favoured with increase in concentration. Some authors **(Okafor and Zheng, 2009; Lorenz and Mansfeld, 1985; Cao, 1996)** classify the modes of the inhibition effect of inhibitors into three categories:1) Geometric blocking effect of adsorbed inhibitive species, 2) Active sites blocking effect by adsorbed inhibitive species, and 3) Electro-catalytic effect of the inhibitor or its reaction products.

From all the obtained results, we can conclude that the investigated polymers acts via the geometric blocking effect, i.e. by blocking the reaction sites on the MS surface without getting involved in the anodic and cathodic reaction process. This represents that more activation energy is required for oxygen and hydrogen reduction when the polymer concentration increases. Hence, there is a definite decrease in the anodic dissolution of the MS, and both oxygen reduction and hydrogen evolution reactions were retarded.

4.4.1.2 Effect of immersion temperature on polarization behaviour of PVA-AAm-PVBS

The effectiveness of the various concentrations of the inhibitor PVA-AAm-PVBS at various temperatures on polarization behaviour of MS in HCl has been studied. Figure 29 is the polarization behaviour of MS in HCl in the presence of 0.45 wt.% optimum concentration of PVA-AAm-PVBS at 303 K-343 K.

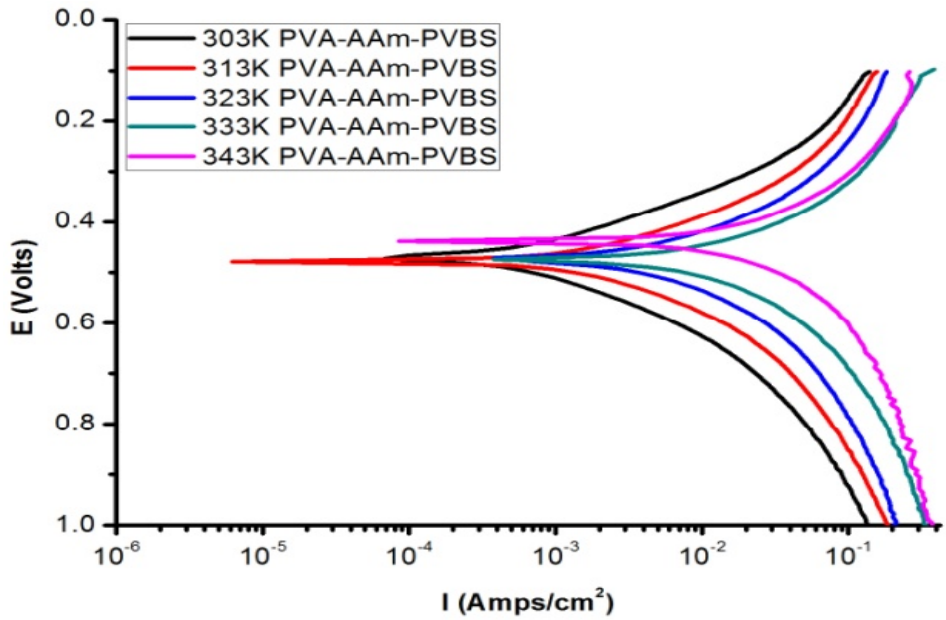

Figure - 29 Potentiodynamic Polarization curves of MS in 1 M HCl in the absence and in the presence of 0.45 wt.% of PVA-AAm-PVBS at various temperatures

When both the cathodic and anodic regions of the Tafel curves are observed, the current density decreases with increasing temperatures till 323 K and then slightly increases. The Tafel plot obtained in the presence of 0.45 wt.% of the inhibitor also show a parallel shift with rise in temperature. The parallel nature of the current-potential curves, indicates that hydrogen evolution reaction is activation controlled. There is no notable shift in corrosion current till 323 K but at higher temperatures the Tafel lines are shifted to the anodic region indicating increased corrosion process. The linearity of the Tafel lines is maintained with different slope values at all the temperature studied. This indicates that the adsorption of the inhibitors in the electrical double layer does not affect the mechanism of the process irrespective of the temperature. When the anodic region is observed, there is no evidence for any passive film formation either in presence or absence of the inhibitors.

The b_a and b_c values in Table 27 show deviations from the expected Tafel behaviour in the cathodic and anodic region at the temperatures studied. The deviation of b_a and b_c from the mentioned values shows that the number of the electrons involved in the reaction is increased due to complexity of the corrosion process with rise in temperature for both the inhibited and uninhibited solutions **(Popova *et al*., 2007).** However, both anodic ad cathodic slopes are affected equally at the temperatures studied which show the mixed type inhibitory action of the inhibitor.

The average value of E_{corr} observed was -0.48 V to -0.43 V for the studied temperature range, which is in agreement with corrosion potential observed by other authors for mild steel corrosion in HCl. In the present study, the corrosion potential values remain almost same or undergo a slight shift among various concentrations of the inhibitor till 323 K. But a pronounced shift in anodic direction is observed for inhibitor concentrations at 333 K and 343 K. The displacement in the E_{corr} values is less than 85 mV till 323 K which is an indication of mixed type inhibitory action of the inhibitors. But at higher temperatures, the E_{corr} values shifts to positive direction which is an indication that inhibitor molecules are more adsorbed on the anodic sites, resulting in an inhibition of the anodic reactions **(Mistry and Jauhari, 2014),** i,e. the inhibitor tends to show a predominant anodic inhibitory action at higher temperatures.

A notable decrease in the corrosion current density and increase in the polarization resistance was observed at all the temperature domains studied. This indicates that the addition of inhibitor reduces the corrosion current values even at high temperatures. Increase in R_p at higher temperatures is an indication of higher protection of the interface against reactions associated with metal dissolution.

As discussed earlier, both anodic and cathodic reactions of mild steel corrosion were inhibited by increasing the concentration of the polymeric inhibitors. With increase in temperature the IE show a minimal decrease till 323 K and decreases rapidly at higher temperatures. However, a highest efficiency in the range of 90-95 % was observed at 303 K-323 K. At subsequent temperatures, the IE calculated from I_{corr} as well as R_p decreases. This indicates that the inhibiting effect of the studied polymers on the mild steel corrosion can be related to its adsorption on the steel surface which is favoured initially with increase in temperature and then decreases.

4.4.1.3 Effect of immersion time on polarization behaviour of PVA-AAm-PVBS

The polarization curves obtained with three different concentrations (0.03, 0.18 and 0.45 wt.%) each at 5 different immersion times (1,3,6,9,12 h) are shown in the Figures 30(a-c). The cathodic and anodic current densities were significantly decreased in the presence of the inhibitors at all the time intervals studied. A small passivation region is seen at 6^{th}, 9^{th} and 12^{th} hour which ensures the formation of a stable film. The graph recorded to demonstrate the change in I_{corr} values and inhibition efficiency (from I_{corr}) as a function of time shows that with increase in immersion time, the inhibition efficiency decreased till 4^{th} hour and then tries to gets stabilized in the forthcoming hours. The paradigm of inhibition efficiency is in corollary with the passivation region noted in the polarization curves.

The passive region denotes the formation of stable, adherent film on the metal surface which is usually perceived in the coating studies **(Tan and Blackwood, 2003).**

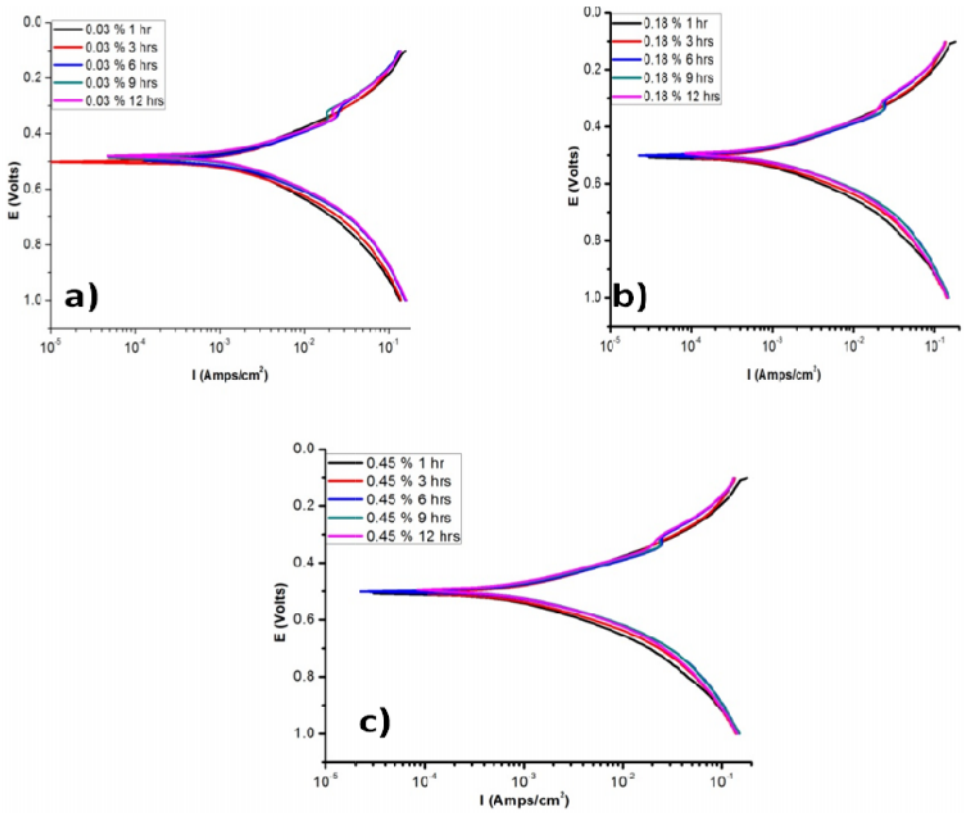

Figure - 30 Potentiodynamic polarization curves of MS in 1 M HCl in the absence and in the presence of a) 0.03 wt.% b) 0.18 wt.% and c) 0.45 wt.%, of PVA-AAm-PVBS at selected time intervals

Hence, the increase in IE_{Icorr} with time is an evidence of formation of adsorbed layer. Furthermore, by increasing immersion time, inhibition efficiency increases and the corrosion rate decreases due to the strong adsorption of the inhibitor. The inhibition efficiency, obtained at all hours of immersion, at the all the studied concentration is more than 80 %. These results confirm a good inhibition effect of the PVA-AAm-PVBS on the corrosion of mild steel.

Figure 31 shows the pattern of I_{corr} and IE values with respect to immersion time for all the concentrations of PVA-AAm-PVBS. The I_{corr} values diminishes with increasing inhibitor concentration with respect to the blank. It is clear that, I_{corr} values in the presence of inhibitor slightly increases till 6^{th} hour of immersion and remains almost same as the time elapses. This increase in the corrosion resistance or inhibitor efficiency with time can be related to the high substitution of inhibitor molecules on the metal surface.

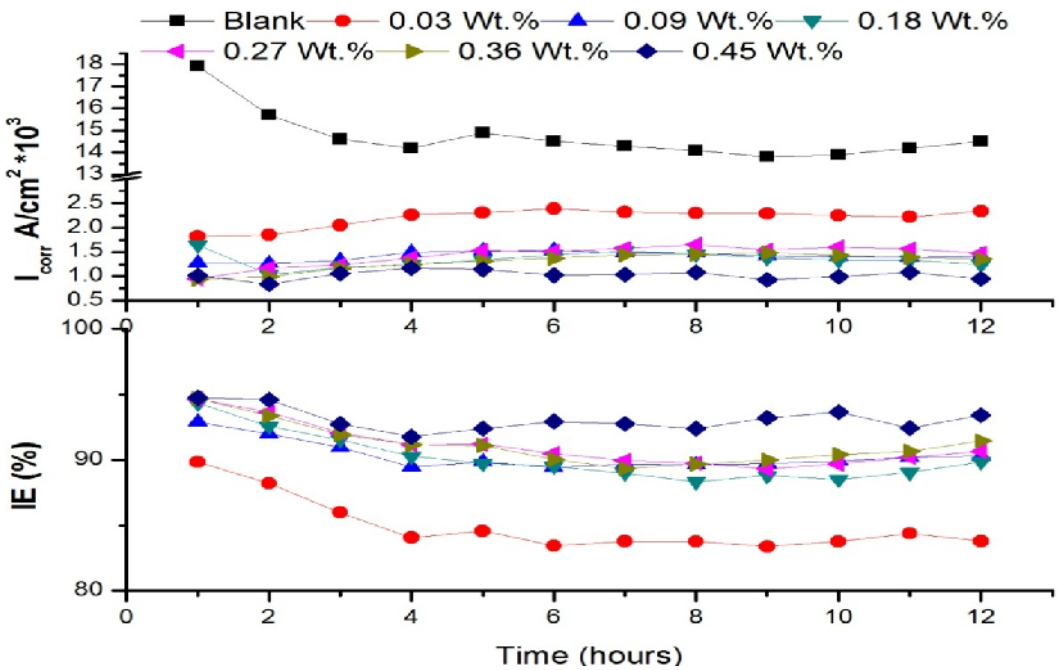

Figure - 31 Change in I_{corr} and IE in the presence and absence of PVA-AAm-PVBS at various time intervals

4.4.1.4 Analysis of polarization behaviour of other investigated terpolymers

The current-potential characteristics of other terpolymers under investigation were analyzed using potentiodynamic polarization measurements. Figures 32(a-d) shows the polarization curves obtained for 0.45 wt.% of PVA-AAm-VSA, PVA-AA-PVBS, PVA-AA-VSA and PVA-VSA-PVBS at various temperatures. From the above discussion, it is understood that concentration has a positive effect on the IE % and a highest IE % is resulted for the optimum concentration (0.45 wt.%). So the polarization data obtained from optimum concentration of the inhibitors at 303-343 K temperature is listed in Table 28.The polarization parameters of all the terpolymers obtained for various concentrations at various temperatures and time intervals are listed in the appendix A(1-4) and A5 respectively.

The current-potential curves (Figure 32) show linear Tafel lines with different slope values at various temperatures studied. This indicates that the adsorption of the inhibitors in the electrical double layer does not affect the mechanism of the process. When the anodic region is observed, there is no evidence for any passive film formation either in presence or absence of the inhibitors. Anodic and cathodic slopes are equally affected and decreased significantly in the presence of inhibitors when compared with that of blank **(Elayyachy *et al*., 2005).** This behaviour suggests that all used inhibitors have inhibition effect on both cathodic and anodic reactions of the corrosion process and can be categorised as mixed type inhibitor.

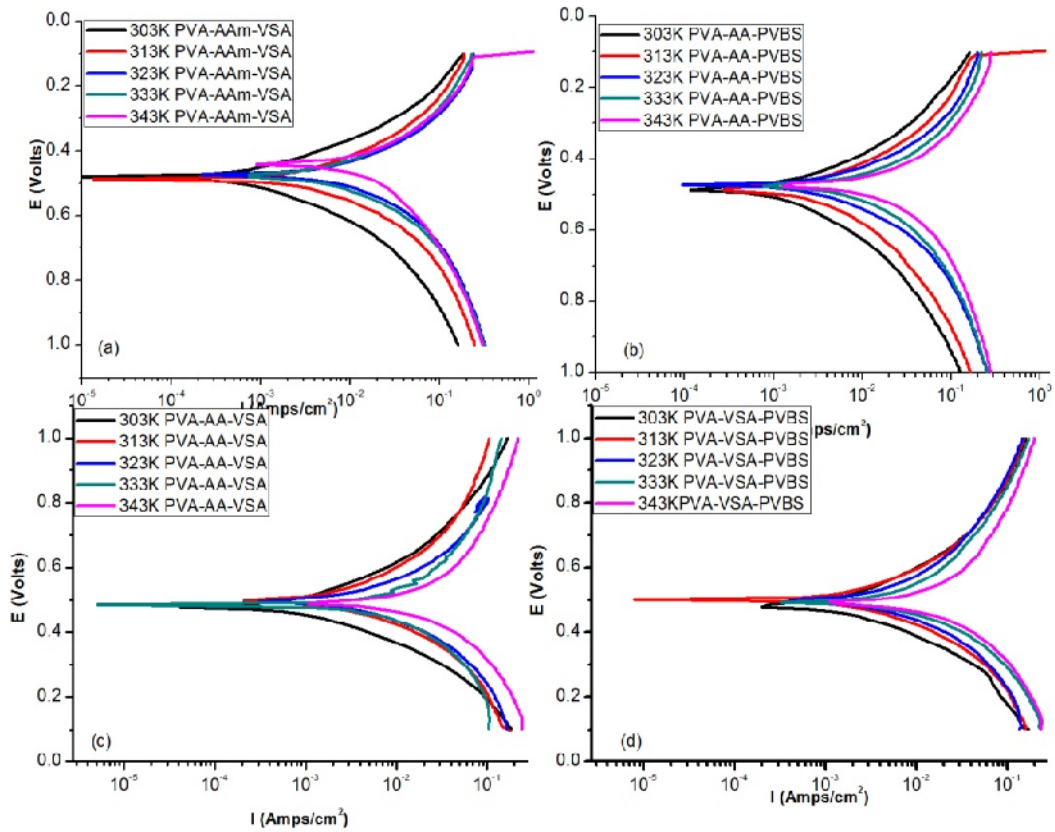

Figure – 32 Potentiodynamic polarization curves of MS in 1 M HCl in the absence and in the presence of 0.45 wt.% of a) PVA-AAm-VSA ;b)PVA-AA-PVBS;C) PVA-AA-VSA; and d) PVA-VSA-PVBS at 303 K-343 K

From the Table 28 it is noted that the corrosion potential values remain almost the same or slightly shifted in both the directions for all the polymers except PVA-VSA-PVBS which is shifted cathodically at all temperatures **(Amin *et al*., 2010).** The relation between the inhibition efficiency and the shift/changes in corrosion potential can be explained as follows **(Herrasti and Ocon, 2001):** the anticorrosion ability of the inhibitors to some extent is due to capability of the inhibitors to displace the electroactive interface from its original localization (metal/solution interface). This will lead to an electrical potential drop at the polymer/solution interface. But there will be almost no potential drop that occurs at the metal/polymer interface. If there is no potential drop, there will be no driving force for metal oxidation. Hence a better inhibition of corrosion can be expected for polymer which is rich in availability of Pi-electrons. Moreover polymers being larger moieties impart a highest surface coverage of the metal surface with which various types of interactions can be established. But the PVA-VSA-PVBS inhibitor displaces the E_{corr} to cathodic direction indicating that it controls cathodic reactions more predominantly than the anodic reaction. However, In the present study the

displacement in the E_{corr} values with respect to the blank HCl is less than 85 mV which is an indication of mixed type inhibitory action of the inhibitors.

Table – 28 Polarization parameters of MS in 1 M HCl containing 0.45 wt.% of investigated terpolymers at 303 to 343 K: Blank(I); PVA-AAm-VSA(II); PVA-AA-VSA(III); PVA-AA-PVBS(IV); PVA-VSA-PVBS(V)

Temp (K)	Conc. (wt.%)	(I)		(II)		(III)		(IV)		(V)	
E_o (V)	303 K	-0.4842		-0.4798		-0.4798		-0.4853		-0.5009	
	313 K	-0.4805		-0.4884		-0.4984		-0.4849		-0.5012	
	323 K	-0.4671		-0.4761		-0.4967		-0.4732		-0.4981	
	333 K	-0.4840		-0.4723		-0.4841		-0.4755		-0.4929	
	343 K	-0.4853		-0.4400		-0.4894		-0.4743		-0.4910	
b_a and b_c (mV)		b_a					b_c				
		(I)	(II)	(III)	(IV)	(V)	(I)	(II)	(III)	(IV)	(V)
	303 K	220	126	131	156	151	269	150	159	209	183
	313 K	298	181	170	174	166	316	184	225	235	201
	323 K	327	209	193	17.	210	355	215	216	211	287
	333 K	373	220	323	242	230	421	238	359	323	431
	343 K	923	318	358	315	340	579	548	551	434	621
I_o (mA/cm^2) % IE $_{Io}$		I_{corr}					% IE $_{Icorr}$				
		(I)	(II)	(III)	(IV)	(V)	(I)	(II)	(III)	(IV)	(V)
	303 K	15.3	1	1.2	2	1	-	93.3	92.1	87.1	84.9
	313 K	37.2	3.1	3.8	4.2	3.1	-	91.7	89.9	88.6	90.5
	323 K	65.9	9.2	7.9	6.6	9.2	-	86.0	88.1	90.0	88.5
	333 K	120.4	17.3	15.6	17.1	17.3	-	85.7	87.1	85.8	84.8
	343 K	231.7	33.8	47.7	55.2	51.0	-	85.4	85.0	82.6	83.9
R_p Ωcm^2 % IE R_p		R_p					% IE $_{Rp}$				
		(I)	(II)	(III)	(IV)	(V)	(I)	(II)	(III)	(IV)	(V)
	303 K	16.4	122.0	127.0	96.0	173.8	-	86.6	87.2	82.9	90.6
	313 K	7.8	38.3	54.2	65.5	80.0	-	79.6	85.6	88.1	90.3
	323 K	3.3	15.3	18.3	59.5	18.8	-	78.2	81.8	94.4	82.3
	333 K	2.6	11.2	13.8	11.2	12.9	-	76.4	80.9	76.6	79.6
	343 K	1.4	5.5	4.9	5.6	5.36	-	74.7	72.0	75.5	74.2

Analysis of data from Table 28 reveals the positive influence of temperature on IE (IE_{Icorr} and IE_{Rp}) till 323 K for PVBS containing polymers (i.e. PVA-AA-PVBS and PVA-VSA-PVBS), and negative influence of temperature on the IE % of PVA-AAm-VSA and PVA-AA-VSA. This shows that the IE of terpolymers containing grafted PVBS affords a better and stable adsorbed film till 323 K. In the static immersion studies, a better inhibition is obtained

at 333 K but in potentiodynamic polarization a better IE is obtained at 323 K for PVBS-containing polymers. With respect to other polymers, the IE is definitely decreased with increase in temperature. The decrease in IE is due to the disturbed stability of the adsorbed film on the metal surface due to the induced polarization combined with high temperature. However, PVBS-containing polymers have additional pi-electron clouds of benzene ring, which can extend linkages with empty d-orbital of the metal, so they impart increased IE till 323 K. Though both the PVBS containing polymer follow the same trend, PVA-AAm-PVBS provides a slightly higher IE of 92 % at 323 K, and PVA-AA-PVBS provides 89.9 K% at 323 K.

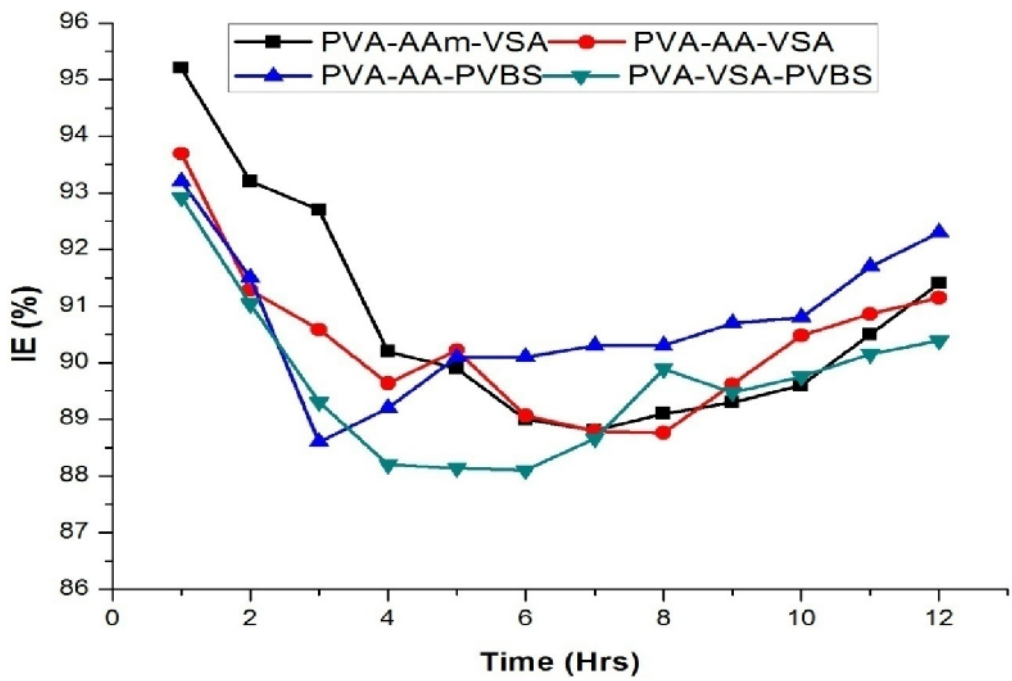

Figure - 33 Trend in IE_{corr}% obtained for PVA-AAm-VSA, PVA-AA-PVBS, PVA-AA-VSA and PVA-VSA-PVBS for 12 hours.

The inhibitive property of the PVA-AAm-PVBS can mainly be attributed to the presence of nitrogen atom coexisting with π-electron clouds which is absent in PVA-AA-PVBS. After all, the longer molecular size ensures the greater adsorption on the MS steel surface and decreases the effective area for corrosion reaction by blocking the reaction sites.

Effect of immersion time: In order to study the current-potential behaviour of the MS in HCl in the presence and absence of terpolymers (PVA-AAm-VSA, PVA-AA-VSA, PVA-AA-PVBS and PVA-VSA-PVBS) at various time intervals. The I_{corr} values and corresponding IE of the investigated terpolymers are presented in appendix A5. Figure 33 shows the trend

in IE_{corr}% obtained for PVA-AAm-VSA, PVA-AA-PVBS, PVA-AA-VSA and PVA-VSA-PVBS with time. The results show that immersion time influences the I_{corr} values and therefore the inhibitive behaviour of the terpolymers under investigation. IE_{corr} % of all the polymers were found to decrease initially till 5 to 7 cycles followed by an increase in the forthcoming hours. This behaviour may be correlated to the formation of adherent film by inhibitor molecules as the time elapses. This is an evidence that the inhibitor tries to form a film initially and then tends to achieve stability. With elapsing time terpolymer molecules adsorb or agglomerate at the surface such that they create no other inhibitive layer **(Azghandi *et al.*, 2013).** Nevertheless, the IE values lay around 86-95 % which shows that the inhibitors have good corrosion mitigating property.

4.4.2 Electrochemical impedance measurements

Electrochemical impedance spectroscopy (EIS) has established itself as a corrosion protection tool for more than two decades and can be considered as the most useful technique presently available. EIS is usually measured by applying an AC potential to an electrochemical cell and then measuring the response in the form of an AC current signal. The AC voltage (10 mV-100 mV) is applied in the form of sinusoidal wave in a wide frequency range, from 10^5 to 10^{-3} Hz. The EIS method is advantageous because it is non-destructive, provides time-dependant data and can be used on even high resistant materials like coatings and paints, and can be applied even to low conducting solutions.

The Ohm's law in the case of DC potential is given as: E=iR, i is the current and R is the resistance. In the case of AC potential: E=iZ: Z is the impedance. Unlike resistance, Z is represented in the form of a complex number.

$$Z(\omega)=E/I; \quad (25)$$

$$Z_o \exp(j\varphi) = Z(\cos\varphi + j\sin\varphi) \quad (26)$$

From the equation 26, we notice that Z is composed of a real and an imaginary part. When real part is plotted in the X-axis and imaginary part is plotted in the Y-axis, we get a Nyquist plot. The Nyquist plot can be represented using an equivalent electric circuit model and is called as Randle's circuit. The circuit has to be designed with different elements like resistor, capacitor and inductor.

Resistor	E=iR	Z=R
Inductor	E=L di/dt	Z=jwL
Capacitor	E= C dE/dt	Z=1/jwC

When phase angle between the applied voltage and current induced is 0 pure resistance operates, when the phase angles is 90^o pure capacitance operates. In angles between these values, both resistance and capacitance operates. One disadvantage with the Nyquist plot is we cannot measure the frequency at each point. Hence it is necessary to plot log of absolute value of impedance in the X-axis and phase shift in Y-axis as a function of frequency, and is called as Bode plot. From the Bode plot frequency information can be acquired.

The equivalent circuit (EC) is generally modelled with a resistor, capacitor and inductor. For iron dissolution in acid, the EC is designed with a resistor and capacitor in parallel with each other. Three types of resistances can be taken into account: solution resistance, polarization resistance or charge transfer resistance. Solution resistance is the ionic solution resistance which depends upon ionic concentration, type of ions, temperature and geometry of the area in which current is carried. The interface of metal in electrolyte is envisioned as space that exists between array of ions on the electrode surface and array of solvated ions away from surface. The two array of ions can store charge in them and acts as a capacitor element. The capacitance thus generated is called the double layer capacitance, C_{dl}. The double layer capacitor can also lead to a resistor providing charge transfer resistance, as the charge is transferred during the metal dissolution. The C_{dl} values were calculated at the frequency f_{max}, at which the imaginary component of the impedance is maximal (Z'') by the following equation:

$$Cdl = \frac{1}{2\pi fmax} R_{ct} \tag{27}$$

The Nyquist Plot for Randle's cell consisting of the above elements is always semicircle. The solution resistance can be determined from the real axis value at the high frequency intercept. This is the intercept near the origin of the plot. The low frequency region gives us the sum of solution resistance and polarization resistance.

4.4.2.1 Effect of concentration on the impedance behaviour of PVA-AA-PVBS

The effects of the inhibitor concentration at 303 K on impedance behaviour of MS in HCl have been studied. Nyquist plot and representative Bode diagram for MS in HCl in the presence of various concentrations of PVA-AA-PVBS are shown in Figure 34. Table 29 represents the list of electrochemical parameters obtained by fitting the data in a Randle's circuit (inset) as shown in Figure 34.

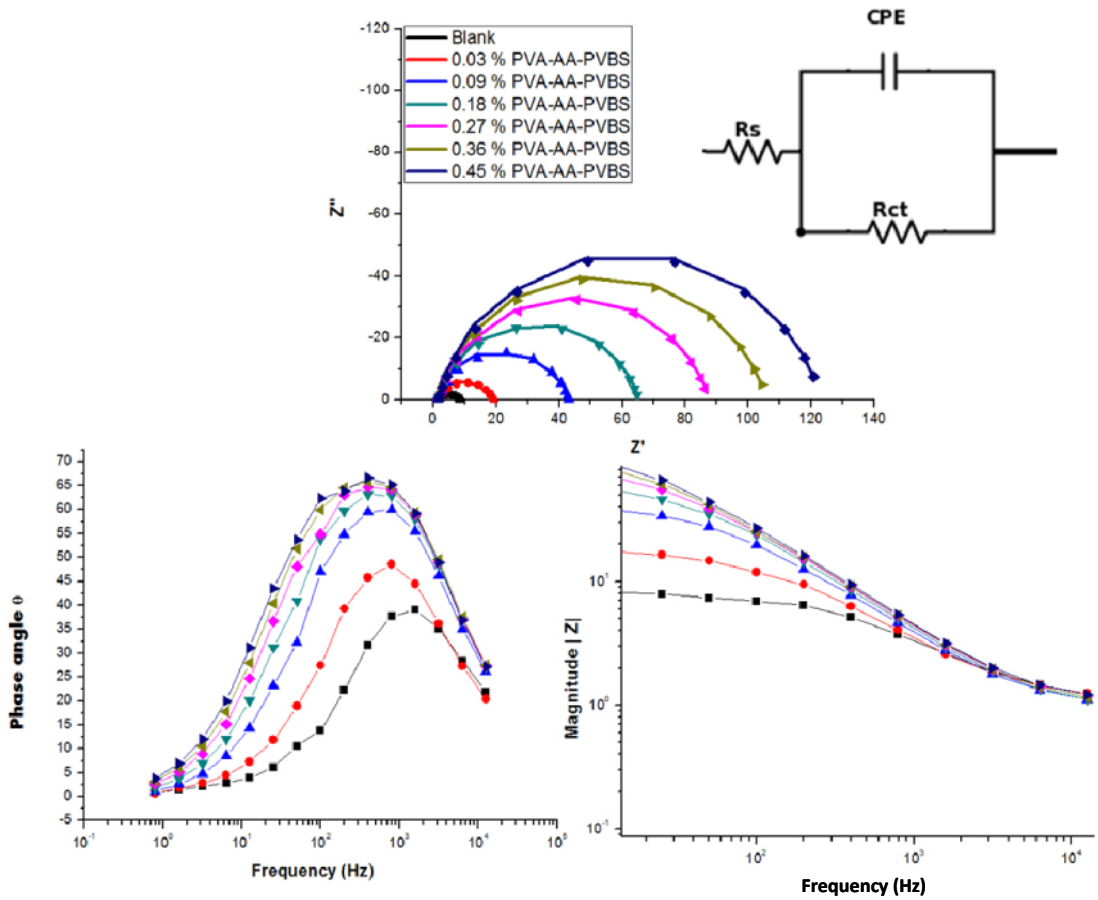

Figure – 34 Nyquist plot, Phase angle plot & Bode plot for MS in 1 M HCl in the presence and absence of various concentrations of PVA-AA-PVBS fitted using the equivalent circuit (inset) ●fit data; ── fit circle

Nyquist plot depicts a set of depressed capacitive loops generated for MS in blank HCl and inhibitor added HCl. This depression at the high frequency region is a characteristic electrochemical corrosion reaction **(Torres *et al*., 2014).** The solid electrodes are usually affected by these inhomogeneities and the resultant effect is termed as frequency dispersion effect **(Ghailane *et al*., 2013; Chen *et al*., 2011).** All the semicircles are single capacitive loop and similar in shape suggesting the geometric blocking effect of the inhibitor **(Bentrah *et al*., 2014)**. These similar shapes of the semicircles can also be attributed to the unmodified mechanism of the corrosion process before and after the addition of inhibitor. The addition of inhibitor pose no changes in the shape of the impedance indicating the activation-controlled nature of the reaction during charge transfer process **(Torres *et al*., 2014)**. But the effect of addition of the inhibitor is reflected as increase in diameter of the semicircle which takes place constantly at each level of inhibitor addition. The increase in diameter of the impedance at increasing concentration of the inhibitor augment the charge transfer resistance as well as the inhibition effect of the polymer **(Chen *et al*., 2011).**

Table - 29 Impedance parameters of the MS in 1 M HCl containing various concentrations of PVA-AA-PVBS at 303 to 343 K calculated from extrapolation of the Tafel lines

Temp. K	Conc. Wt.%	R_s Ωcm^2	Yo* 10-6	n	R_{ct} $k\Omega cm^2$	IE_{Rct} (%)	C_{dl} $*10^3$ μFcm^{-2}	Surface coverage (θ)
303 K	Blank	0.544	606.4	0.794	6.853	-	9.98	-
	0.03	1.018	305.1	0.831	17.91	61.74	8.98	0.10
	0.09	0.858	190.6	0.839	42.02	83.69	2.85	0.71
	0.18	0.854	165.6	0.834	63.99	89.29	1.18	0.88
	0.27	0.881	164.9	0.836	86.26	92.06	0.98	0.90
	0.36	0.874	161.3	0.837	104.5	93.44	1.10	0.89
	0.45	0.921	157.0	0.794	122.2	94.39	1.09	0.89
313 K	Blank	0.771	546.7	0.749	4.135	-	1.08	-
	0.03	0.446	197.2	0.866	29.01	85.75	0.72	0.33
	0.09	0.296	169.8	0.874	42.11	90.18	0.75	0.30
	0.18	0.228	152.8	0.883	52.12	92.07	0.61	0.43
	0.27	0.466	179.1	0.856	61.02	93.22	0.50	0.54
	0.36	0.586	188.1	0.849	66.03	93.74	0.85	0.21
	0.45	0.226	161.3	0.872	66.88	93.82	0.10	0.91
323 K	Blank	0.751	1236.1	0.684	2.264	-	48.10	-
	0.03	0.659	273.6	0.807	14.31	84.18	1.97	0.96
	0.09	0.602	243.3	0.814	22.5	89.94	1.75	0.96
	0.18	0.602	240.8	0.811	26.33	91.40	1.85	0.96
	0.27	0.638	218.7	0.819	29.68	92.37	1.51	0.97
	0.36	0.678	228.8	0.814	32.27	92.98	1.75	0.96
	0.45	0.743	217.5	0.819	33.83	93.31	1.55	0.97
333 K	Blank	0.552	894.0	0.756	1.42	-	8.93	-
	0.03	0.527	530.9	0.822	3.32	57.16	2.68	0.70
	0.09	0.717	486.3	0.833	4.20	66.12	2.24	0.75
	0.18	0.648	550.2	0.821	5.05	71.84	3.11	0.65
	0.27	0.603	521.3	0.827	5.59	74.57	2.77	0.69
	0.36	0.666	551.9	0.822	5.79	75.45	3.17	0.65
	0.45	0.574	546.2	0.824	5.90	75.88	3.05	0.66
343 K	Blank	0.729	883.2	0.723	0.69	-	10.04	-
	0.03	0.527	710.8	0.822	1.73	60.03	3.33	0.68
	0.09	0.500	691.7	0.827	2.27	69.42	3.24	0.69
	0.18	0.395	716.1	0.823	2.74	74.70	3.67	0.65
	0.27	0.406	637.6	0.837	3.01	76.98	2.77	0.73
	0.36	0.411	685.9	0.832	3.22	78.48	3.26	0.69
	0.45	0.431	714.3	0.830	3.17	78.17	3.49	0.66

The Bode plot is used to verify the results acquired from the Nyquist plots, and the frequency of every data point can be identified. The Bode-phase diagram consists of a single wave crest and all the curves lie above the zero degree phase angle. The recorded Bode plot lies in the frequency range of 10^0-10^4 Hz. The shapes of the Bode plots for both the inhibited electrodes and uninhibited electrode are similar. This phenomenon reveals that the presence of the inhibitor increases the charge transfer impedance by forming a protective layer on the MS surface, but it does not change other aspects of the corrosion behaviour **(Chen *et al*., 2011).**

Bode plot plotted using Z_{mod} can be explained by dividing the curve into three frequency regions: low, middle and high frequency phase angle ranges **(Hegazy *et al*., 2012)**. The high frequency phase angle range (10^4–10^3 Hz) of the impedance spectra relates to the properties of an outer layer, the middle frequency range (10^3–10^2 Hz) represents the properties of an inner barrier layer, and the low frequency range (10^0-10^2 Hz) provides details of the electrical-double layer **(Duan *et al.,* 2006).** So the high frequency region denotes the increase in thickness of the adsorbed outer porous layer. Therefore, the high frequency region can be attributed to the ohmic resistance of the films of corrosion product and the electrolyte, middle frequency region can be ascribed to the inclusion of chloride ions and water through the defect of the adsorbed inhibitor inner barrier layer **(Hegazy *et al*., 2012).** When the phase angle is -90^o the system behaves as an ideal capacitor. A phase angle of around -75^o is obtained for highest concentration of the inhibitor which is another evidence of non-ideal behaviour of the electrochemical system. The more the negative phase angle, more is the capacitive behaviour of the system. In the high frequency region, the values of log|Z| and phase angle shows the resistive nature of MS electrode with respect to the solution resistance that prevail between the reference and working electrodes **(Ansari *et al*., 2014).**

In the figure recorded at 303 K, it can be noticed that the Z_{mod} increases with respect to the concentration confirming the highest inhibition efficiency of the polymer. The Z_{mod} is drastically improved for concentration ranging more than 0.03 wt.% of the inhibitor. Similarly the phase angles of the Bode plot increases as the concentration increases at 303 K. This is again an evidence for the increased surface coverage of inhibitor with respect to concentration.

Introduction of CPE element, and fitting the data in an equivalent circuit

The Nyquist plots as discussed above are not ideal plots as described in the theoretical point of view. This is because the double layer does not behave as an ideal capacitor. Usually at the metal/solution interface, the charge transfer reaction is controlled by

the charges from the metal side and ions from the solution side. The presence of ions in electrolyte is plenty than the charges present on metal. Hence the equivalent ions to the charges on the metal occupy a huge volume in the double layer from the solution side of the interface. This characteristic behaviour deviates the double layer from an ideal capacitive behaviour, and therefore double layer capacitance values are replaced by a constant phase element CPE **(Hegazy *et al*., 2012).** The use of CPE is generally required for the distribution of relaxation time arising as a result of inhomogeneity, roughness, adsorption or diffusion at micro and nano level of the metal surface **(Navvaro-Flores *et al*., 2005)**. All EIS data were analysed by fitting into the equivalent circuit shown in Figure 35.

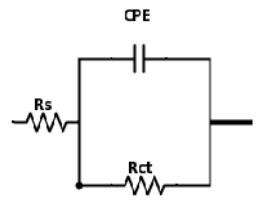

Figure - 35 Equivalent circuit used for fitting the data

Where R_s is the solution resistance and R_{ct} is the charge transfer resistance. Double layer capacitance associated with the CPE element is calculated using the following formula:

$$CPE_{dl} = (Y_o.R_{ct}1\text{-}n)^{1/n} \quad (28)$$

Where Y_o is the magnitude of the CPE, and n value is a parameter that quantifies surface phenomena like surface inhomogeneities resulting from surface roughness, inhibitor adsorption, porous layer formation, etc. The n value usually lays around -1 to 1. When n value is 1, 0 or -1 it corresponds to the capacitance (C), resistance (R) or inductance (L) respectively. For other values, n approximately describes combination of the C, R and/or L of the frequency distribution behaviour **(Lebrini *et al*., 2007).**

The charge transfer resistance values increased from 7**Ω** cm^2 to 122 **Ω** cm^2 at 303 K for the concentration ranging from 0.03 wt. % to 0.45 wt.% of PVA-AA-PVBS. This shows the adsorption of the inhibitor on the metal surface and decrease in the reaction rate of charge transfer reaction. The double layer capacitance values for inhibitor-added solution are comparatively lesser than that of inhibitor-free solution. The decrease in C_{dl} values is attributed to the formation of a protective layer on the surface. The decrease of C_{dl} and increase in surface coverage can be proved by the parallel-plate model **(Chen *et al*., 2011; Bockris and Reddy, 1972).** According to the parallel-plate model, the C_{dl} is given as follows:

$$C_{dl} = \varepsilon/4\pi d \quad (29)$$

where C_{dl} is the capacitance per unit area of the parallel-plate capacitor, d is the distance between the capacitor plates, and e is the dielectric constant of the materials between the plate. According to the equation, if the water molecules and other ions are gradually replaced by larger polymeric inhibitor molecules through adsorption, dielectric constant decreases with increase in the thickness of the electrical double layer **(Bentiss et al., 2004)** resulting in decreased C_{dl} values. The values of heterogeneity factor n range from 0.79-0.84 at 303 K. The changes of n value does not vary significantly and its ongoing stability with inhibitor addition accounts for the charge-transfer controlled dissolution mechanism of MS in HCl medium **(Ansari *et al*., 2014).**

4.4.2.2 Effect of immersion temperature on the impedance behaviour of PVA-AA-PVBS

The effects of the inhibitor concentration at various temperatures on impedance behaviour of MS in HCl have been studied. Figure 36 is the impedance behaviour of MS in HCl in the presence of 0.45 wt.% optimum concentration of PVA-AA-PVBS at 303 K-343 K. The Nyquist plot at various temperatures is a set of depressed capacitive loops which are due to the frequency dispersion effect **(Ghailane *et al*., 2013).** The shape of the semicircles are not affected with increasing temperature suggesting the geometric blocking effect of the inhibitor and unmodified mechanism of the corrosion process.

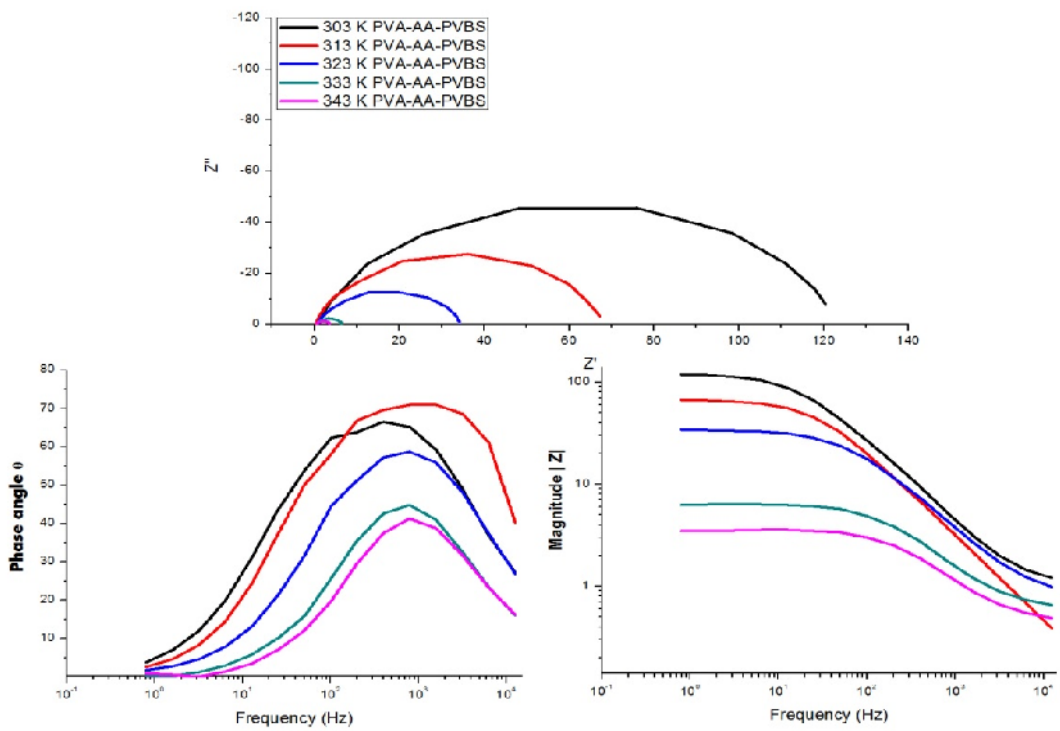

Figure - 36 Nyquist plot , Phase angle plot & Bode plot for MS in 1 M HCl in the presence and absence of 0.45 wt.% of PVA-AA-PVBS at various temperatures

In the figure recorded for optimum inhibitor concentration at different temperatures 303-343 K, Z_{mod} decreases and phase angles gets depressed with increase in temperature. This shows that the thickness of the outer porous layer of the inhibitor is decreased at high temperatures thereby furnishing decreased protection effect. This is an evidence for the desorbed or deprived adsorption of film at higher temperatures. The impedance data were fitted into the equivalent circuit same as that used for fitting the data at 303 K, and the parameters R_s, R_{ct} and C_{dl} were obtained.

Analysis of Table 29 shows that the values of heterogeneity factor n range from 0.80-0.88 at higher temperatures. The increase in n value with increase in temperature is an indication of the homogeneous metal surface due to the adsorption of the inhibitor **(Morad and El-Dean, 2006)**. The double layer capacitance values for inhibitor-added solution are comparatively lesser than that of inhibitor-free solution at all the temperatures studied denoting the protective ability of the inhibitor. With rise in temperature R_{ct} values tend to decrease, but still the IE_{Rct} shows no appreciable change till 323 K and then decrease.

4.4.2.3 Effect of immersion time on the impedance behaviour of PVA-AA-PVBS

Electrochemical impedance analysis is a useful technique for studying the effect of immersion time because it does not perturb the system significantly and helps to follow the behaviour of the system over time **(Moretti *et al*., 2004).** The effectiveness of PVA-AA-PVBS was ensured by recording EIS spectra for every 1 hour for 12 hours. Nyquist plots for MS in 1M HCl in the presence of 0.03, 0.18 and 0.45 Wt.% of PVA-AA-PVBS, for different immersion times (1, 3, 6, 9 and 12 hours) are shown in Figure 37.

The equivalent circuit used for fitting the experimental data obtained for 1,3,6,9,12 hours were the same as that used in previous section (Figure 35). From the shape of the obtained Nyquist plots, it is worth noting that the curves are approximated by single capacitive semicircles, indicating that the corrosion process was mainly charge-transfer controlled and also there is almost no change in the corrosion mechanism for various immersion times or to the inhibitor addition. The diameter of the semicircles is maintained approximately the same during 1-6 hrs for 0.45 % concentration of the inhibitor which can be accounted to the formation of a protective film and the continued improvement in the protectiveness of this film. The magnitude of impedance then decreases after 6 hrs immersion time due to desorption of the film **(Jiang *et al.,* 2006*).*** Figure 36 shows the change in R_{ct} values and C_{dl} values with immersion time. From the figures it is clear that for lowest concentration of inhibitor studied, the R_{ct} of the Nyquist plot increases till 3rd hour and then decreases during the consecutive hours of immersion. For the 0.18 wt.% concentration,

this behaviour slightly changes, the diameter and R_{ct} values increases till 6 hours and then decrease. For highest concentration studied, the time dependency provided a positive effect on diameter and R_{ct} values for all the hours of immersion considered.

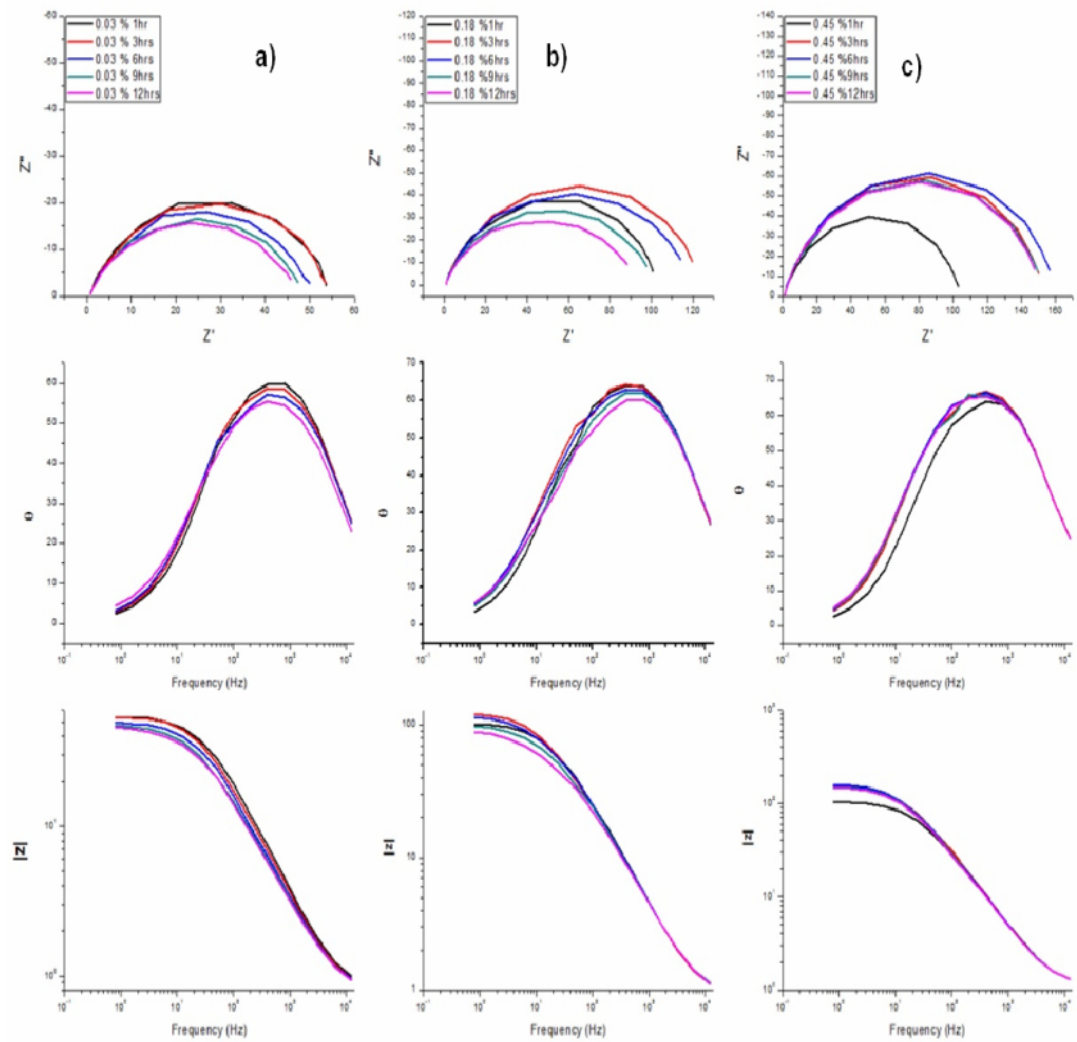

Figure-37 a) Nyquist plot; b) & c) Bode plot for MS in 1 M HCl in the presence and absence of 0.45 wt.% of PVA-AA-PVBS at various temperatures.

From the time dependant behaviour studied, it is understood that concentration plays an important role. Due to the increase in availability of hetero atoms with increase in concentration, effective surface coverage is favoured in highest concentration, followed by a slower and smaller change with time. As the immersion of time increases the charge transfer resistance decreases in the case of lowest concentration and the electrode becomes less passive **(Rosliza *et al*., 2008).** This behaviour is entirely opposite for highest concentration studied.

Table - 30 Impedance parameters of MS in 1 M HCl containing 0.03, 0.18 and 0.45 wt.% of PVA-AA-PVBS at 1-12 h of immersion time

PVA-AA-PVBS	Time in hrs	R_s Ωcm^2	Y_o* 10-6	n	R_{ct} $k\Omega cm^2$	IE R_{ct}	C_{dl} $*10^3$ μFcm^{-2}
0.03 Wt.%	1	0.7416	247.3	0.8063	54.39	80.7	1.76
	2	0.7105	265.7	0.8024	57.34	79.1	2.47
	3	0.7028	306.5	0.7889	54.78	76.0	3.09
	4	0.6992	333.3	0.7822	53.21	74.7	3.55
	5	0.6881	372.2	0.7720	52.32	74.4	4.00
	6	0.6868	371.6	0.7738	50.59	73.3	3.48
	7	0.6864	401.9	0.7667	49.34	73.0	3.64
	8	0.6962	388.4	0.7721	48.68	72.2	3.90
	9	0.6756	448.6	0.7580	48.11	72.0	4.37
	10	0.6829	456.8	0.7579	47.27	71.2	7.01
	11	0.6858	458.2	0.7586	46.36	70.6	7.40
	12	0.6845	482.3	0.7538	46.42	71.1	7.65
0.18 Wt.%	1	0.8266	187.4	0.8149	102.5	89.7	1.51
	2	0.7952	209.3	0.8036	116.8	89.7	2.05
	3	0.7847	224.8	0.7960	123.1	89.3	2.10
	4	0.7778	235.7	0.7910	121.5	88.9	2.18
	5	0.7656	242.5	0.7862	123.0	89.1	3.01
	6	0.7689	231.8	0.7902	115.9	88.3	3.26
	7	0.7640	237.0	0.7881	109.7	87.9	4.14
	8	0.7657	243.9	0.7850	102.1	86.8	4.06
	9	0.7584	254.5	0.7808	98.1	86.3	5.72
	10	0.7322	297.7	0.7644	94.8	85.6	5.02
	11	0.7266	302.3	0.7617	90.7	85.0	6.37
	12	0.7258	308.7	0.7608	88.2	84.8	6.34
0.45 Wt.%	1	1.0230	150.5	0.8301	103.7	89.9	1.09
	2	1.0350	139.7	0.8384	137.8	91.3	0.94
	3	1.0240	141.9	0.8368	153.3	91.4	1.00
	4	1.0210	148.2	0.8322	159.4	91.6	1.13
	5	1.0100	153.0	0.8325	163.0	91.8	1.17
	6	1.0230	151.6	0.8368	160.6	91.6	1.09
	7	1.0230	152.2	0.8317	162.0	91.8	1.18
	8	1.0120	153.5	0.8267	159.6	91.5	1.28
	9	1.0230	158.6	0.8267	153.0	91.2	1.32
	10	1.0160	163.9	0.8234	152.8	91.1	1.44
	11	1.0120	167.3	0.8242	146.3	90.7	1.44
	12	1.0120	169.5	0.8205	152.7	91.2	1.57

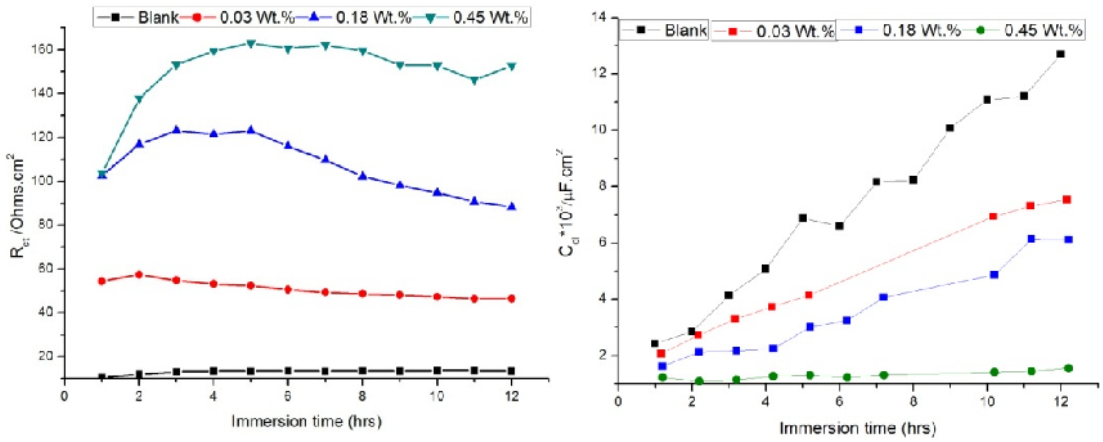

Figure - 38 Change in R_{ct} and C_{dl} values with respect to immersion time for selected concentrations of PVA-AA-PVBS

Figure 38 shows the pattern of R_{ct} and C_{dl} values with respect to immersion time for selected concentrations of PVA-AA-PVBS. It is clear that, R_{ct} values for 0.03 wt.% does not show an appreciable change with increase in time of immersion. But at higher concentrations the R_{ct} values increases till 6th hour and then decreases. For optimum concentration studied, even after the 6th hour the decrease in R_{ct} values are less pronounced. The C_{dl} values increase with respect to time for 0.03 and 0.18 wt.% concentration, and remains almost same for highest concentration studied. This indicates the quality of the inhibitor film formed on the MS surface with time at optimum concentration. The change in the R_{ct} and C_{dl} values is due to the replacement of water molecules by chloride ions followed by adsorption of inhibitor molecules. **(Bentiss *et al.*, 2000)**. The n values decrease with increase in time denoting the surface roughness of the mild steel surface with time **(Bouanis *et al.*, 2010).**

4.4.2.4 Analysis of impedance behaviour of other investigated terpolymers

The Nyquist plots and Bode plot for mild steel obtained in the absence and presence of inhibitors at optimum concentrations at various temperatures are given in Figures 39 and 40. The calculated impedance parameters of all the investigated terpolymers at various temperatures are presented in appendix A(6-9) section.

All the plots contain single capacitive loop with one capacitive time constant in the Bode-phase plot and the diameter of the semicircle decreases with increasing the temperature. It is worth mentioning that for polyacrylamide-containing polymers, the diameter or R_{ct} values almost remain same till 313 K, followed by notable decrease with increase in temperature. This fact suggests that the resistive nature of inhibitor film towards temperature. But for other polymers, the diameter and R_{ct} values recorded at 303 K is much greater than

those obtained at higher temperatures. This vast difference is clearly seen in figures and is due to the shift of the adsorption–desorption equilibrium towards desorption and roughening of the metal surface which results from enhanced corrosion.

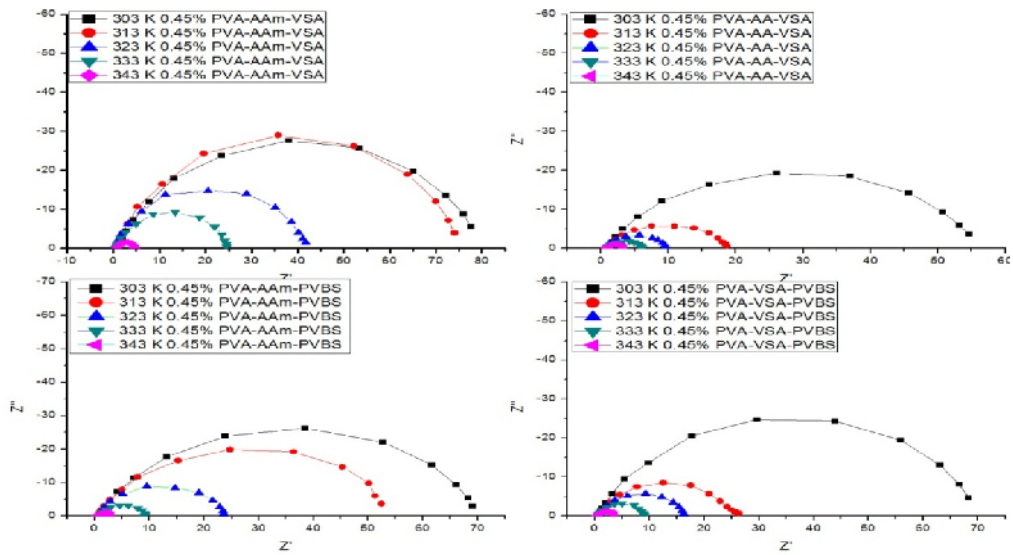

Figure – 39 Nyquist plot for MS in 1 M HCl in the presence and absence of 0.45 wt.% of PVA-AAm-VSA, PVA-AA-VSA, PVA-AmA-PVBS and PVA-VSA-PVBS at various temperatures

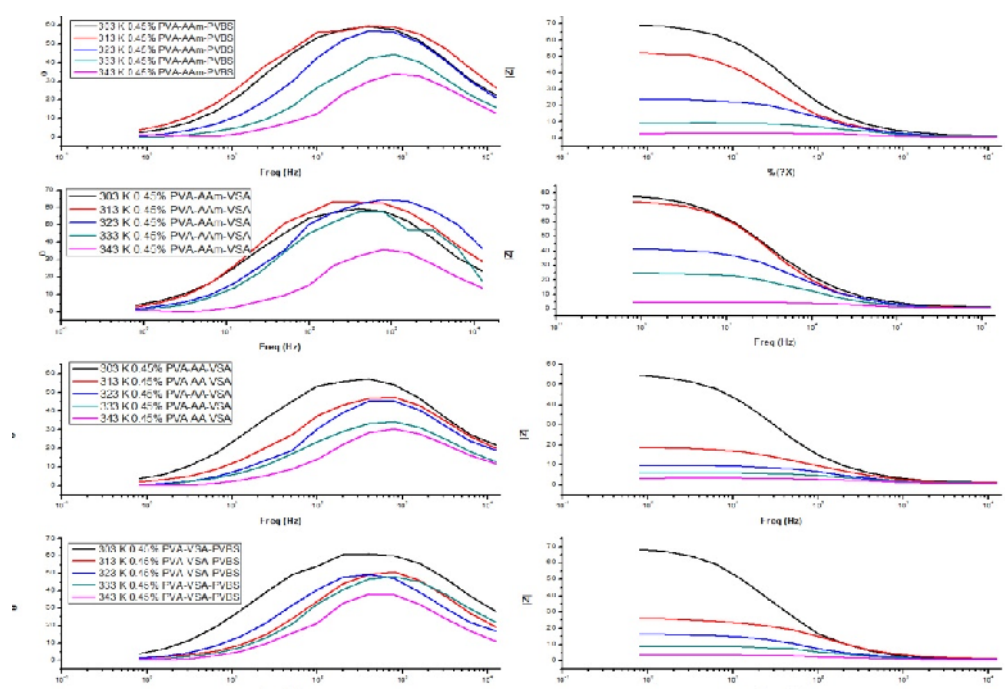

Figure - 40 Bode plot for MS in 1 M HCl in the presence and absence of 0.45 wt.% of PVA-AAm-VSA, PVA-AA-VSA, PVA-AmA-PVBS and PVA-VSA-PVBS at various temperatures

Table - 31 Impedance parameters obtained for other polymers for optimum concentration at various temperatures

Temperature (K)	Conc.	R_s Ωcm^2	Y_o* 10-6	n	R_{ct} $k\Omega cm^2$	IE R_{ct}	C_{dl} $*10^3$ μFcm^{-2}
303	Blank	0.544	606.4	0.748	6.85		9.98
313		0.771	546.7	0.749	4.14		7.29
323		0.751	1236.1	0.684	2.26		8.10
333		0.552	894.0	0.756	1.42		8.93
343		0.729	883.2	0.723	0.69		10.04
PVA-AAm-PVBS							
303	0.45	1.168	201.5	0.809	69.82	90.20	1.94
313		0.553	350.9	0.800	56.61	92.70	4.17
323		0.747	274.1	0.835	23.26	90.30	1.54
333		0.893	403.7	0.815	8.49	83.20	2.56
343		0.540	615.0	0.837	2.44	71.60	2.57
PVA-AAm-VSA							
303	0.45	1.117	250.6	0.789	78.34	91.25	3.53
313		0.694	234.0	0.818	75.78	94.54	2.07
323		0.378	214.7	0.828	41.27	94.51	1.42
333		0.495	339.6	0.816	10.85	86.89	2.17
343		0.735	486.8	0.829	3.91	82.26	2.31
PVA-AA-VSA							
303	0.45	1.001	395.2	0.860	55.37	87.62	2.01
313		0.830	654.0	0.742	18.11	77.17	1.69
323		0.725	688.5	0.782	10.06	77.50	8.05
333		0.810	1135.2	0.738	5.45	73.89	2.53
343		0.694	842.2	0.806	2.61	73.44	**5.37**
PVA-VSA-PVBS							
303	0.45	0.671	327.0	0.789	70.09	90.22	4.82
313		1.152	253.1	0.806	27.25	84.83	2.11
323		0.843	595.2	0.787	14.02	83.85	6.83
333		0.490	617.1	0.791	8.00	82.23	5.82
343		0.486	1102.8	0.816	3.15	77.97	**6.96**

Thus, with increase in temperature in the presence of inhibitors

(i) R_{ct} value decreases, C_{dl} increases (ii) the adsorption/desorption equilibrium is most probably shifted towards desorption. But at highest concentration of the inhibitor the inhibiting adsorption layer is sustained. It may be due to the decrease in thickness of the adsorbed particles within outer Helmholtz layer (OHL) while the diffused portion of electrical double layer increases **(Popova *et al*., 2003**).

(ii) Inspection of a set of data corresponding to a polymer reveals that the decrease in values of the CPE's exponent, n, with the rise of temperature is an indication for the increase of electrode surface roughness. The increase of n values with temperature reflects that the electrode surface becomes more homogeneous as a result of adsorption of the polymeric inhibitors **(Morad and El-Dean, 2006)**. The values of n are lower in pure acid than in the presence of inhibitors. This can be explained from an energetic point of view, i.e. The inhibitor's adsorption takes place at the most active sites on the metal surface isolation resulting in a homogenous surface **(Popova *et al*., 2003).**

(iii) The relative Values of IE% deduced from R_{ct} values are also included in Table 31 and it is clearly seen that the acrylamide based polymers are efficient till 323 K, whilst the IE_{Rct} of other polymers decrease gradually with increase in temperature. The IE of the polymers were found to follow the following order: Polyacrylamide polymers and PVA-AA-PVBS exhibited highest film resistance obviously due to the higher electron density. Polyacrylic acid polymers ranked second in rendering highest charge transfer resistance. PVA-VSA-PVBS shows about 90 % IE at 303 K and in the consequent higher temperatures the IE decreased.

Effect of immersion time: In order to study the stability of the adsorbed layer, the effect of immersion time was investigated using AC impedance technique. The calculated impedance parameters of the investigated terpolymers are presented in appendix A(10-13). Figure 41 shows the trend in IE_{Rct}% obtained for PVA-AAm-PVBS, PVA-AAm-VSA, PVA-AA-VSA and PVA-VSA-PVBS for every 1 hour during 12 hours immersion. The results show that immersion time influences the R_{ct} values and therefore the inhibitive behaviour of the terpolymers under investigation. IE_{Rct} % of all the polymers were found to increase initially till 5 to 7 cycles followed by a minimal decrease and stabilization in the forthcoming hours. This behaviour may be correlated with adsorption of inhibitor molecules thereby decreasing active area of metal dissolution. This is an evidence that the inhibitor tries to form a film initially and then tends to achieve stability. With elapsing time terpolymer molecules adsorb

or agglomerate at the surface such that they create no other inhibitive layer **(Azghandi *et al*., 2013).** But in the case of PVA-VSA-PVBS, the IE% is initially high which decreases gradually till 12th hour. This is because of the least stability of the inhibitor film where desorption starts immediately in the 2nd hour and the protection efficiency gradually falls till 12th hour.

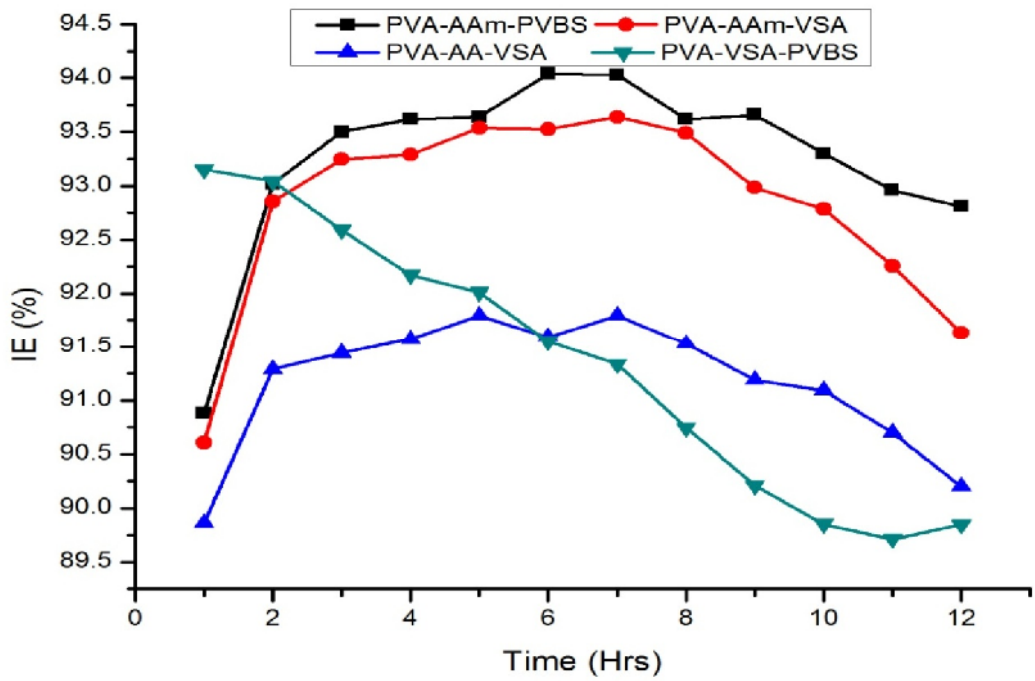

Figure - 41 Change in IE % values of 0.45 wt.% of the investigated terpolymers at various immersion times

4.5 Adsorption considerations

The inhibiting action of the inhibitor compounds is mainly pertained to the type of interactions with metallic surfaces. The inhibitors get adsorbed on the metal surface thereby resulting in the transition of active dissolution of metal/solution interface to passive state. The metal is thus shielded from the corrosive environment. In other words, adsorption is a phenomenon that occurs when the interaction energy between metal and inhibitors are more when compared with the interaction energy between water molecules with metal surface. Since corrosion inhibition primarily occurs through adsorption, a detailed insight into the adsorption properties of the inhibitor on the metal surface is highly essential.

Adsorption is operative in most natural physical, biological, and chemical systems, and is a consequence of surface energy of the adsorbent. In the bulk material the bonding requirements of the adsorbate are satisfied in the form of ionic, covalent or metallic bonds. But in the surface of the adsorbent, the bonding requirements of the adsorbate are not

fulfilled because of lack of holistic surrounding atoms. This makes them energetically favourable to extend bonding with the surrounding material. The nature of the bonding primarily depends on the surrounding environment, and however the adsorbed material is concluded as exhibiting physical or chemical nature of adsorption **(Kopecký *et al*., 1996)**.

Physisorption or physical adsorption is a type in which the adsorption between adsorbate and the surface is achieved through VanderWaal's weak intermolecular interactions. Chemisorption is a type of adsorption in which the molecule adheres to a surface through the formation of a chemical bond.

The adsorption of any organic/polymeric compounds on the metal surface is governed by certain physicochemical properties of the inhibitor molecules viz. functional groups, steric effect, electronic density of the π-orbitals and capability of π-orbitals to interact with the empty d-orbitals of the metal atom. These interactions are not always direct linkage between metal and inhibitor, but in some cases the adsorption takes place through the ions adsorbed on metal surface **(Rengamani *et al*., 1994; Murakawa and Hackerman, 1964)**. In aggressive acid media the following four types of interactions are generally expected **(Shokry *et al*., 1998)**:

- Electrostatic interactions between charged molecules and charged metal
- Interaction of uncharged electron pairs in the molecule with the metal
- Interaction of pi electrons with the metal
- Combination of 1 and 2.

4.5.1 An overview of Adsorption isotherms

Based on the types of interactions, adsorption is classified into physical adsorption, chemical adsorption and comprehensive physical adsorption which is a combination of both. Information regarding such interactions can be obtained by fitting the surface coverage values on various adsorption models, selecting the best fit model and analyzing the adsorption parameters.

In general, adsorption isotherm is an invaluable curve describing the mobility of ions or molecules (inhibitor) from the solution phase (acid) to solid phase (metal) at constant temperature or pH **Foo and Hameed (2010).** In this perspective, seven types of isotherms were considered for fitting: Langmuir, Temkin, El-Awady, Freundlich, Flory-Huggins, Frumkin and Bockris-Swinkles. A quick glimpse on the types of isotherms and their significance is given in Table 32.

Table - 32 List of adsorption isotherms models and significance of the deduced parameters

Name of the isotherm	Formula	Significance of the parameters	Reference
Langmuir	$\frac{C}{\theta} = \frac{1}{k} + C$ Assumptions: monolayer, homogenous, no lateral interaction between molecules	Slope=1 and R_L=1/1+KC_o R_L > 1; adsorption unfavourable R_L = 1; linear, 0-1=favourable R_L < 1; adsorption favourable or irreversible	**Obot *et al*. (2009);** **Webber and Chakkravort, (1974)**
Temkin	$\theta = \frac{1}{f}\ln K + \frac{1}{f}\ln C$	Slope= 1/f f=molecular interaction parameter	**Umoren and Ebenso, (2008)**
El-Awady	$log\frac{\theta}{1-\theta} = \log K' + y\log C$	Slope =y; y< 1 ; monolayer adsorption,y> 1 ; multilayer adsorption	**Foad El-Sherbini *et al*. (2003)**
Freundlich	$\ln\theta = \ln K + \frac{1}{n}\ln C$ Monolayer and Heterogenous systems	Slope = 1/n; 1/n > 1; co-opertive,1/n < 1; chemisorption Nearly 0; heterogenous surface	**Freundlich, (1906)**
Flory-Huggins	$log\frac{\theta}{C} = \log xK + x\log(1-\theta)$	Slope=x(1/y);no. of inhibitor molecues occupying one active site/no. of water molecules replaced by one inhibitor molecule x < 1 ; inhibitor occupies more than 1 active site	**Foad El-Sherbini *et al*. (2003)**
Frumkin	$log\frac{\theta}{1-\theta} = \log B + \log C + 2a\theta$	Slope=a a > 0; interaction, a < 0; repulsion, a = 0; no interaction	**Popova, (2007)**
Bockris-Swinkles	$[\theta/(1-\theta)^x]\{[\theta + \frac{x(1-\theta)^{(x-1)}}{x^x} = \left(\frac{C}{55.5}\right)\exp(-\frac{\Delta G}{RT})$	a'= molecular interaction parameter a = -ve; free energy of adsorption decrease and surface coverage increase and vice versa	**Das *et al*. (2000)**

Basically all the isotherms follow a standard equation 30 (**Umoren *et al.*, 2012**):

$$f(\theta,x)\exp(-2a\,\theta)=K_{ads}+C \quad (30)$$

Where θ is the surface coverage of the inhibitor, 'a' is the molecular interaction parameter signifying the molecular interactions in the adsorbed layer and degree of inhomogeneity, C is the concentration and K is the equilibrium constant of adsorption.

The data when fits into a particular isotherm model, several conclusions on the mode of adsorption, type of layers formed, attraction/repulsion that exist between the adsorbed molecules etc. can be drawn. In the endeavour to explore inhibitors accessing an ideal adsorption system, it is essential to perform a statistical analysis which is indispensable for reliable prediction of adsorption parameters and quantitative comparison of adsorbent behaviour for different adsorbent systems **(Gimbert *et al.*, 2008)**. The best fit isotherm was chosen based on the R^2 values that were closer to 1. One-way analysis of variance (ANOVA) was performed for comparison of significance of the isotherm studied. The results of R^2 and F values were obtained through statistical analysis by employing SPSS v.20 statistical software.

4.5.2 Analysis of adsorption properties of terpolymers from weight loss technique

In the present study, the degree of surface coverage (θ) for the various inhibitor concentrations in 1 M HCl at 303-343 K for 1/2 h immersion time has been evaluated from weight loss studies. In the attempt to fit the θ values to various isotherms, Langmuir isotherm provided a best fit with regression values close to unity, but the slope values deviated from one. The deviation of slope values from unity strongly restricted the use of Langmuir isotherm model. Among the other isotherm models tested, the best fit was achieved with Temkin's adsorption isotherm. The strong correlation (R^2 >0.9) and F values for Temkin's isotherm plot confirms the validity of this model. The Temkin isotherm is generally used for the characteristic adsorption of uncharged molecules on a heterogenous surface, where θ is the linear function of ln C. The general form of Temkin isotherm is given as:

$$\theta = \frac{1}{f}\ln K + \frac{1}{f}\ln C \quad (31)$$

Where, f is a factor of energetic inhomogeneity in the surface, θ is the surface coverage, C is the concentration and K is the equilibrium adsorption constant. The linear regression between θ vs. ln C for PVA-AA-PVBS at various temperatures is depicted in Figure 42. Figure 43 shows the isotherms of other terpolymers studied at 333 K. Table 33 summarises the adsorption parameters derived from Temkin isotherm.

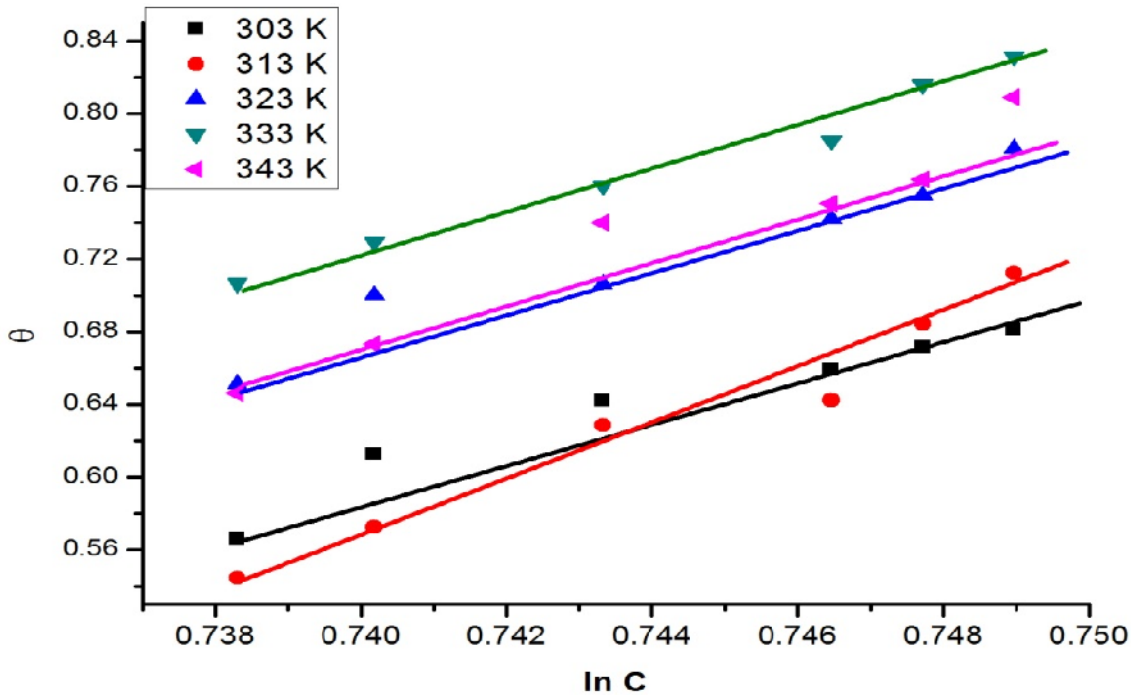

Figure - 42 Temkin isotherm for MS in 1 M HCl in the presence of different concentrations of PVA-AA-PVBS (Data from weight loss technique)

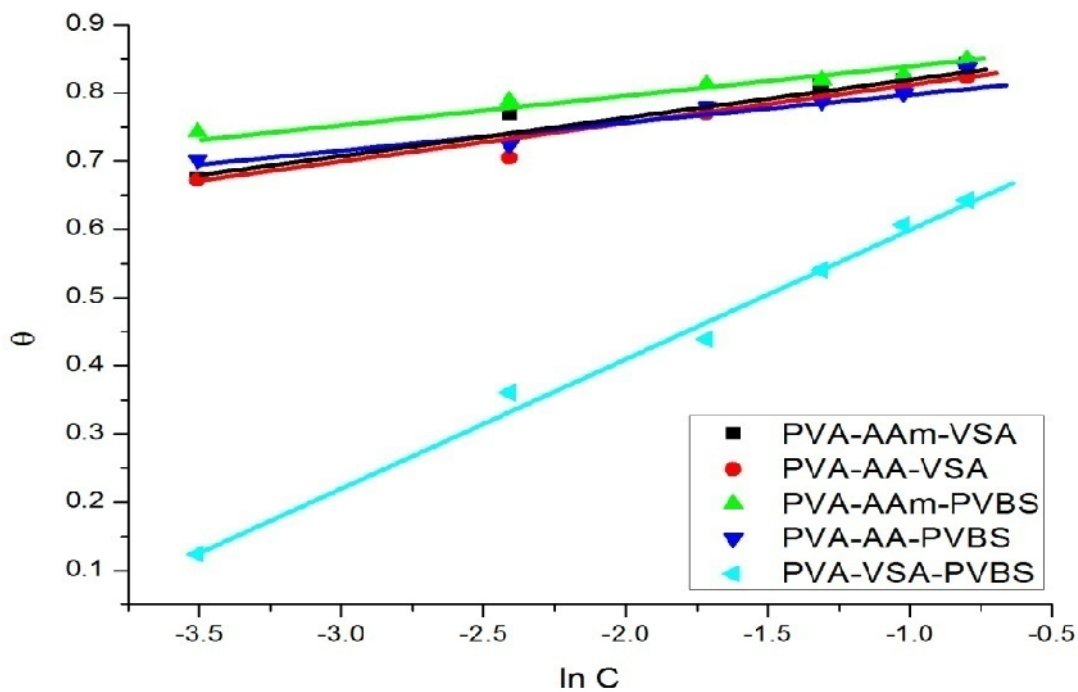

Figure - 43 Temkin isotherm for MS in 1 M HCl in the presence of optimum concentration of all investigated terpolymers (Data from weight loss technique)

Table - 33 Thermodynamic parameters of adsorption of the investigated terpolymers on MS electrode surface in 1 M HCl solution (Data from weight loss technique)

Temperature	Statistical analysis		f	K_{ads} 10^5	ΔG_{ads} ($kJmol^{-1}$)	ΔH_{ads} ($kJmol^{-1}$)	ΔS_{ads} ($Jmol^{-1}\ K^{-1}$)
	R^2	F					
PVA-AAm-VSA							
303	0.99	46.88[0.002]	18.35	$5.31*10^5$	-43.33	127.19	554.5
313	0.94	62.93[0.001]	17.50	$5.24*10^5$	-44.73		
323	0.97	46.01[0.002]	16.83	$2.58*10^6$	-50.44		
333	0.95	49.92[0.002]	17.52	$5.40*10^6$	-54.05		
343	0.92	33.19[0.005]	22.93	$2.91*10^8$	-67.04		
PVA-AA-VSA							
303	0.93	44.90[0.003]	15.62	$6.19*10^4$	-37.92	187.45	729.8
313	0.97	128.68[0.000]	12.56	$1.54*10^4$	-35.55		
323	0.99	415.04[0.000]	16.22	$1.55*10^6$	-49.08		
333	0.96	154.10[0.000]	16.91	$2.40*10^6$	-51.80		
343	0.92	65.35[0.001]	22.93	$2.91*10^8$	-67.04		
PVA-AAm-PVBS							
303	0.92	44.90[0.003]	17.20	$1.54*10^5$	-40.21	346.13	1258.1
313	0.94	128.68[0.000]	16.11	$2.88*10^5$	-43.17		
323	0.92	415.04[0.000]	18.26	$6.65*10^6$	-52.98		
333	0.93	154.10[0.000]	28.03	$3.89*10^{10}$	-78.65		
343	0.89	65.35[0.001]	30.83	$2.40*10^{11}$	-86.20		
PVA-AA-PVBS							
303	0.91	46.88[0.002]	23.53	$2.03*10^7$	-52.51	136.9	193.13
313	0.97	62.93[0.001]	15.68	$1.19*10^5$	-40.87		
323	0.99	46.01[0.002]	22.29	$5.92*10^7$	-58.86		
333	0.97	49.92[0.002]	21.01	$6.58*10^7$	-60.97		
343	0.94	33.19[0.005]	16.93	$1.41*10^6$	-51.85		
PVA-VSA-PVBS							
303	0.90	46.88[0.002]	34.75	$1.41*10^{10}$	-69.00	-122.2	-216.9
313	0.80	62.93[0.001]	19.73	$2.38*10^6$	-48.67		
323	0.93	46.01[0.002]	11.22	$2.32*10^4$	-37.79		
333	0.99	49.92[0.002]	11.29	$2.34*10^4$	-38.97		
343	0.96	33.19[0.005]	23.63	$2.24*10^8$	-66.30		

The efficiency of an inhibitor is pertained to the magnitude of its binding constant, 'K' **(Khalil *et al*., 2003)**, therefore larger values of K implies a stronger interaction of the inhibitor molecules with the metal surface. Also the increase in K values indicates the increase in strength of the adsorption between inhibitor molecules and metal. The increase in K values with temperature is directly proportional to the adsorption efficiency of the inhibitor with temperature **(Shukla and Ebenso, 2011).** In this study, the magnitude of the K values is larger which is attributable to the effective adsorption of the inhibitor (**Singh *et al*., 2010)**.

Basically, the constant f describes the intermolecular interaction in the adsorbed layer and on the heterogeneity of the surface. If f is positive, mutual repulsion of molecules occurs and if f is negative mutual attraction of molecules takes place. The values of f retrieved from the present investigation are positive indicating repulsive forces that exist between inhibitor molecules in the adsorbed layer.

4.5.2.1 Thermodynamic parameters of adsorption calculated from weight loss technique

Thermodynamic adsorption parameters are a useful tool for clarifying the adsorption behaviour of an inhibitor The free energy of adsorption ΔG_{ads} is calculated using the relationship (**Umoren *et al*., 2012)**:

$$\log K_{ads} = -\log C_{H2O} - \frac{\Delta G_{ads}}{RT} \quad (32)$$

Where C_{H2O} is the molar concentration of water expressed in g/L, R is the molar gas constant J/mol/K and T is the temperature in K.

Thermodynamic parameters such as entropy of adsorption ΔS_{ads} and enthalpy of adsorption ΔH_{ads} were deduced from the integrated form of Van't Hoff equation **(Obi-Egbedi and Obot, 2011).**

$$\ln K_{ads} = -\frac{\Delta H_{ads}}{RT} + \frac{\Delta S_{ads}}{R} + \ln\frac{1}{55.5} \quad (33)$$

In the plot of ln K versus 1/T, ΔS_{ads} and ΔH_{ads} can be calculated from the slope ($-\Delta H_{ads}/R$) and intercept ($\Delta S_{ads}/R+\ln 1/55.5$) respectively. The calculated thermodynamic parameters of adsorption are listed in Table 33.

Free energy of adsorption: The negative values of ΔG indicate the spontaneity of the adsorption process. Generally, the free energy values less than -20 kJ mol^{-1} are attributed to the electrostatic interaction between charged molecules and charged metal surface, and the

phenomenon is termed as physisorption. The free energy values greater than -40 kJ mol^{-1} or more involve charge sharing or transfer from the inhibitor molecules to the metal surface to form a coordinate covalent bond, and the phenomenon is associated with chemisorption **(Ahamad and Quraishi, 2009; Obot and Obi-Egbedi, 2008; Noor and Al-moubaraki, 2008b)**. The values in the range of 21 kJ mol^{-1}– 39 kJ mol^{-1}can be attributed to the threshold for chemical adsorption in combination with physical adsorption **(Noor and Al-moubaraki, 2008b, Li *et al*., 2008b).** In the present investigation the ΔG values are negative indicating the spontaneous adsorption process, and the magnitude is greater than -40 KJ mol^{-1}(-40 to -86 KJ mol^{-1}) which is consistent with the chemical mode of adsorption as a result of sharing of electrons between the inhibitor molecule and metal surface to form a co-ordinate bond. The ΔG values increase with increasing temperature which can be assigned to the fact of strong chemical adsorption at higher temperatures. The magnitude of ΔG values of individual polymers listed in Table 33 shows the extent to which a polymer a can be chemisorbed. PVA-AAm-PVBS assumes a highest mean ΔG value -60.2 KJ mol^{-1} indicating the highest charge transfer had taken place between the terpolymer and metal surface. PVA-AAm-VSA and PVA-AA-VSA ranks second with ΔG values more than 50 KJ mol^{-1}. PVA-AA-VSA and PVA-VSA-PVBS ranks third with ΔG values around 50 KJ mol^{-1}. Though the magnitude of ΔG values greater than 40 KJ mol^{-1} is unequivocally related to chemisorption, the variation in the values can be pertained well to the hetero atom population that can extend co-ordination with metal surface. The various interactions that is possible for each polymer is discussed in detail in mechanism of adsorption (section 4.5.6)**.**

Enthalpy of adsorption and Entropy of adsorption: The sign of the ΔH can be used for distinguishing the adsorption of inhibitor as exothermic process or endothermic process. The positive ΔH reflects the endothermic process and negative values of ΔH reflects the exothermic process. Endothermic process is generally attributed to chemisorption. But exothermic process can be associated with physisorption or chemisorption, depending on absolute values. A physisorption process reflects an enthalpy around 40 kJ mol^{-1} while chemisorption process results an enthalpy around 100 kJ mol^{-1} **(Noor and Al-moubaraki, 2008b; Awad, 2006)**. The orderliness/disorderliness of an adsorption process can be determined using entropy of adsorption. The decrease in entropy or negative entropy is a due to free movement of inhibitor molecules from the bulk solution that gets adsorbed in an orderly fashion onto the mild steel **(Li *et al*., 2009)**. Similarly, the positive entropy is attributed to the solvent entropy that is associated with the disorderliness of the solution during the adsorption process.

The ΔH_{ads} obtained for the investigated polymers were positive except that obtained for PVA-VSA-PVBS. But the absolute value of ΔH_{ads} for PVA-VSA-PVBS is -122 kJ mol^{-1},which supports the chemical nature of adsorption through exothermic process. Hence the adsorption of terpolymers can be concluded to have chemically adsorbed on the metal surface. As a contrary to the observations from the literature, positive values of ΔH are associated with the positive entropy. **Tahir and Rauf (2003)** reported the same trend and explain the reason as follows: when the inhibitor molecules are well solvated in water, during the adsorption process they have to be denuded from the hydration sheath. The author assumes that this dehydration process also requires energy and this energy overlies the exothermic energy of ions that tends to attach to the surface. But in this case of polymers the positive enthalpy can be explained in a different manner. Polymers are generally larger molecules, and terpolymer under investigation is a bigger macromolecule with hetero atoms like N, S and O. Hence, before getting adsorbed onto the metal surface the macromolecule has to orient itself in the solution state to extend the bonding with the metal surface. The total enthalpy of the system is an algebraic sum of adsorption enthalpy, enthalpy assumed by polymer molecules and desorption enthalpy. Hence, desorption of water molecules and orientation energy of the polymer molecules are implicitly an endothermic process resulting a positive enthalpy for the whole system. Since the adsorption is endothermic, the adsorption process is spontaneous with positive entropy change **(Qadeer *et al*., 1992)**. This means that adsorption is accompanied by increased entropy. This can be explained as follows**: Singh and Quraishi (2010a), Wang *et al*. (2010)**: Adsorption of inhibitors from the aqueous solution is considered as quasi-substitution process between the organic compound in the aqueous phase and water molecules at the mild steel surface. The adsorption of inhibitors on metal surface takes place at the cost of desorption of water molecules. The total entropy is calculated as algebraic sum of adsorption of organic inhibitor molecule and desorption of water molecules. So the gain in entropy is related with the solvent entropy. That is from the solvent side, the disorderliness increases resulting in increased entropy.

Usually negative enthalpy is associated with the decreased entropy. PVA-VSA-PVBS follows the same trend. The sign of entropy of adsorption is negative, meaning that the process of adsorption is accompanied by a decrease in entropy. This may be explained as follows: the chaotic degree at the metal/solution interface is higher before the adsorption of inhibitor molecules. But once when the inhibitor molecules start adsorbing on the metal solution interface, the orderliness of the adsorption is increased resulting in decreased entropy **(Li *et al*., 2010)**.

4.5.2.2 Supporting evidences for the proposed chemical adsorption

According to **Oguzie *et al*. (2004) and El-Sayed *et al*. (2010),** a decrease/increase in inhibition efficiency with rise in temperature is one of the criteria for differentiating the adsorption as physical or chemical in nature. When the IE decreases with temperature, it is attributed to the physical nature of adsorption and vice versa. In the present study the IE increases with temperature which satisfies the primary criterion for chemical adsorption.

The adsorption is mainly governed by functional groups present in a molecule and its orientation. The orientation of the inhibitor molecule is decided by several factors that includes molecular structure and its reactivity. Each functional group has its own interaction ability. The terpolymers under investigation includes polyvinyl alcohol, polyacrylamide, polyacrylic acid, polyvinyl sulfonate and polyvinyl benzene sulfonate which contain functional groups that are responsible for adsorption. it is reported that sulphur-containing substances easily chemisorb onto the metal surface whereas nitrogen-containing substances prefer physisorption **(Oguzie *et al*., 2005). Umoren (2006)** has reported the chemical adsorption of polyvinyl alcohol on MS during the exploration of effect of halide ions on the inhibitive action of PVA on MS in acid medium. The physical adsorptive nature of Polyacryic acid was reported by corrosion scientists. **Umoren *et al*. (2011)** has reported that the polyacrylic acid can interact with metal through protonated form or molecular form. Protonated form gets poorly adsorbed on a metal surface with positive charge while molecular species is easily adsorbed on the metal surface. The chelating ability of poly(acrylic acid-co-vinyl sulfonic acid) with metal ions in solution was discussed by **Rivas and Nicolas, (2003).**

The acrylic terpolymer under investigation can form complex with iron in solution and gets adsorbed on the metal surface, during corrosion studies. These studies support the physical adsorption of polyacrylic acid through electrostatic interactions **(Umoren, *et al*., 2010). Chamovska *et al*. (2007)** analysed the adsorption of different molecular weights of polyacrylamide on iron in HCl. The thermodynamic parameters revealed ΔG values in the range of 50-60 KJ mol^{-1} ensuring the chemical adsorption of polyacrylamide. The PVBS polymers also get attracted to the metal surface through the π electrons on the benzene ring. Though both physical adsorption and chemical adsorption favouring groups are present in the terpolymer, chemical adsorption predominantly takes place which is well corroborated by the results obtained from thermodynamic adsorption parameters.

4.5.3 Analysis of adsorption properties of PVA-AAm-PVBS from potentiodynamic polarization and PVA-AA-PVBS from impedance spectroscopy

Establishment of adsorption isotherm is an important phenomenon which can help us to assess the nature of the interactions existing between the metal and inhibitor. It is difficult to reach real adsorption equilibrium during the corrosion process. But still the adsorption steady state can be achieved when the corrosion rate is small and the steady state is transformed into quasi-equilibrium state. Therefore, the quasi-equilibrium adsorption can be considered in a thermodynamic manner using the appropriate equilibrium isotherms **(Umoren *et al*., 2010).**

The degree of surface coverage is plotted against inhibitor concentration during the construction of an isotherm, and for the present study surface coverage values were calculated from R_{ct} and I_{corr} values as follows:

$$\theta = \frac{R_{ct} - R_{ct}^{o}}{R_{ct}} \quad (34)$$

$$\theta = \frac{I_{corr}^{o} - I_{corr}}{I_{corr}^{o}} \quad (35)$$

where R^{o}_{ct} and I^{o}_{corr}, are charge transfer resistance and corrosion current density of blank solution; R_{ct} and I_{corr} charge transfer resistance and corrosion current density of inhibitor added solution respectively. In an effort to fit the θ values obtained from I_{corr} values in the absence and presence of various concentrations of the inhibitor, Temkin isotherm was found to give the best description of the adsorption behaviour of the studied inhibitors with high regression values (Table 34). Though Langmuir isotherm gave best regression values, there is a deviation of slope values from unity indicating the non-applicability of the model. Hence Temkin isotherm was used for further studies.

Figure 44 a&b depicts the application of Temkin isotherm model for adsorbed layer of the grafted terpolymer PVA-AA-PVBS (from impedance) and PVA-AAm-PVBS (from polarization) on MS during the electrochemical measurements respectively. The Temkin isotherm is generally used for the characteristic adsorption of uncharged molecules on a heterogenous surface, where θ is the linear function of ln C. The general form of Temkin isotherm is given as:

$$\theta = \frac{1}{f}\ln K + \frac{1}{f}\ln C \quad (36)$$

Where, f is a factor of energetic inhomogeneity in the surface, θ is the surface coverage, C is the concentration and K is the equilibrium adsorption constant. The derived adsorption parameters are listed in Table 34.

Table - 34 Thermodynamic parameters of adsorption of PVA-AA-PVBS and PVA-AAm-PVBS on MS electrode surface in 1 M HCl solution by impedance method and potentiodynamic polarization method respectively

PVA-AA-PVBS	therm fit of surface coverage from impedance R_{ct}					
	R^2	f	K_{ads}	ΔG_{ads} ($kJmol^{-1}$)	ΔH_{ads} ($kJmol^{-1}$)	ΔS_{ads} ($Jmol^{-1}\ K^{-1}$)
303 K	0.92	8.53	$9.01*10^{3}$	-62.91	-103.2	-125
313 K	0.97	32.99	$7.63*10^{13}$			
323 K	0.95	30.48	$6.11*10^{12}$			
333 K	0.98	13.97	$1.08*10^{5}$			
343 K	0.98	14.33	$2.09*10^{5}$			
PVA-AAm-PVBS	**Temkin isotherm fit of surface coverage from potentiodynamic polarization I_{corr}**					
	R^2	f	K_{ads}	ΔG_{ads} ($kJmol^{-1}$)	ΔH_{ads} ($kJmol^{-1}$)	ΔS_{ads} ($Jmol^{-1}\ K^{-1}$)
303 K	0.95	9.50	$1.52*10^{4}$	-96.26	709.83	2495.7
313 K	0.98	26.32	$1.11*10^{11}$			
323 K	0.97	47.11	$1.30*10^{19}$			
333 K	0.94	34.42	$3.93*10^{12}$			
343 K	0.90	56.22	$1.18*10^{12}$			

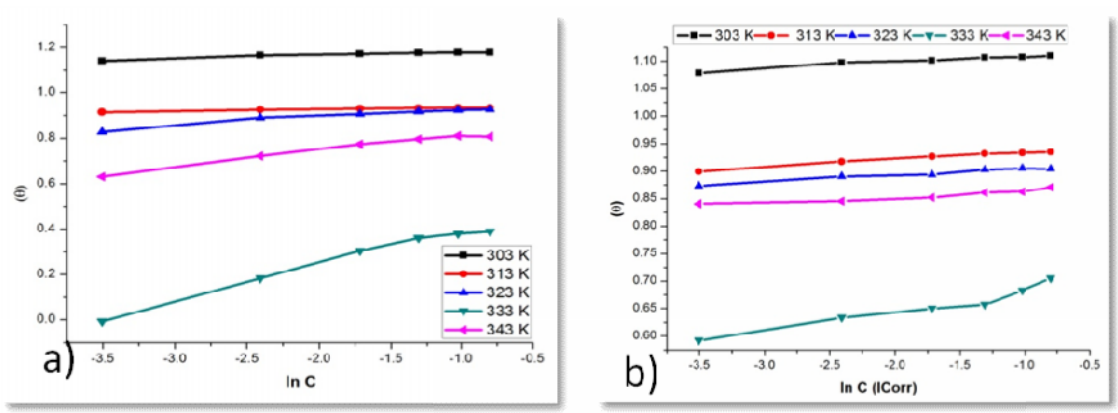

Figure - 44 Temkin isotherm of PVA-AA-PVBS from a) impedance and Temkin isotherm of PVA-AAm-PVBS from b) potentiodynamic polarization

The high values of K_{ads} obtained up to 333 K in HCl reveal the formation of a stable layer of the inhibitor on the metal surface **(Wang *et al*., 2004).** The slight decrease in K_{ads} values at higher temperatures is due to the large surface energy that is capable of releasing/desorbing the adsorbed molecules.

Basically, the constant f describes the intermolecular interaction in the adsorbed layer or the heterogeneity of the surface. If f is positive, mutual repulsion of molecules occurs and

if f is negative mutual attraction of molecules takes place. The values of f retrieved from the present investigation are positive indicating repulsive forces that exist between inhibitor molecules in the adsorbed layer.

Thermodynamic adsorption parameters are a useful tool for clarifying the adsorption behaviour of an inhibitor. The free energy of adsorption ΔG as computed using the equation 30 shows negativity in all the cases studied. This indicates the spontaneous nature of adsorption under all the conditions studied. The magnitude of the ΔG values presented in the table is greater than -40 KJ mol^{-1}, which is consistent with the chemical nature of adsorption. This may be because of the strong adsorption of inhibitor molecules on the mild steel surface through the lone electron pairs on O and S atoms as well as π-electrons of the aromatic rings **(Trabanelli, 1987).**

Literature reports show three types of relations between enthalpy and entropy: positive enthalpy-positive entropy, negative enthalpy-negative entropy and negative enthalpy-positive entropy. In the present study, PVA-AA-PVBS exhibits negative enthalpy associated with negative entropy and PVA-AAm-PVBS exhibits positive enthalpy associated with positive entropy.

ΔH values are another criterion which can explain the mode of adsorption. Based on the ΔH values, the nature of adsorption can be probed as endothermic or exothermic. Positive ΔH values unequivocally represent endothermic process associated with chemisorption. In the present study, the value of enthalpy (ΔH_{Icorr}) is positive for PVA-AAm-PVBS indicating endothermic chemisorption process. The value of enthalpy (ΔH_{Rct}) is negative for PVA-AA-PVBS indicating exothermic process. An exothermic adsorption process is explicated either to physisorption or chemisorption based on their absolute values. The absolute value of ΔH_{Rct} of PVA-AA-PVBS is greater than 40 KJ mol^{-1} indicating chemisorption **(Noor and Al-moubaraki, 2008b; Awad 2006).**

The negative ΔS values associated with negative enthalpy can be explained as follows: Entropy decreases when the orderliness of the system increases. So during the adsorption process the free movement of inhibitor molecule (which basically results in positive entropy) are reduced and gets adsorbed onto the mild steel surface in an orderly fashion. As a result of this a negative entropy is observed **(Awad, 2006).**

The positive ΔS values associated with positive enthalpy is due to the following reasons: Adsorption of inhibitors on mild steel surface is in equilibrium with desorption of water molecules from the mild steel surface:

$$inh(sol) + nH_2O(ads) \rightleftharpoons inh(ads) + nH_2O(sol)$$

From the above reaction scheme, it is understood that total entropy of the system is an algebraic sum of adsorption of inhibitor molecules and desorption of water molecules. Increase in entropy is a result of increased disorderliness from the solvent side which in turn increases the total entropy of the system. **(Deng et al., 2010; Yadav et al., 2010).**

4.5.3.1 Analysis of adsorption properties of other investigated terpolymers from potentiodynamic polarization and impedance spectroscopy

Basic information that deals with the interaction between inhibitor molecules and metal surface is analysed using adsorption isotherm. The previous section discusses in detail the adsorption isotherm and the derived thermodynamic parameters of PVA-AA-PVBS from R_{ct} and PVA-AAm-PVBS from I_{corr}. Similarly the surface coverage values calculated from R_{ct} and I_{corr} for the remaining polymers were found fit well in Temkin isotherm model. Table 35 summarises the mean values of regression R^2, heterogeneity factor f, adsorption coefficient K_{ads}, free energy of adsorption $\mathbf{\Delta G_{ads}}$, enthalpy of adsorption $\mathbf{\Delta H_{ads}}$ and entropy of adsorption $\mathbf{\Delta S_{ads}}$ of the other terpolymers from impedance and polarization experiments.

Table - 35 Thermodynamic parameters of adsorption of the other investigated terpolymers on MS electrode surface in 1 M HCl solution by impedance method and potentiodynamic polarization method respectively

Inhibitor	Temkin isotherm fit of surface coverage from impedance R_{ct}					
	R^2	f	K_{ads}	ΔG_{ads} ($kJmol^{-1}$)	ΔH_{ads} ($kJmol^{-1}$)	ΔS_{ads} ($Jmol^{-1}\,K^{-1}$)
PVA-AAm-VSA	0.95	22.154	$5.36*10^{15}$	-66.63	340.32	1259.90
PVA-AA-VSA	0.93	13.736	$1.54*10^{7}$	-41.28	-90.76	-153.20
PVA-AAm-PVBS	0.92	23.332	$4.08*10^{13}$	-65.24	-73.74	-26.18
PVA-VSA-PVBS	0.90	12.25	$3.81*10^{11}$	-40.88	-332.9	-904.10
Inhibitor	**Temkin isotherm fit of surface coverage from potentiodynamic polarization I_{corr}**					
	R^2	f	K_{ads}	ΔG_{ads} ($kJmol^{-1}$)	ΔH_{ads} ($kJmol^{-1}$)	ΔS_{ads} ($Jmol^{-1}\,K^{-1}$)
PVA-AAm-VSA	0.95	9.50	$1.52*10^{4}$	-79.33	605.13	2119.10
PVA-AA-VSA	0.98	26.32	$1.11*10^{11}$	-40.44	-186.40	-455.10
PVA-AA-PVBS	0.97	47.11	$1.30*10^{19}$	-96.26	709.83	2495.71
PVA-VSA-PVBS	0.94	34.42	$3.93*10^{12}$	-46.74	-357.20	-961.23

The mean regression coefficient values of the trend lines thus obtained from the Temkin plot was found to be very close to unity (>0.92) denoting the validity of the adsorption isotherm model. The positive f values observed in all the systems describe the repulsive molecular interactions of adsorbed inhibitor molecules in the adsorption layer

The higher equilibrium constant values determined in presence of acrylamide terpolymers is an added proof that demonstrates their ability of enhanced adsorption on the MS surface. The ΔG_{ads} values also confirm the chemical mode of adsorption of all the inhibitors calculated using θ_{Rct} and θ_{Icorr}. However, the higher values of K_{ads} **and** ΔG_{ads} were obtained for acrylamide polymers indicating their extensive co-ordinating capability. The enthalpy and entropy of adsorption of PVA-AAm-VSA is positive in both the cases. The ΔH_{Rct} and ΔS_{Rct} of PVA-AAm-PVBS is positive while the ΔH_{Icorr} and ΔS_{Icorr} is negative. All the other polymers exhibit negative enthalpy and negative entropy from both R_{ct} and $I_{Corr.}$

4.5.4 Surface imaging techniques- i) Scanning electron microscopy/energy dispersive X-ray analysis

The application of adsorption isotherms provided a clear insight into the nature of adsorption. In order to analyse the external morphology (texture), crystalline structure, chemical composition, and orientation of materials, the present research work has taken advantage of the benefits offered by surface characterisation techniques: Scanning electron microscopy/energy dispersive X-ray analysis (SEM/EDX). *Ex-situ* corrosion product analysis was performed after 6 hours immersion in the respective inhibited solution and uninhibited solution.

4.5.4.1 SEM analysis of polished and corroded metal surface

Since the corrosion inhibition is ascribed basically to the adsorption of inhibitors on the metal surface, SEM is a veritable tool used to behold those adsorbed inhibitor layers formed on the metal surface. The SEM micrographs provide a visual proof for the corrosion inhibition of the polymers under investigation through adsorption. SEM analysis was performed using a Bruker field emission SEM EDX. Literature reports from various laboratories show that the polymer deposits occur in the forms of granules, fibers or smooth structures **(Beck *et al*., 1992; Herrasti and Ocon, 2001).** The component ratio of the polymeric particles deposited on the mild steel can be determined using EDX analysis.

Figure 45b is the surface of the polished mild steel. No cracks or pits are seen and the streaks are created during the surface preparation with emery paper. The element aspect ratio retrieved from the *EDX* analysis shows 100 at. Wt.% of iron content and absence of oxygen. This is an indication that the surface is free from any oxides of iron and the corresponding surface is free from corrosion.

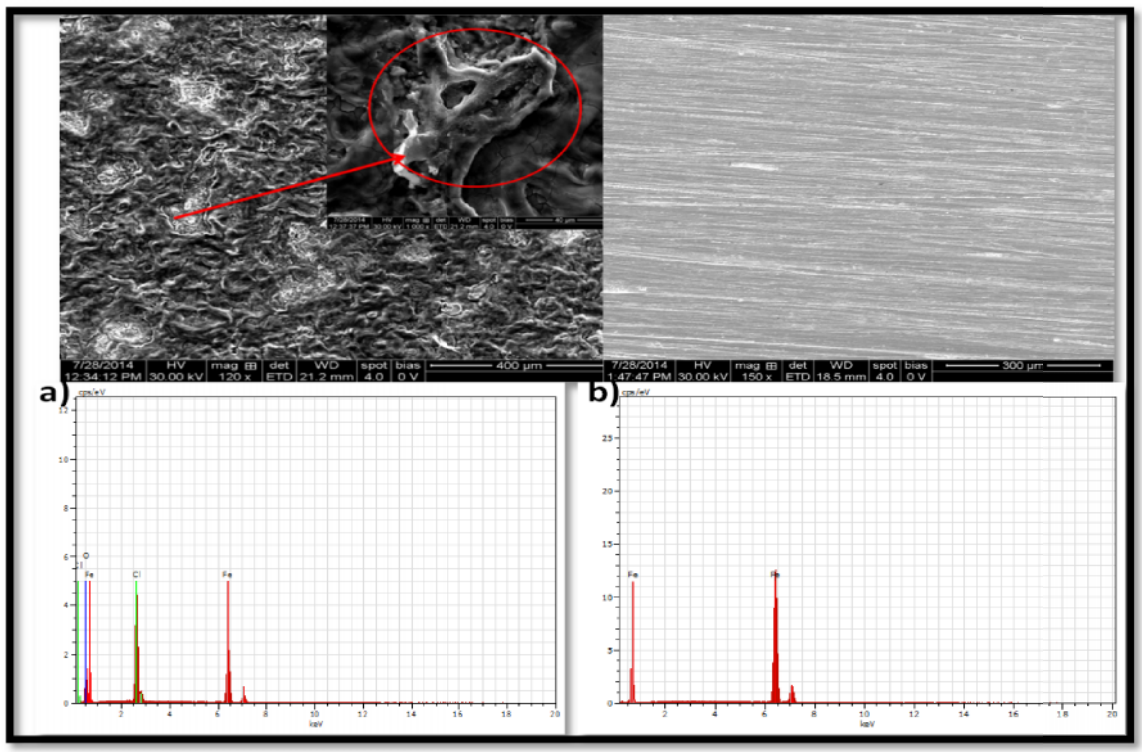

Figure - 45 SEM images and EDX spectra of mild steel (a) immersed in 1M hydrochloric acid solution and (b) Polished surface

Figure 45a is the surface of the mild steel deposited with corrosion products after immersion in 1M HCl for a period of 6 hours. Examination of the layer reveals the presence of densely packed crystalline aggregates of the corrosion products on the surface and resulting in a porous and rough surface. The aggregates consist of oxyhydroxides (FeOOH) of Fe and a part of these oxyhydroxides may also tend to transform into other types of oxyhydroxides and/or oxides in the due course **(Balasubramaniam, 2000)**. Though, the oxide layers are densely packed which were primarily meant to inhibit corrosion, close examination (Figure 45a inset) reveals the presence of cracks through which Fe tends to dissolve and diffuse outwards due to the lowest reduction potential of Fe^{2+}/Fe compared to other elements **(Nam *et al.*, 2010)** i.e. These oxide layers easily break up allowing the HCl to penetrate and contact the metal in the due time increasing the chances of pit formation. The elemental analysis of the layers formed reveals the presence of Fe, O and Chlorine. The content of iron is reduced to 15.45 at. Wt. % and content of oxygen is increased to 65.01 at.wt. %, due to formation of iron oxides.

4.5.4.2 SEM analysis of metal surface inhibited with Acrylamide terpolymers

The morphological dependence of the steel specimen on grafted terpolymer containing acrylamide is illustrated through SEM micrographs. Figure 46a show the SEM micrograph of

the MS coupon in the presence of PVA-AAm-VSA. In the presence of PVA-AAm-VSA, a non-uniform distribution of non-spherical particles as well as some clusters can be observed **(Amin *et al.*, 2010)**, and the surface is smooth with respect to the MS (Figure 45b). Further magnification (Figure 46a inset) of distributed polymer particles to 2000 X reveals clearly agglomerated particles of the polymer. The corrosion products are absent in the general view, and pits or crevices are not found when compared to the corroded metal specimen (Figure 45a). The EDX analysis of the clustered polymeric particles confirms the presence of nitrogen and sulphur in the particulates deposited on the surface. The presence of these elements are absent in the blank assay which is an evidence for the surface coverage by the polymer on MS surface.

Figure 46b show the surfaces of MS specimen immersed in the optimum concentration of 0.45 Wt.% of PVA-AAm-PVBS. The surface of the steel is extensively covered by white-coloured crystallites of the polymer and surface of the MS appears to be comparably smooth. The white coloured needle like particles when magnified to 3000 X revealed a protruding crusty crystal-like growth from the surface. The coverage of the particles ensures the prevention of hostile attack of the acid medium. Acquisition of elemental composition of the selected portion (Figure 46b inset) confirms the presence of iron, nitrogen, oxygen and sulphur.

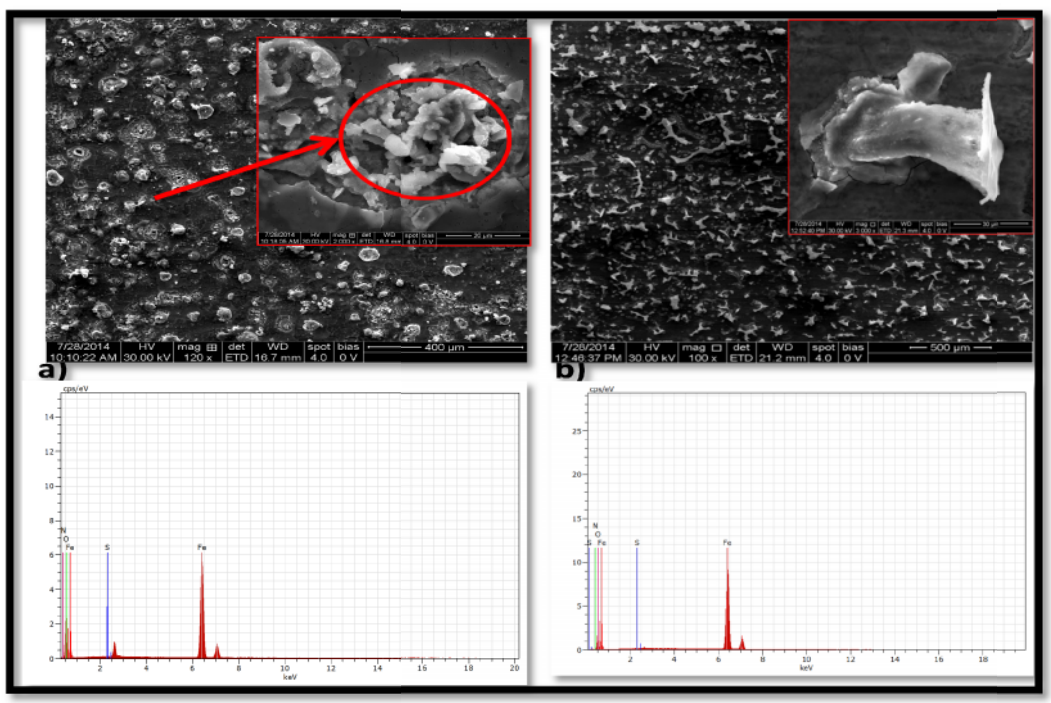

Figure – 46 SEM images and *EDX* spectra of mild steel immersed in the presence of (a) PVA-AAm-VSA (b) PVA-AAm-PVBS

4.5.4.3 SEM analysis of metal surface inhibited with Acrylic acid terpolymers

Typical photomicrographs of mild steel samples in the presence of PVA-AA-VSA are shown in Figure 47a. The inhibited metal surface is smoother than the uninhibited surface (Figure 45a) indicating the presence of a protective layer of adsorbed inhibitor preventing chloride attack in 1 M HCl. The protective layer comprises scattered polymeric structures as clearly seen in the inset of Figure 47. When one such portion is magnified to 12000 X (Figure 47a inset) a floral structure exhibiting interlinked structure is perceived. The elemental distribution maps obtained for the floral portion by means of SEM–EDX, detected the high deposition rates of oxygen. The content aspect ratio of oxygen is more in this case when compared to that of PVA-AAm-VSA because of oxygen rich sources; PVA and acrylic acid. However, the element nitrogen is obviously absent in PVA-AA-VSA.

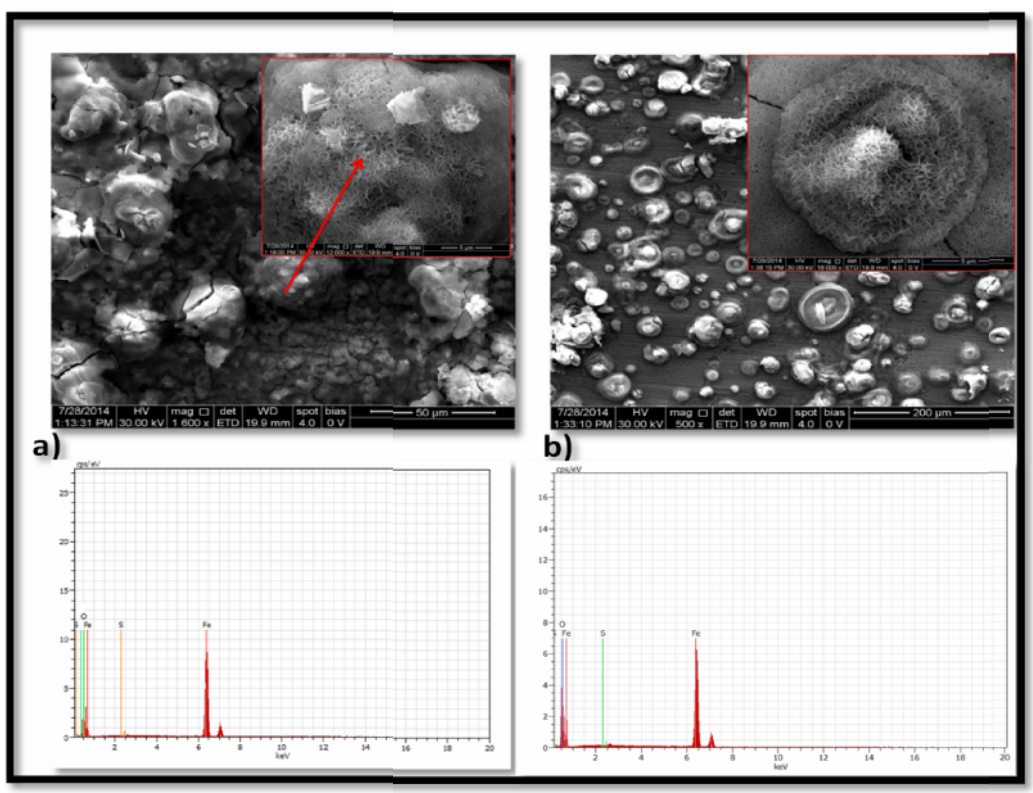

Figure - 47 SEM images and EDX spectra of mild steel immersed in the presence of (a) PVA-AA-VSA (b) PVA-AA-PVBS

Figure 47b shows the electronic image acquisition of the MS surface in the presence of PVA-AA-PVBS. The coverage of the metallic surface is considered as the primary factor to prevent the corrosion as explained previously. In this sense the coverage of the MS by PVA-AA-PVBS is very similar to that of PVA-AA-VSA. The SEM image shows a uniform layer covering the surface with distributed spherical particles of various sizes. The image clearly

shows the presence of two phases. Extensively cross-linked floral structure located in the ring shaped aggregated white particles. EDX mapping of the portion confirmed the presence of Fe, O and S.

4.5.4.4 SEM analysis of metal surface inhibited with PVA-VSA-PVBS

Figure 48 shows the visual aspect of the mild steel surface after immersion in HCl containing PVA-VSA-PVBS. The surface morphology of the sulphur containing terpolymers deposited on mild steel clearly shows the distribution of spherical and non-spherical particles as well as some clusters**.** This may be interpreted as due to the adsorption of the inhibitor on the metal surface and forming a passive film in order to block the active site present on the mild steel surface. However, the magnified image of spherical structure of the polymer shows a few cracks. As a result of this, the film formed on the surface may rupture in the due course of immersion. This nature of the less adherent or cracked film of PVA-VSA-PVBS may be the reason for less IE % when compared to other polymers. The elemental analysis results of the selected portion reveal the presence of O, Fe and sulphur.

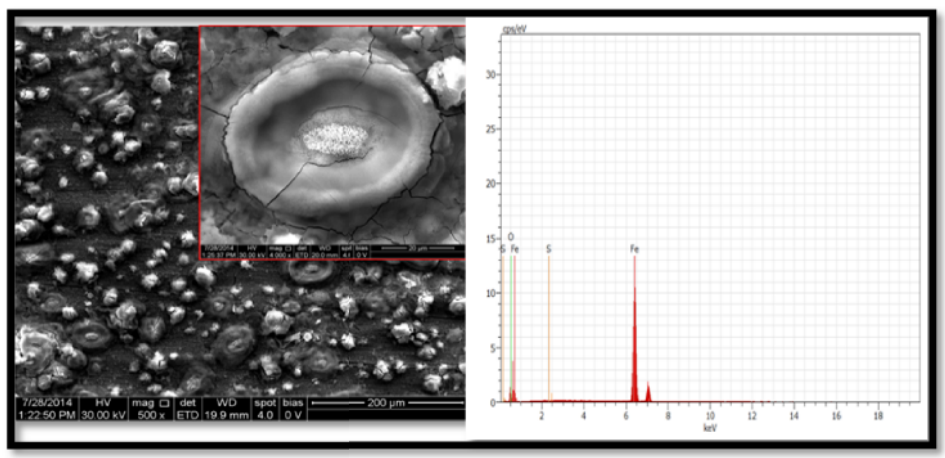

Figure - 48 SEM image and EDX spectra of mild steel in the presence of PVA-VSA-PVBS

Table - 36 Atomic wt.% of the elements observed in *EDX* analysis

Surface analysed	Atomic wt.%				
	Fe	O	Cl	N	S
Polished	100	-	-	-	-
Corroded	15.45	65.01	19.54	-	-
PVA-AAm-VSA	30.82	68.87	-	0.21	0.10
PVA-AA-VSA	29.18	69.49	-	-	0.08
PVA-AAm-PVBS	49.23	49.07	-	1.59	0.11
PVA-AA-PVBS	24.63	75.29	-	-	0.09
PVA-VSA-PVBS	31.40	68.53	-	-	0.07

The comparative elemental composition of MS surface in 1 M HCl in the presence and absence of inhibitors acquisitioned by EDX mapping are presented in Table 36. It is clear that Fe percentage in the absence of inhibitors in acid medium was 15 %. But in the presence of inhibitors the percentage of Fe content was increased and lies in the range of 24-49 %. This increment in the percentage of Fe values in the presence of inhibitors confirms the reduction of dissolution of metal by virtue of adsorption on mild steel **(Hari Kumar and Karthikeyan, 2014).** The corroded surface has chloride content of 19.54 % as a result of adsorption of chloride ions from the HCl medium on steel surface. The atomic % of nitrogen and sulphur is an evidence for the adsorbed layer of the respective terpolymers on the MS surface.

4.5.5 Surface imaging techniques- ii) Atomic force microscopic analysis

Atomic force microscope has emerged as a contemporary choice for investigating the influence of inhibitors on the metal surface from nano to micro scale level **(Xianghong and Guannan, 2005).** Because AFM uses a sharp tip to probe the surface features by raster scanning and can image the surface topography with extremely high magnifications, up to 1,000,000 X, comparable or even better than electronic microscopes. The measurements are depicted as three dimensional images as horizontal X-Y plane and the vertical Z plane. Resolution (magnification) at Z-direction is larger than X-Y.

The integrity and persistence of inhibitor films formed on the metal surface is of paramount importance in the corrosion inhibition studies. The AFM technique reveals the extent of inhibitor film adsorption on the MS surface in terms of calculating the roughness parameter and through 3D images of the surface.

In the present study, morphological analysis of the surfaces of the mild steel were carried out by AFM in the range 0 to 50 μm at room temperature after immersion in different test solutions for 6 h. Three-dimensional AFM images of mild steel, mild steel immersed in 1 M HCl and mild steel immersed in 1 M HCl containing various terpolymeric inhibitors are shown in Figures 49(a&b) and 50(a-e) respectively. The roughness parameter Ra and root mean square roughness Rms were calculated using software called Gwyddion and are tabulated in Table 37.

The polished mild steel is absolutely smooth with very least surface roughness. In the absence of the inhibitors (Figure 49b), the surface of the film shows several mountain like formations that correspond to rough surface **(Quraishi and Shukla, 2009)**. The Ra and Rms corresponding to the MS corroded in blank HCl is 0.567 μm and 0.693 μm which are very higher than the roughness parameters obtained for inhibited surfaces. In the presence of

inhibitors, the ridges caused by corrosive environment are decreased to a greater extent and a smooth surface is perceived. But still the surface resembles sand dunes which can be correlated to the uneven inhibitor film formed on MS surface during the course of the study.

Table - 37 Surface roughness parameters obtained for MS under various conditions using atomic force microscope

Polished	Ra (µm)	Rms (µm)
Polished MS	0.112	0.146
Corroded	0.567	0.693
PVA-AAm-VSA	0.313	0.401
PVA-AA-VSA	0.257	0.319
PVA-AAm-PVBS	0.220	0.294
PVA-AA-PVBS	0.290	0.369
PVA-VSA-PVBS	0.329	0.404

The roughness parameter given in the Table 37 has the following order:

Polished MS<PVA-AAm-PVBS<PVA-AA-PVBS<PVA-AA-VSA<PVA-AAm-VSA<PVA-VSA-PVBS<Corroded MS

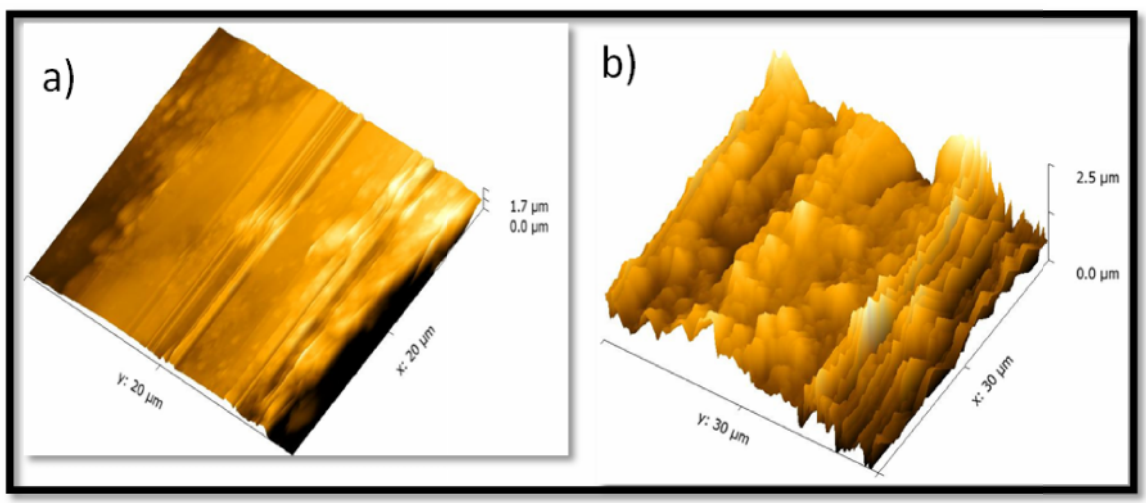

Figure - 49 Atomic force microscopic images of a) Polished MS; b)MS immersed in 1M HCl

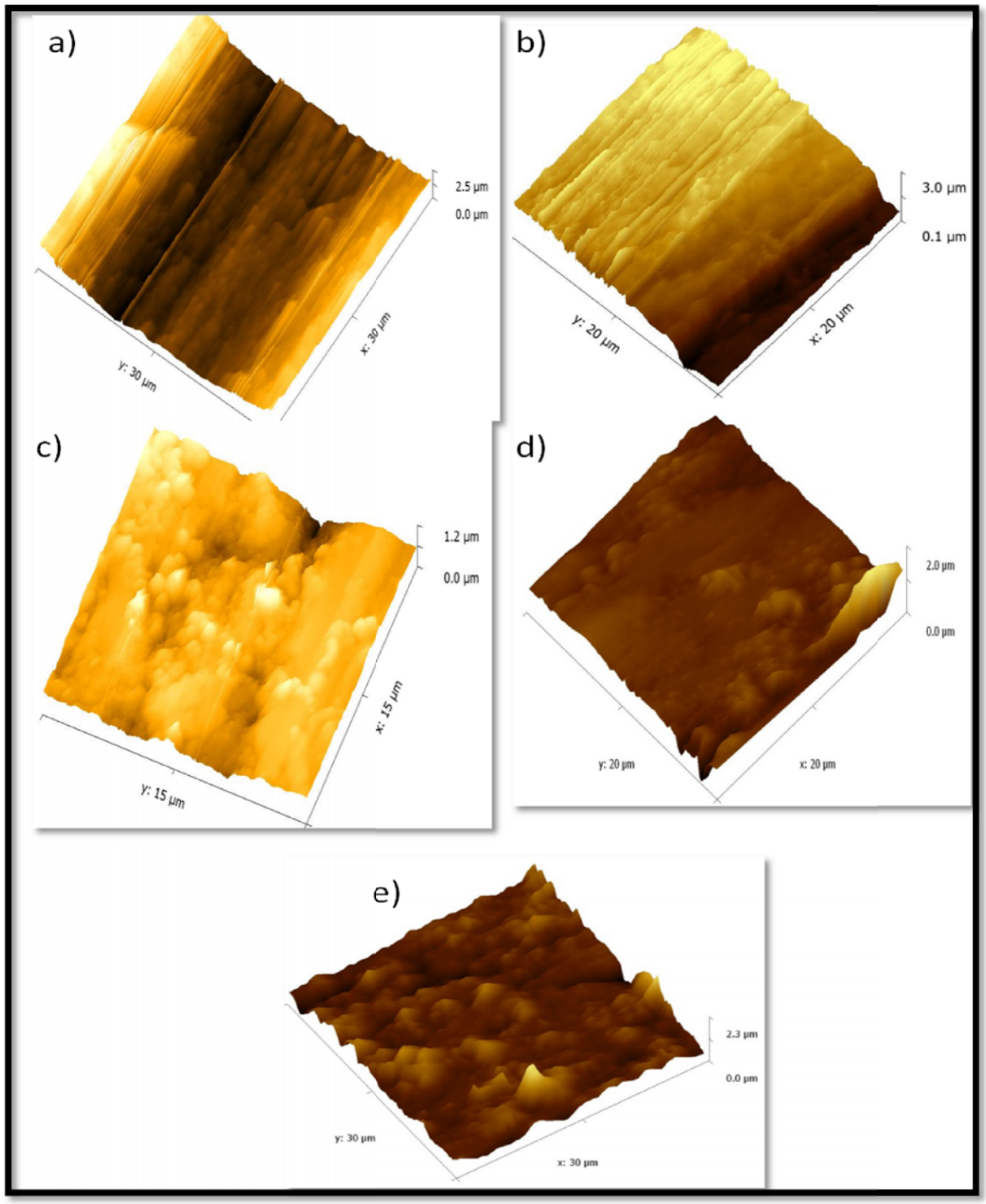

Figure - 50 Atomic force microscopic images of MS immersed in 1M HCl in the presence of a) PVA-AAm-VSA ; b)PVA-AAm-PVBS;c)PVA-AA-VSA; d)PVA-AA-PVBS;e)PVA-VSA-PVBS

4.5.6 Mechanism of inhibitive action of terpolymers

Inhibition of corrosion in acid medium is achieved through adsorption. The adsorption of any inhibitor molecule on the metal surface is a substitutional process by replacing the water molecules on the metallic surface $H_2O_{(ads)}$.

$$Inh_{(sol)} + xH_2O_{(ads)} \rightarrow Inh_{(ads)} + xH_2O_{(sol)}$$

where $Inh_{(sol)}$ and $Inh_{(ads)}$ are the inhibitor molecules in the acidic solution and adsorbed on metallic surface respectively. $H_2O_{(ads)}$ is the water molecule adsorbed on the metallic surface, x is the number of water molecules replaced by one adsorbed inhibitor molecule **(Benchettara and Amara, 2008).**

The adsorption process basically is affected by many factors including charge on metal surface, charge/dipole moment of the inhibitor molecules, hetero atom population, structural properties of the inhibitor and type of the aggressive medium. According to **Hackerman and Mackrides (1954)** a corrosion inhibitor actually functions by reacting with the metal ion that is newly produced in the corrosive medium but in a plane very near or on the metal surface **(Ebenso *et al*., 1999).** The adsorption can be physical or chemical in nature.

Four types of adsorption may take place by inhibitor molecules at the metal-solution interface **(Shokry *et al*., 1998).**

- electrostatic attraction between the charged molecules and the charged metal
- interaction of uncharged electron pairs in the molecule with the metal
- interaction of π electrons with the metal and
- combination of 1 and 3.

Electrostatic attraction is mainly due to the physical adsorption of the inhibitors while sharing of lone pair of electrons and interaction with π electrons can lead to chemisorption. Potential zero charge (pzc) is an important factor in determining electrostatic adsorption process. AC impedance technique is used to determine potential zero charge of the electrode. Figure 51 shows the impedance curves obtained at various applied potentials and Figure 52 shows the relationship between R_{ct} and applied potential. The charge on the metal surface can be determined using the potential zero charge (pzc) on the correlative scale using the equation **(Shukla and Quraishi, 2010)**.

$$\psi_c = E_{corr} - E_{q=0} \quad (35)$$

where $E_{q=0}$ is the potential of zero charge and E_{corr} value obtained for mild steel in 1 M HCl. Depending upon the charge of ψ_c values, the charge of the metal surface can be determined. From the Figure 52, it is clear that the value of $E_{q=0}$ is -0.475 mV and E_{corr} for mild steel in 1M HCl is -0.450 mV. ψ_c = 25 mV. This shows that the surface of the metal is positively charged.

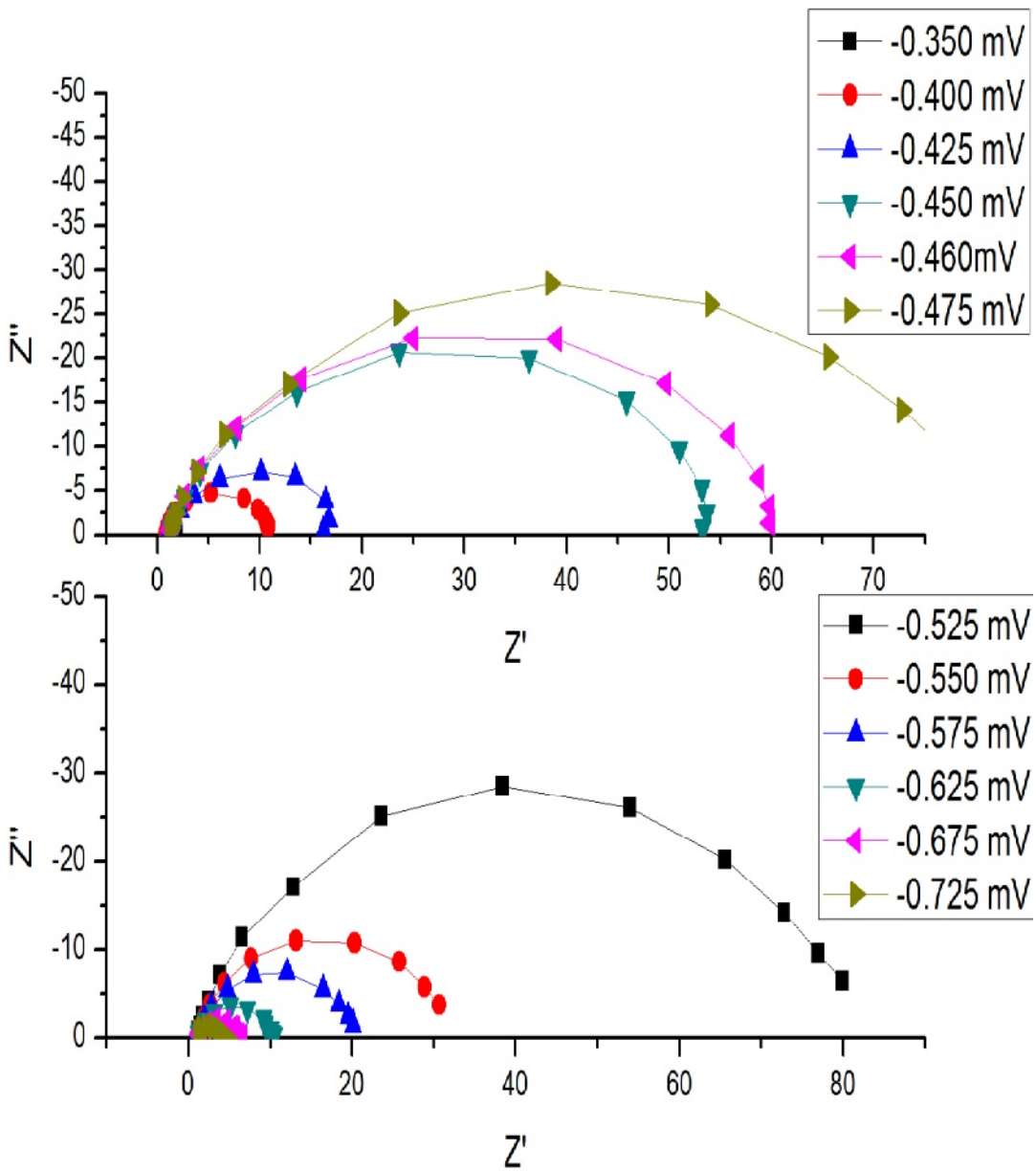

Figure - 51 Impedance curves obtained for MS at various applied potentials

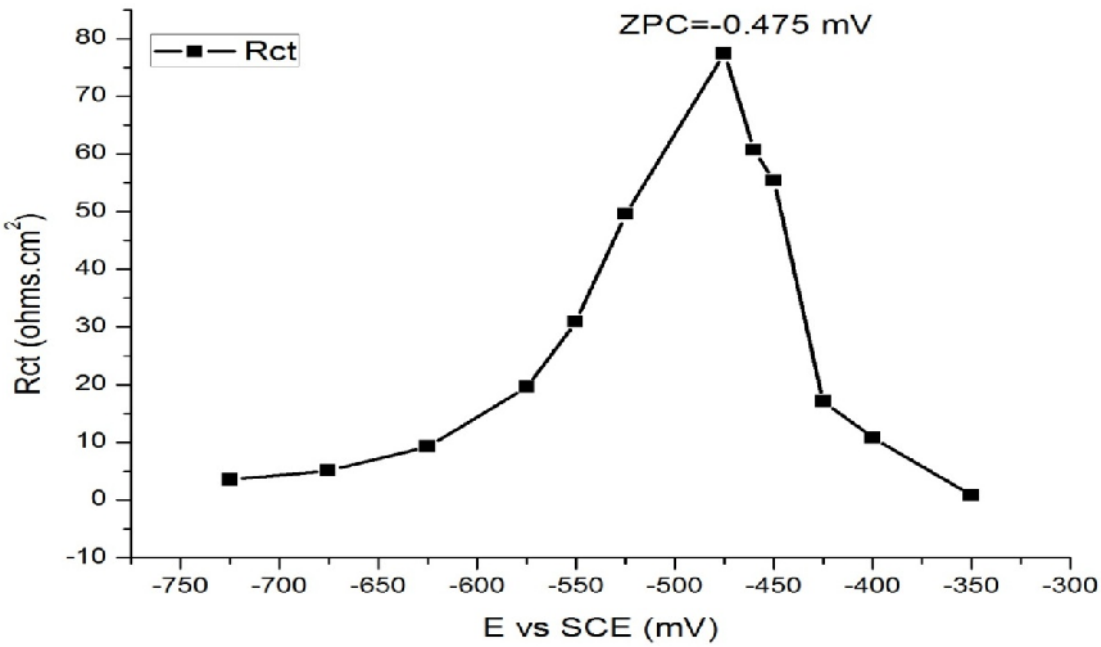

Figure - 52 A plot of R_{ct} vs. applied potential (E vs. SCE) for MS in 1 M HCl solution

4.5.6.1 Mode of adsorption of grafted terpolymers

The terpolymers under investigation have several adsorption centres that favour combination of the above interactions. i.e. both the physical adsorption and chemical adsorptions are favourable. Physical adsorption or electrostatic interactions are proved by the zpc and chemical adsorption is proved from the thermodynamic parameters of adsorption and activation energy in the previous chapters.

As far as the electrostatic interactions are considered, polyacrylamide can form protonated groups to interact with negative sites and polyacrylic acid/polysulfonate can exist in anionic form to interact with positive sites of the metal. In the present study, polyacrylamide (cationic) containing terpolymeric inhibitors function by electrostatic adsorption between the positively charged nitrogen atom (N^+) and the negatively charged metal surface (through chloride ion bridges in HCl) to prevent any H^+ getting nearer to the metal surface. In the case of anionic polymers, COO^- anions of Polyacrylic acid and SO_3^- anions of sulfonate polymers electrostatically form linkages with the positive sites of the metal. A hydrophobic, dense and defect-free monolayer is formed by the neighbouring alkyl chains through Vander Waal forces, which acts as a barrier between the metal surface and corrosive environment, thereby protecting the iron surface from corrosion **(Ren *et al*., 2008; Rivas and Nicolas, 2003)**. It is worth mentioning the metal chelating property of the polychelatogen poly(acrylic acid-co-vinyl sulfonic acid) discussed by **Rivas**

and Nicolas (2003), which further supports the inhibitive mechanism of polyacrylic acid containing terpolymers through complex formation. These complexes might be adsorbed on the steel surface through Vanderwaal's force and forms a barrier layer to prevent from corrosion. Figure 53 is the pictorial representation of plausible electrostatic interactions of the functional groups in the terpolymer.

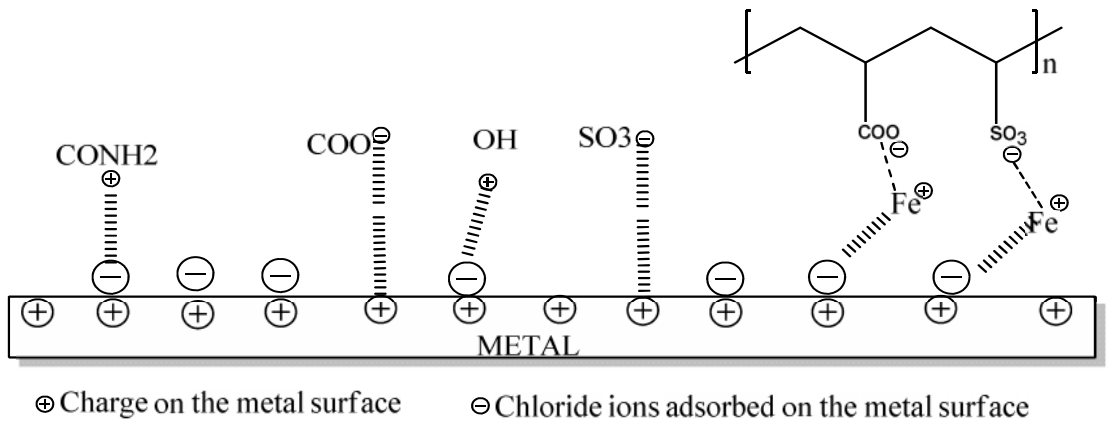

Figure - 53 Plausible electrostatic interactions favoured by the functional groups in terpolymer- Physical adsorption

The process of chemical adsorption takes place by charge sharing or transferring from the molecules to the metal surface thereby forming a co-ordinate type of bond. This type of co-ordination occurs between the low energy vacant orbitals of transition metals and loosely bound electrons of the inhibitor molecules **(Amin and Khaled, 2010).** The terpolymer under investigation has electron rich centres that aid in the chemical adsorption or co-ordinate bond formation with the low energy vacant d-orbitals of the mild steel surface. Figure 54 is the pictorial representation of plausible co-ordinations of electron rich centres with the metal. The electron rich centres for chemisorption are listed below, and the function of each active centre in adsorption can be described as follows:

PVA-AAm-VSA	N, S, O
PVA-AA-VSA	O,S
PVA-AAm-PVBS	N, S, O,C=C (Ar.)
PVA-AA-PVBS	S, O,C=C (Ar.)
PVA-VSA-PVBS	O,S, C=C (Ar.)

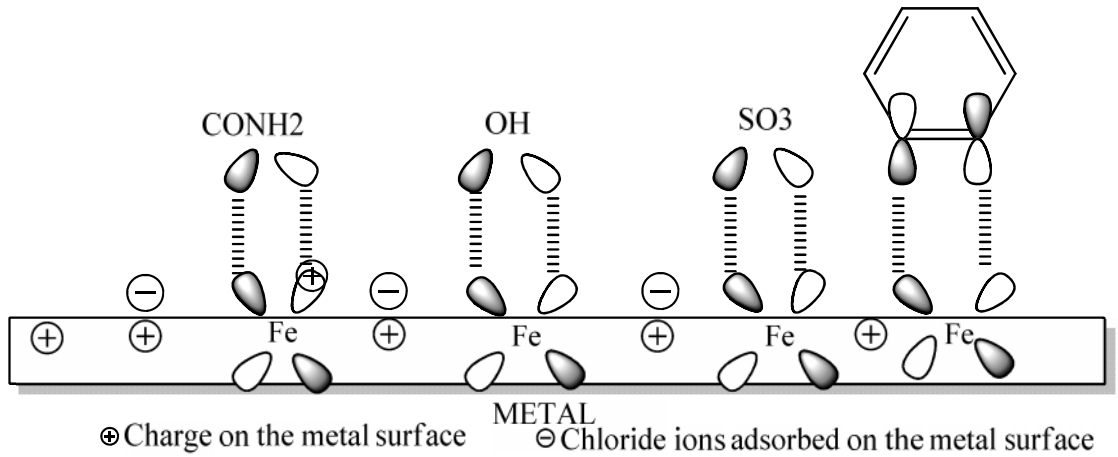

Figure - 54 Plausible interactions of uncharged electron pairs and π electrons with the vacant orbitals of metal atom-Chemisorption

All the investigated polymers have hydrophilic segments in which the lone electron pairs of the oxygen atoms form coordinate bonds with the empty orbitals of iron atoms. The nitrogen atom has an electron pair and sulphur atom has two electron pairs which are capable of chemically interacting with empty d-orbitals of the metal atom. The protective ability of the sulphur compounds depends on the polarization of the sulphur atom **(Oguzie, 2004).**

In the structure of the PVBS-containing polymers, the π electrons of the benzene ring can interact with the mild steel surface. While the π orbital of the inhibitor molecule donates electrons to the empty orbital of the metal atom, there is also possibility of π* orbital to accept electrons from the metal orbital thereby forming feedback bonds **(Behpour *et al*., 2008).**

Depending upon the population of hetero atoms, pi bonds, unshared electron pair and electrostatic charges, the order of inhibition of the terpolymers obtained in different techniques are well in agreement with the order as shown below.

PVA-AAm-PVBS(O+N+S+phenl moiety) >PVA-AAm-VSA (O+N+S) >PVA-AA-PVBS (O+S+phenyl moiety) >PVA-AA-VSA (O+S) >PVA-VSA-PVBS (O+S+phenyl moiety)

4.5.6.2 Quantum chemical calculations

Various factors have to be considered for elucidating the mode of action of inhibition on the metal surface. Quantitative structure–activity relationship (QSAR) calculations were conducted to optimize a part of geometry of the synthesized terpolymers to study the effect of molecular structure on the inhibition efficiency. The theoretical computations were carried out using semi-empirical PM3 method using the Hyperchem software. As an optimization

procedure, the built-in Polak–Ribiere algorithm was used with root mean square gradient of 0.05 kcal/mol in-vacuo method. The quantum chemical indices calculated were: the energy of the highest occupied molecular orbital (E_{HOMO}), the energy of the lowest unoccupied molecular orbital (E_{LUMO}), the dipole moment (μ) and energy band gap ($\Delta E = E_{LUMO} - E_{HOMO}$) are listed in Table 38. Figures 55&56 shows the optimized molecular structure, molecular orbital plots of investigated terpolymers obtained from PM3 method.

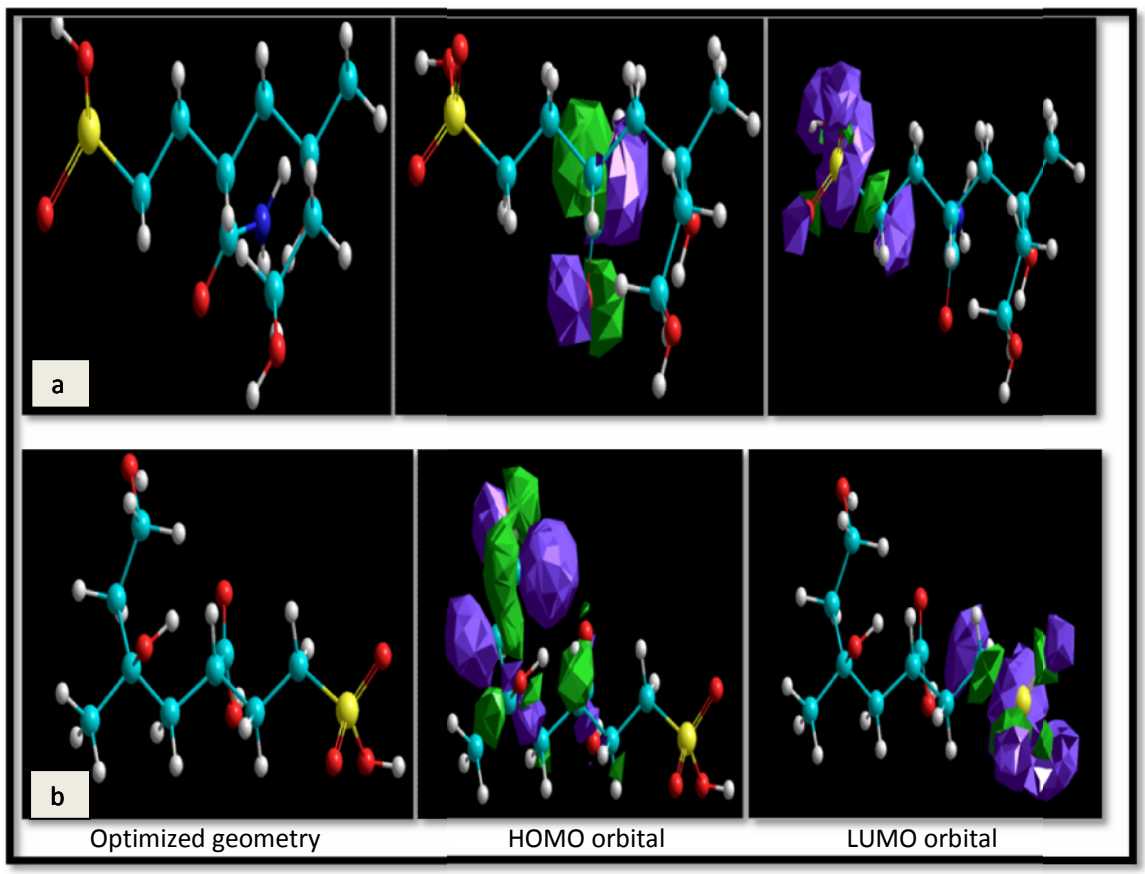

Figure - 55 Molecular structure, molecular orbital plots of a) PVA-AAm-VSA and b) PVA-AA-VSA obtained from PM3 method

Table - 38 Quantum chemical parameters calculated using PM3

Inhibitor	E_{HOMO} eV	E_{LUMO} eV	ΔE	μ Debye
PVA-AAm-VSA	-10.307	-0.1157	10.19	6.616
PVA-AA-VSA	-11.192	-0.2778	10.92	4.836
PVA-AAm- PVBS	-10.4159	-0.9080	9.5079	7.258
PVA-AA-PVBS	-10.3909	-0.6190	9.7719	5.387
PVA-VSA-PVBS	-10.8953	-1.2941	9.6012	5.616

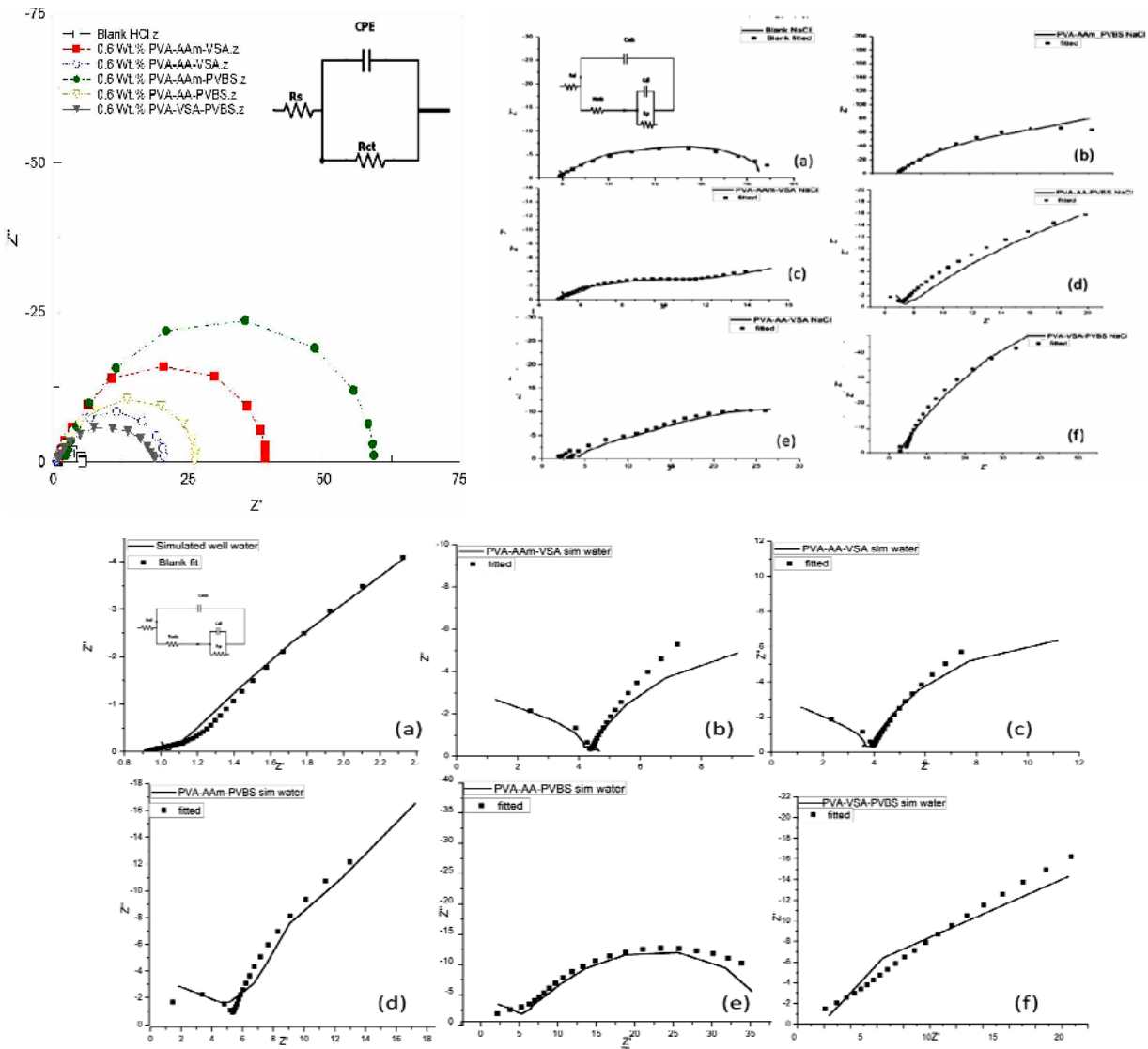

Figure - 58 Nyquist plot for 0.6 wt.% of terpolymers in 10 % HCl, 3.5 % NaCl and simulated oil well water

5.2.1 Analysis of impedance behaviour of N80 steel in HCl

For iron dissolution in acid, the equivalent circuit is designed with a resistor and capacitor in parallel with each other. Three types of resistances can be taken into account: solution resistance, polarization resistance and charge transfer resistance. Solution resistance is the ionic solution resistance which depends upon ionic concentration, type of ions, temperature and geometry of the area in which current is carried. The interface of metal in electrolyte is envisioned as space that exists between array of ions on the electrode surface and array of solvated ions away from surface. The two arrays of ions can store charge in them and acts as a capacitor element. The capacitance thus generated is called

the double layer capacitance, C_{dl}. The double layer capacitor can also lead to a resistor providing charge transfer resistance, as the charge is transferred during the metal dissolution. The Nyquist Plot for Randle's cell consisting of the above elements is always semicircle. The solution resistance can be determined from the real axis value at the high frequency intercept. This is the intercept near the origin of the plot. The low frequency region gives us the sum of solution resistance and polarization resistance.

Figure 58 shows the impedance response of 0.6 wt.% of each inhibitor on N80 steel in 10 % HCl and Table 42 lists the impedance parameters for N80 steel in HCl . The impedance diagram consists of single semicircle indicating a single charge transfer reaction. The shape of the semicircle is depressed in nature from high to medium frequency region which is an indication of micro-roughness and other inhomogeneties of the working electrode during the reaction **(Ostovari *et al*., 2009)**. Nevertheless introduction of the inhibitors increases the diameter of the capacitive semicircle with respect to corrosion mitigating capability of the inhibitor.

Table - 42 Impedance parameters for N80 steel in HCl

Inhibitor	Conc. Wt.%	R_s/ Ωcm^2	CPE Fcm^{-2}* 10^{-6}	n	R_{ct} $k\Omega cm^2$	IE R_{ct} %
Blank	-	0.9178	1806	0.860	4.50	-
PVA-AAm-VSA	0.09	1.1800	699	0.892	11.13	59.57
	0.45	0.7977	788	0.809	13.69	67.13
	0.6	0.8598	223	0.826	40.12	88.78
PVA-AAm-PVBS	0.09	1.2840	340	0.812	37.35	87.95
	0.45	1.2020	925	0.806	43.21	89.59
	0.6	1.9210	262	0.802	60.46	92.56
PVA-AA-VSA	0.09	0.6872	738	0.796	8.94	49.69
	0.45	0.7690	1369	0.827	15.15	70.30
	0.6	0.6718	1247	0.828	21.08	78.65
PVA-AA-PVBS	0.09	0.9074	506	0.754	23.16	80.57
	0.45	0.7910	548	0.807	23.72	81.03
	0.6	0.8114	444	0.782	28.40	84.15
PVA-VSA-PVBS	0.09	1.2840	340	0.812	37.35	49.69
	0.45	1.2020	925	0.806	43.21	56.01
	0.6	1.9210	262	0.802	60.46	75.32

The values of R_{ct} in the presence of inhibitors are higher than in absence indicating the formation of protective film on the metal/solution interface (**Rosliza *et al*., 2008**).

The C_{dl} values were calculated at the frequency f_{max}, at which the imaginary component of the impedance is maximal (Z'') by the following equation:

$$Cdl = \frac{1}{2\pi fmax}\ R_{ct} \tag{36}$$

But the double layer capacitance (C_{dl}) value is affected by certain imperfections of the surface, and this effect is simulated via a constant phase element (CPE). The C_{dl} value is calculated using the following formula:

$$\text{CPE}_{dl} = Y_o(Rct^{1-n})^{1/n} \tag{37}$$

It is worth mentioning that the parameter n quantifies different physical phenomena like surface in homogeneities in the form of surface roughness, adsorption of inhibitor, and pores in the adsorbed layer and so on. CPE can correspond to resistor (when n=0), capacitor (when n =1), inductor (when n=-1) and Warburg impedance (when n=0.5). In this case, n value is close to unity representing that the CPE is a capacitor element **(Wanying *et al*., 2014).**

The addition of polymeric inhibitors obviously increased the values of R_{ct} and lowered the values of double layer capacitance. The constant phase elements (CPEs) with their n values close to unity represent double layer capacitors with some pores **(Sherif and Park, 2006)**. When the value of n, ranges between 0.74 and 0.86, it can be an indication of the charge transfer process controlling the dissolution mechanism **(Wanying *et al*., 2014)**. The decrease in CPEs with increase in inhibitor concentrations, are expected as an effect of coverage of charged surfaces and thereby reduction of capacitive effects **(Khaled, 2008b)**. **Singh and Quaraishi (2010b) and Bentiss *et al*. (2000)** explain that decrease in C_{dl} values is probably an effect of decrease in local dielectric constant and/or an increase in the thickness of the inhibitor layer on metal/solution interface. The decrease in the effective surface area which acts as a place for charging is also a reason for decrease in C_{dl}. The IE calculated from the R_{ct} values shows that maximum IE is rendered by acrylamide terpolymers followed by acrylic acid terpolymers and sulfonate polymers.

5.2.2 Analysis of impedance behaviour of N80 steel in 3.5 % NaCl and Simulated oil well water

Observation of the Figures 58(a-f) shows that the diameter of the semicircles is higher (from high frequency to low frequency region) for the inhibited solution when compared to that of the blank solution indicating the formation of a protective film or reduction in corrosion rate after the addition of inhibitors. The Nyquist plots for NaCl reflects unduly elongated

semicircle indicating that there is a dispersion of time constants, i.e the elongated semicircle can be considered as two overlapping semicircles. This high frequency semicircle is associated with the dielectric property of the film whereas the low frequency semicircle is attributed to the diffusion process. The flattened Nyquist plots reveal that there is formation of corrosion products and/or incrustation, hence the corrosion process at the low frequency region can be assumed to be controlled by diffusion **(Perez *et al*., 2007).** The change in the shape of the impedance plots among the investigated polymers reveals the difference in the protective layer formed by the inhibitors, which is reinforced on the charge transfer surface layer **(Azghandi *et al*., 2012).** Various resistances may operate in the neutral corrosion reactions that includes, charge transfer resistance R_{ct}, diffuse layer resistance R_d, resistance of film R_f and resistance created by accumulated species R_a. The total resistance of the system is taken as R_p;$R_p = R_{ct} + R_d + R_a + R_f$. The IE calculated from the R_{ct} values for 0.6 wt.% inhibitor concentration has the following trend: PVA-AAm-PVBS>PVA-AA-VSA>PVA-AAm-VSA>PVA-AA-PVBS> PVA-VSA-PVBS.

Table - 43 Impedance parameters for N80 steel in NaCl

Inhibitor	Conc. Wt.%	R_s/ Ωcm^2	R_{ads}/ $k\Omega cm^2$	C_{ads} $\mu F\ cm^2$	CPE		C_{dl} $\mu F\ cm^2$	R_p $k\Omega cm^2$	IE %
					A $S^n\Omega^{-1}\ cm^{-2}$	n			
Blank	-	3.00	100	2.77	0.095	0.7070	1939.7	15.25	-
PVA-AAm-VSA	0.09	5.53	152	2.76	0.0025	0.6800	16.6	22.32	31.68
	0.45	4.95	183	2.70	0.0030	0.7000	21.6	33.50	54.48
	0.6	2.66	652	2.50	0.0039	0.5200	36.7	81.85	81.37
PVA-AAm-PVBS	0.09	1.76	130	3.08	0.0210	0.7968	117.1	40.24	62.1
	0.45	1.50	102	2.03	0.0168	0.7968	101.2	68.00	77.57
	0.6	1.50	120	2.03	0.0262	0.7677	287.8	105.00	85.48
PVA-AA-VSA	0.09	1.21	120	3.50	0.0335	0.7126	792.1	76.06	79.95
	0.45	1.21	148	3.50	0.0265	0.7826	227.0	86.00	82.27
	0.6	1.21	169	3.50	0.0352	0.8026	259.7	96.00	84.11
PVA-AA-PVBS	0.09	2.00	113	2.71	0.0032	0.5982	73.0	32.90	53.65
	0.45	3.52	257	2.50	0.0008	0.7366	2.8	40.50	62.35
	0.6	3.58	307	2.01	0.0053	0.8370	16.1	57.36	73.41
PVA-VSA-PVBS	0.09	3.09	198	2.55	0.0037	0.7976	10.8	18.30	16.67
	0.45	4.25	120	2.55	0.0020	0.7415	8.7	34.15	55.34
	0.6	4.44	105	2.55	0.0011	0.7269	5.1	54.01	71.76

The Nyquist plot obtained for simulated well water (Figure 58a-f) shows a straight line at the high frequency region and an unduly elongated semicircle at the low frequency region. The low frequency region in the real axis is attributed to the total resistance i.e. sum of electronic resistance of the active material, contact resistance with the current collector, and electrolyte resistance. The straight line in the low frequency region is an indication of diffusion-controlled process. The straight lines appear with slopes of 45–90° indicating diffusive resistance of the electrolyte in electrode pores and the cation diffusion in the host materials **(Feliu *et al*., 1993).** The slope of the straight line is larger for the inhibitor added solution when compared with that of blank simulated well water solution which denotes a lower diffusive resistance of the electrode after inhibitor addition.

Table - 44 Impedance parameters for N80 steel in simulated well water

Inhibitor	Conc. Wt.%	R_s/ Ωcm^2	R_{ads}/ $k\Omega cm^2$	C_{ads} μF cm^2	CPE		C_{dl} μF cm^2	R_p $k\Omega cm^2$	IE_t%
					A $S^n\Omega^{-1}$ cm^{-2}	n			
Blank	Blank	3.00	12.003	2.77	0.085	0.707	191.7	25.15	
PVA-AAm-VSA	0.09	2.23	399.89	2.71	0.0149	0.440	229.1	72.37	65.25
	0.45	2.23	200.28	2.50	0.0084	0.392	94.2	114.08	77.95
	0.6	4.49	254.02	2.01	0.0104	0.699	143.4	198.02	87.30
PVA-AAm-PVBS	0.09	3.35	224.78	2.55	0.0008	0.545	39.3	158.60	84.14
	0.45	3.87	204.18	2.55	0.0007	0.501	50.8	220.30	88.58
	0.6	2.87	113.01	2.55	0.0005	0.505	37.7	330.60	92.39
PVA-AA-VSA	0.09	1.58	120.02	2.72	0.0079	0.530	104.3	125.00	79.88
	0.45	1.57	225.36	2.04	0.0089	0.780	56.3	165.00	84.76
	0.6	1.58	299.47	2.07	0.0089	0.770	46.8	185.00	86.41
PVA-AA-PVBS	0.09	5.41	541.02	3.50	0.0176	0.605	310.1	136.90	81.63
	0.45	4.60	561.25	3.50	0.0143	0.607	139.1	201.50	87.52
	0.6	4.68	586.23	3.50	0.0143	0.607	52.8	245.65	89.76
PVA-VSA-PVBS	0.09	3.4	108.20	2.76	0.0046	0.916	14.2	53.23	52.55
	0.45	3.6	158.92	2.70	0.0015	0.716	5.9	65.23	61.31
	0.6	3.1	188.93	2.50	0.0014	0.716	7.1	85.02	70.41

The circuit used for fitting NaCl/simulated well water contains elements that can be described as follows: R_{ads}/C_{ads} is the high frequency time constant attributed to the adsorption of the inhibitor and R_p/C_{dl} is the low frequency time constant attributed to the defect sites where charge transfer processes take place **(Azghandi *et al*., 2012; Geethanjali *et al*., 2014).** This situation arises when the charge transfer resistance for anion exchange is larger than the relaxation of cations at the surface of the film **(Venugopal and Raja, 1997)**. The data presented in Tables 43 and 44 reveals that progressive addition of polymeric inhibitors obviously increased the values of R_p and inhibition efficiency calculated from R_p and lowered the values of double layer capacitance corresponding to the high-frequency semicircle. The decrease in C_{dl} values is due to the adsorption of the inhibitor on the electrode surface. The IE rendered by the terpolymers in simulated oil well water was found to follow the same trend as that of HCl medium.

5.3 Weight loss measurements

The persistency of inhibitor action is a vital aspect in assessing the efficiency of an inhibitor. During the application of inhibitors in oil and gas wells and flow lines, continuous supply of an inhibitor may not be possible. When inhibitor is applied at a low concentration continuously it is cumbersome to meet the adequate requirement throughout the pipeline **(Tan *et al*., 1996).** Hence, persistency of inhibitive action can therefore be considered as a primary criterion for evaluation of inhibitors, and in the present study it is carried out under static and dynamic conditions by weight loss method. From the electrochemical studies, it can be observed that a maximum inhibition efficiency (IE) was obtained for the highest concentration (0.6 wt.%) of the inhibitors under investigation. Hence 0.6 wt.% was fixed as optimum inhibitor concentration and further evaluation of corrosion protection efficiency was carried out under static and dynamic conditions. Table 45 collects the IE obtained for five grafted terpolymers on N80 steel under static and dynamic conditions. The values of IE obtained under static conditions are lesser than that obtained for dynamic conditions. This can be attributed to the following reasons:

1. The easy adsorption of inhibitor molecules on the metal surface even in short contact time. i.e. In dynamic conditions metal comes in contact with the inhibitor solution in gradual intervals during each rotation.
2. The splashing force of the inhibitor solution could have also helped the adsorption of inhibitors.
3. The persistency of the adsorbed molecules on the surface which also shows the chemisorption of the inhibitor molecules.

Table - 45 Comparative results of IE obtained for the different polymers in static and dynamic conditions

Inhibitor	Corrodant					
	HCl		NaCl		Simulated oil water	
	Static	Dynamic	Static	Dynamic	Static	Dynamic
PVA-AAm-VSA	72.3	75.52	72.39	74.26	79.56	86.61
PVA-AAm-PVBS	74.36	76.80	71.87	74.85	78.54	82.52
PVA-AA-VSA	70.25	75.12	68.25	71.70	69.36	72.33
PVA-AA-PVBS	72.36	74.62	70.14	72.02	75.45	79.62
PVA-VSA-PVBS	69.75	75.73	65.25	67.77	68.55	72.71

As far as the corrosive mediums are concerned, the inhibitors were found to work well in simulated well water followed by HCl and NaCl. Sulphuric acid is formed in simulated well water by reaction of H_2S with dissolved oxygen. The sulphur-containing compounds generally work well in sulphuric acid medium thus imparting a highest efficiency **(Loto *et al*., 2012, Shen *et al*., 2006).** All the inhibitors under investigation contain sulphur which could have contributed to the highest inhibition in simulated well water. The highest efficiency is however observed for inhibitors containing acryalmide along with sulfonate. The inhibition efficiency is slightly reduced in HCl medium. In HCl medium the adsorption of inhibitors predominantly occurs through electrostatic interaction with the chloride ions on the metal surface. This electrostatic interaction could have reduced at the studied temperature (60 ^{o}C). In 3.5 % NaCl solution, due to weak electrostatic interactions the inhibition efficiency is least than the others. From these observations, the inhibition efficiency of the terpolymers can be related to the hetero atom population and their interaction with the metal which will be discussed in detail the forthcoming section.

5.4 Mechanism of inhibition

The adsorption process is affected by many factors including chemical structure of the inhibitor, hetero atom population, total charges present and their distribution over the inhibitor molecule. A corrosion inhibitor actually functions by reacting with the metal ion that is newly produced in the corrosive medium but in a plane very near or on the metal surface **(Ebenso *et al*., 1999)**. The adsorption can be physical or chemical in nature. Four types of adsorption may take place by inhibitor molecules at the metal-solution interface **(Shokry *et al*., 1998).**

- electrostatic attraction between the charged molecules and the charged metal
- interaction of uncharged electron pairs in the molecule with the metal

- interaction of p electrons with the metal and
- Combination of 1 and 3.

As far as the metal surface is considered, it undergoes following types of reactions in different corrosive mediums. The anodic reaction of iron in HCl is given by **Solamaz *et al*. (2011).**

$$Fe + Cl^- \leftrightarrow (FeCl^-)_{ads}$$

$$(FeCl^-)_{ads} \leftrightarrow (FeCl)_{ads} + e^-$$

$$(FeCl)_{ads} \leftrightarrow FeCl+ + e^-$$

$$FeCl+ \leftrightarrow Fe^{2+} + Cl^-$$

The cathodic hydrogen dissolution is given as follows

$$Fe + H^+ \leftrightarrow (FeH^+)_{ads}$$

$$(FeH^+)_{ads} + e- \leftrightarrow (FeH)_{ads}$$

$$(FeH)_{ads} + H+ + e- \leftrightarrow Fe + H_2 \text{ (hydrogen evolution)}$$

The corrosion of iron in neutral or saline media is given as **(Solmaz *et al*., 2011; Sherif, *et al*., 2010)**

$$\mathbf{F}e \rightarrow Fe^{2+} + 2\ e-$$

$$Fe^{2+} \rightarrow Fe^{3+} + e-$$

$$Fe + Cl^- \rightarrow FeCl + e-$$

$$FeCl + Cl^- \rightarrow FeCl_2^- + e-$$

Meanwhile, iron develops oxide layers that partially protect the surface being attacked by chloride ions. It was also found that iron could develop nine different types of oxide phases on their surfaces. The oxide formation occurs according to the following equation.

$$Fe + 1/2\ O_2 + H_2O \rightarrow Fe(OH)_2$$

$$3Fe(OH)_2 + 1/2\ O_2 \rightarrow Fe_3O_4 + 3H_2O$$

The chemical reaction proposed for iron dissolution in neutral media containing hydrogen sulphide is shown below.

$$Fe + H_2S \rightarrow FeS + H_2$$

It is also assumed that iron dissolution does not occur immediately, before which a fast oxidation of solid iron occurs and transforms directly into iron sulphide. Then the iron sulphide is strongly adhered on the metal surface, but still this mechanism is under question

including the role of various factors that influence the formation of different types of sulphide products.

The terpolymer under investigation has electron rich centres that aid in adsorption of the inhibitors as given in Figure 59. In the present study, polyacrylamide (cationic) polymeric inhibitors probably adsorb by electrostatic interaction between the positively charged nitrogen atom (N^+) and the negatively charged metal surface. The metal surface becomes negative charged due to the adsorption of chloride ions from HCl/NaCl and and HS^- ions from simulated well water. This prevents any H^+ getting nearer to the metal surface (**Shen *et al*., 2006; Migahed *et al*., 2003**). The COO^- anions of Polyacrylic acid polymers, and SO_3^- anions of sulfonate polymers electrostatically form linkages with the positive sites of the metal. All the investigated polymers have hydrophilic segments in which the lone electron pairs of the oxygen atoms form coordinate bonds with the empty orbitals of iron atoms. The inhibitive effect can also be due to the formation of bonds between the empty d-orbital of iron atoms and the lone pair of electrons present in the N, O and S atoms of whole terpolymer (**Chandra *et al*., 2014; Apparao *et al*., 2009**)**.** The protective ability of the sulphur compounds is governed by the fact of greater polarization of C-S bonds (**Oguzie, 2004**)**.**

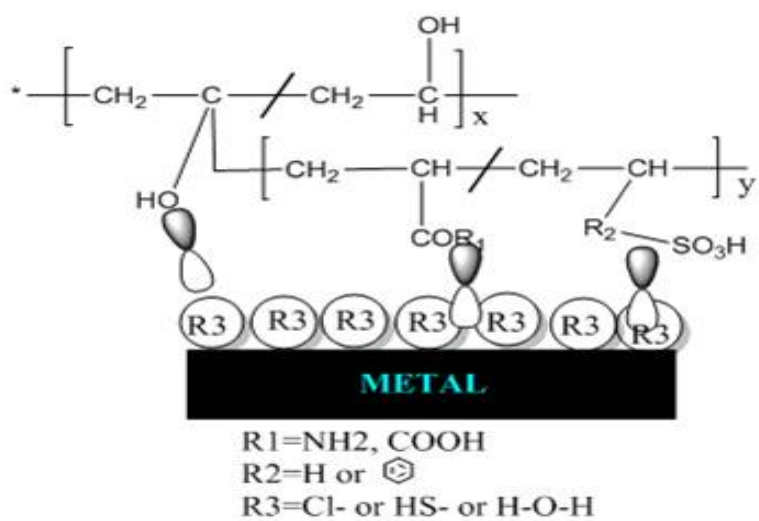

Figure - 59 Plausible mechanism of inhibition on N80 steel in investigated systems by terpolymers

The PVBS polymers also get attracted to the metal surface through the π electrons on the benzene ring. While the π orbital of the inhibitor molecule donates electrons to the empty orbital of the metal atom, there is also possibility of π* orbital to accept electrons from the metal orbital thereby forming feedback bonds **(Behpour *et al*., 2008).**

A hydrophobic, dense and defect-free monolayer is formed by the neighbouring alkyl chains through Vander Waal forces, which acts as a barrier between the metal surface and corrosive environment, thereby protecting the iron surface from corrosion **(Ren *et al*., 2008, Rivas 2003**). It is worth mentioning the metal chelating property of the polychelatogen poly(acrylic acid-co-vinyl sulfonic acid) discussed by **Rivas (2003)**, which further supports the inhibitive mechanism of polyacrylic acid containing terpolymers through complex formation. These complexes might be adsorbed on the steel surface through Vanderwaal's force and forms a barrier layer to prevent from corrosion. Depending upon the population of hetero atoms, pi bonds, unshared electron pair and electrostatic charges, the order of inhibition of the terpolymers obtained in different techniques are well in agreement with the order as shown below.

PVA-AAm-PVBS(O+N+S+phenl moiety) >PVA-AAm-VSA (O+N+S) >PVA-AA-PVBS (O+S+phenyl moiety) >PVA-AA-VSA (O+S) >PVA-VSA-PVBS (O+S+phenyl moiety)

Among the five terpolymers investigated, acrylamide terpolymers were found to be effective in controlling the corrosion of N80 steel in different mediums. The potentiodynamic polarization study shows that the corrosion currents are minimized by the addition of inhibitor. The IE was well pronounced in simulated oil well water followed by HCl and 3.5% NaCl. The inhibitors action persistency analysed by static and dynamic weight loss method shows that the inhibitor action is persistent in dynamic conditions. Hence the inhibitors can be optimized and recommended for usage in oil wells containing sour corrosion problems.